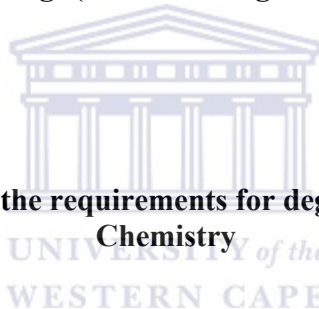


**SYNTHESIS AND CHARACTERIZATION OF
MICRO- AND MESOPOROUS MATERIALS FOR
LOW TEMPERATURE SELECTIVE CATALYTIC
REDUCTION OF NITROGEN OXIDES**

By:

**JEAN BAPTISTE KASONGO WA KASONGO
BSc Eng: (Chemical Engineering)**



**Submitted in fulfillment of the requirements for degree of Magister Scientiae in
Chemistry**

**Department of Chemistry
University of the Western Cape**

Supervisor: Associate Professor L.F. Petrik

Co-supervisor: Dr Eric Hums

May 2011

SYNTHESIS AND CHARACTERIZATION OF MICRO- AND MESOPOROUS MATERIALS FOR LOW TEMPERATURE SELECTIVE CATALYTIC REDUCTION OF NITROGEN OXIDES

JEAN BAPTISTE KASONGO WA KASONGO
BSc Eng: (Chemical Engineering)

KEYWORDS

Catalysis

Selective catalytic reduction

NO_x

DeNO_x

Microporous

Mesoporous

MCM-41

H-Beta-25

Wet impregnation

Ion exchange

Theoretical loading

Calculated loading

Physicochemical



DECLARATION

I declare that *“SYNTHESIS AND CHARACTERIZATION OF MICRO- AND MESOPOROUS MATERIALS FOR LOW TEMPERATURE SELECTIVE CATALYTIC REDUCTION OF NITROGEN OXIDES”* is my own work, that it has not been submitted for any degree or examination in any other university, and that all the sources I have used or quoted have been indicated and acknowledged by complete references

Jean B. KASONGO WA KASONGO

May 2011

Signed.....



ABSTRACT

Electricity generated from coal combustion has its own advantages and draw backs; one of its draw backs is the pollution of the surrounding atmosphere. Finding economical ways to reduce the exhaust formed during coal combustion will be a plus for the environment since the gases will be reduced from the source. The cost of flue gas treatment needs to be reduced. One way of treating gases coming from power plants is the use of selective catalytic reduction at low temperatures. The technology itself has been on the market for three decades but ways to improve it are still under investigation.

In the present work, two substrates of choice were used to provide answers to a challenging environmental problem of the 21st century. The two substrates as chosen were subjected to two methods of incorporating active sites upon which the reduction process will take place. The two substrates, mesoporous silica (MCM-41) and microporous Beta (H-Beta-25) were used to prepare a series of catalysts. The metal oxides chosen as active species were Fe and Mn and loading of metal was investigated using two preparation methods of choice, namely ion exchange or wet impregnation. The MCM-41 was loaded with the bimetallic system (Fe and Mn) while the H-Beta-25 zeolite was only loaded with a single metal (Fe).

In order to investigate the final products (catalysts), different techniques were used and meaningful results were obtained to support the key questions and the hypothesis of the present work. Techniques such as SEM coupled with mapping of elements as well as EDS were used; quantitative results with AAS and ICP were also used in order to investigate the metal content of the catalyst; XRD, BET, TGA FTIR and TPR were also among the techniques used to characterize the final products.

The results (SEM, mapping and EDS) showed the porous nature of the silica host and resolved some sub-micron bimetallic structures formed on the support, but due to the limitations of the equipment no scientific conclusion were able to be drawn. EDS analysis proved that the atomic ratio of the two metals on the support was not of one to one when

ABSTRACT

wet impregnation was used as the metal loading technique; the atomic ratio of one to one could not also be achieved with the ion exchange method. An interesting finding from the elemental mapping was that well dispersed catalysts were achieved in the two cases, wet impregnation and ion exchange. However, manganese was found to be absent on the support when ion exchange was used as the metal loading method. This was also confirmed by ICP results where the highest concentration of Mn was found to be in the washing solution and no loading of Mn could be achieved on the mesoporous substrate, although Fe was successfully loaded according to the specified mass percentage, confirming the competition of the two metals to attach onto the support when the ion exchange process was used.

The BET surface area and pore size distribution results showed that the Fe/Mn-MCM-41 had a large pore size around 2.8 nm depending on the metal loading achieved while the pore size of the Fe-beta was found to have a bi-model distribution (meso and micro). The surface area of the Fe/Mn-MCM-41 synthesized by both wet impregnation and ion exchange was found to be large enough (above 600 m²/g for the wet impregnated catalysts and above 850 m²/g for the ion exchanged catalysts) even after the metal loading process whereas the Fe-beta-25 surface area was around 450 m²/g after loading of metal onto the support.

The XRD of the Fe/Mn-MCM-41 did not resolve metal crystallinity supporting the FTIR and TGA but confirmed the mesoporosity of the substrate when the low angle XRD was conducted. In the case of the Fe-Beta-25 catalyst new metal phases were confirmed and their qualitative presence was shown by EDS.

The TPR conducted on the Fe/Mn-MCM-41 was a powerful tool used in this study. For the wet impregnated as well as ion exchange samples, the hydrogen consumption in both cases increased in direct proportion to an increase in the amount of the metal salt loaded. The presence of two peaks (310 °C and 400 °C) in the case of the wet impregnated samples confirmed the loading of two different metals on the support whereas only one peak at 400 °C (for Fe) was observed when ion exchange was used as the preparation

ABSTRACT

method for the synthesis of the ion exchanged catalysts. During the temperature programmed reduction process of the ion exchanged samples only one peak (420 °C) was observed on the catalyst, this conclusion supports the elemental mapping results where Mn was absent on the ion exchanged catalyst.

In summary, it has been shown during this study that bimetallic Fe and Mn containing catalysts can be prepared by wet impregnation and not by ion exchange because of the competition between two different metals at different oxidation number. Only a single metallic phase catalyst could be prepared successfully by using ion exchange.



CONFERENCE CONTRIBUTION

Poster title: “Characterization of iron/manganese oxides loaded onto ordered mesoporous silica materials for use as nitrogen oxides (NO_x) reduction catalysts” presented at the annual research open for post graduate students at The University of The Western Cape (2009).

Poster title: “Characterization of iron/manganese oxides loaded onto ordered mesoporous silica materials for use as nitrogen oxides (NO_x) reduction catalysts” presented at the Catsa conference held at Goudini SPA, Rawsonville (2009).



ACKNOWLEDGEMENT

The writing of this thesis has been a wonderfully transformative yet sometimes difficult experience for me personally. It has been an undertaking that I could not have completed without the help and support of a number of important and in some instances “pivotal people” at the university.

I would like through these few lines, to acknowledge the hand of God that has been there always for the renewal and strength and hope for the future.

Special thank goes to the promoter of the present work, Associate Professor Dr. Leslie Petrik for the financial support and the wonderful opportunity of being part on the Environmental and Nano Sciences Research Group, where I have grown up, not only as a student but also as a human being.

I would like also to express my gratitude to my family for their moral and encouragement during tough times, my sister Mujinga Pascaline and my brother Dieudonne Kazadi. To my lovely wife and companion Binene Kayiba Kasongo for being there all along during the good and bad times.

To those who have been in the field of environmental catalysis before us, Patrick Ndungu, Dr Gillian Balfour, thank you for your support and mentorship. To my colleagues and friends from the ENS group who have always being there since the beginning and the end of this project.

This work could not been accomplished without the technical aspect being put aside, I would like here to say thank you to Joe Macke from UCT, Dr. Remy from Ithemba Lab, Adrian Joseph from the Physics department UWC for their multiple interactions and the knowledge that I have acquired through them.

LIST OF ABBREVIATIONS

AAS	Atomic Adsorption Spectroscopy
AH	Air Heater
At%	Atomic Percentage
BET	Brunauer – Emmett -Teller
Cu-OFF	Copper Offretite
DHT	Direct Hydrothermal Synthesis
EDS	Energy Dispersive Spectroscopy
FGD	Flue gas desulphurization
FTIR	Fourier Transformed Infrared Spectroscopy
FWRHM	Full Width at Half Maximum
GGH	Gas – Gas – Heater
GHSV	Gas Hourly Space Velocity
H-ESP	High - Electrostatic Precipitator
ICP	Inductive Coupled Plasma
IES	Ion – Exchange in solution
MCM	Mobil Composition of Matter
NMR	Nuclear Magnetic Resonance
SCR	Selective Catalytic Reduction
SEM	Scanning Electron Microscopy
SSIE	Solid – State - Ion - Exchange
TIE	Template Ion Exchange
TGA	Thermo Gravimetric Analysis
TPD	Temperature Programmed Desorption
TPR	Temperature Programmed Reduction
XRD	X-ray Diffraction
UV	Ultra-Violet
Wt %	Weight Percentage
ESR	Electron-Spin Resonance

TABLE OF CONTENTS

KEYWORDS.....	ii
ABSTRACT.....	iii
DECLARATION.....	iv
PUBLICATION.....	v
ACKNOWLEDGEMENTS.....	vi
TABLE OF CONTENTS.....	vii
LIST OF FIGURES.....	viii
LIST OF TABLES.....	ix
LIST OF ABBREVIATION.....	x
1 INTRODUCTION.....	1
1.1 NO _x abatement techniques to control pollution	1
1.2 Overview of the selective catalytic reduction process.....	4
1.3 Problem statement.....	4
1.4 Research questions.....	5
1.5 Hypothesis.....	6
1.6 Aims and objectives of the study	6
1.7 Research approach	7
1.8 Scope and delimitation of the thesis	9
1.9 Thesis structure	9
2 LITERATURE REVIEW	12
2.1 Mechanism and kinetics of the SCR process applied to coal fired power stations..	12
2.2 Place of the SCR in the flow sheet.....	12
2.2.1 Mechanism and kinetics.....	15
2.3 Impact of parameters triggering the SCR reactions.....	19
2.4 Requirement for low temperature SCR system	20

TABLE OF CONTENTS

2.5	Overview of the different NO _x abatement techniques	21
2.5.1	Selective catalytic reduction using ammonia as reducing agent.....	23
2.5.1.1	Low temperature catalysts	26
2.5.1.2	High temperature catalysts	38
2.5.1.3	Partial summary	44
2.5.2	Selective catalytic reduction using hydrocarbons as reducing agent (High temperature)	45
2.6	Loading techniques of catalysts and characterization methodology.....	49
2.6.1	Introduction.....	49
2.6.2	Deposition techniques on substrates	49
2.6.2.1	Impregnation techniques in general.....	49
2.6.2.2	Ion exchange technique in general	51
2.6.3	Methods for introducing catalytic active species into mesoporous silica support.....	52
2.6.3.1	Direct hydrothermal synthetic method	52
2.6.3.2	Impregnation method.....	52
2.6.3.3	Grafting method.....	53
2.6.3.4	Chemical vapour deposition (vapour grafting) method.....	53
2.6.3.5	Template – ion exchange method.....	53
2.6.4	Methods for introducing catalytic active species into zeolites	54
2.6.4.1	Introduction	54
2.6.4.2	Ion exchange with zeolites	54
2.6.4.3	Impregnation of zeolites	55
2.6.5	Characterization techniques	55
2.6.5.1	Introduction	55
2.6.5.2	Morphology study by scanning electron microscopy.....	56
2.6.5.3	Elemental composition study by energy dispersive spectroscopy.....	56
2.6.5.4	Composition study inductive coupled plasma mass spectroscopy	57
2.6.5.5	Composition study by atomic absorption spectroscopy	58

TABLE OF CONTENTS

2.6.5.6	Surface structure and topology study by high resolution transmission microscopy.....	60
2.6.5.7	Crystalline phases study by diffraction pattern study by selected-area diffraction.....	60
2.6.5.8	Crystalline phases study by X-ray diffraction spectroscopy	61
2.6.5.8.1	Principle	61
2.6.5.9	Surface area and pore size distribution study by N ₂ -BET	63
2.6.5.10	Chemical bonding study by Fourier transformed infrared spectroscopy.. ..	66
2.6.5.11	Structural stability study by thermo-gravimetric analysis.....	67
2.6.5.12	Reducibility study by temperature programmed reduction	67
2.7	General summary	69
3	EXPERIMENTAL APPROACH	71
3.1	Introduction.....	71
3.2	Carrier description	72
3.2.1	Introduction.....	72
3.2.2	Mesoporous silica (SiO ₂ /Al ₂ O ₃)	72
3.2.2.1	Description.....	72
3.2.2.2	Properties.....	72
3.2.3	H-Beta-25 zeolite (SiO ₂ /Al ₂ O ₃ : 11)	72
3.2.3.1	Description.....	72
3.2.3.2	Properties	73
3.3	Synthesis of SCR metal loaded catalysts	73
3.3.1	Introduction.....	73
3.3.2	Catalysts prepared by wet impregnation using MCM - 41 as support.....	73
3.3.2.1	Methodology.....	73
3.3.2.2	Equipment.....	74
3.3.2.3	Chemicals	74
3.3.2.4	Calculated metal loading results.....	75

TABLE OF CONTENTS

3.3.3	Catalysts prepared by ion exchange using MCM - 41 as support.....	77
3.3.3.1	Methodology.....	77
3.3.3.2	Calculated metal loading results.....	77
3.3.4	Catalysts synthesized by wet and ion exchange using H-Beta-25 as support.....	79
3.3.4.1	Ion exchange.....	79
3.3.4.2	Wet impregnation	79
3.4	Characterization and set up conditions details.....	80
3.4.1	Scanning electron microscopy and electron dispersive spectroscopy (Elemental mapping).....	80
3.4.1.1	Sample preparation.....	80
3.4.1.2	Set up conditions	80
3.4.2	High resolution transmission electron microscopy.....	81
3.4.2.1	Sample preparation.....	81
3.4.2.2	Instrumental set up conditions.....	81
3.4.3	Selected area electron diffraction.....	82
3.4.4	X-ray diffraction spectroscopy	82
3.4.4.1	Sample preparation.....	82
3.4.4.2	Set up conditions	83
3.4.5	N ₂ -B.E.T (BRUNAUER- EMMET-TELLER).....	84
3.4.5.1	Sample preparation.....	84
3.4.5.2	Set up conditions	84
3.4.6	Fourier transformed infrared spectroscopy.....	84
3.4.6.1	Sample preparation.....	84
3.4.6.2	Set up conditions	85
3.4.7	Thermo-gravimetric analysis	85
3.4.7.1	Sample preparation and experimental conditions.....	85
3.4.7.2	Set up conditions	86
3.4.8	Temperature programmed reduction.....	86
3.4.8.1	Sample preparation and experimental conditions.....	86

TABLE OF CONTENTS

3.4.8.2	Set up conditions	87
3.5	Experimental set-up for SCR.....	87
3.5.1	Schematic of the rig design.....	87
3.6	Nitrogen oxide screening tests.....	89
4	RESULTS AND DISCUSSION	90
4.1	Characterization of catalysts.....	90
4.1.1	Introduction.....	90
4.1.2	Morphological study by scanning electron microscopy and electron dispersive spectroscopy (Elemental mapping).....	91
4.1.3	Elemental composition study by electron dispersive spectroscopy on wet impregnated samples.....	96
4.1.4	Elemental composition study by electron dispersive spectroscopy on ion exchange samples.....	98
4.2	Catalyst preparation and mass balance of the synthesis procedure	99
4.2.1	Metal content determination of catalysts prepared by wet impregnation. 99	
4.2.1.1	Elemental composition study by inductive coupled plasma of wet impregnated samples (Fe – Mn/MCM - 41)	100
4.2.1.2	Elemental composition study by atomic adsorption spectroscopy after digestion of wet impregnated samples.....	101
4.2.2	Metal content determination of ion exchange catalysts.....	103
4.2.2.1	Elemental composition study by inductive coupled plasma of ion exchanged samples (Fe – Mn/MCM - 41)	103
4.2.2.2	Elemental composition study by atomic adsorption spectroscopy after digestion of wet impregnated samples.....	103
4.2.2.3	Elemental composition study by Inductive Coupled Plasma of the filtrate after washing the ion exchanged samples.....	105
4.2.2.4	Mass balance of ion exchanged catalysts	106
4.2.3	Surface structure and topology study by High resolution transmission microscopy	108

TABLE OF CONTENTS

4.2.4	Crystalline phases study by selected area electron diffraction	110
4.2.5	Crystalline phases study by X-ray diffraction spectroscopy.....	112
4.2.6	Surface area and pore size distribution study by N ₂ -B.E.T	119
4.2.7	Chemical bonding study of the catalysts by Fourier transformed infrared spectroscopy.....	126
4.2.8	Structural study of the catalysts by thermo-gravimetric analysis	133
4.2.9	Reducibility study of the catalysts by temperature programmed reduction... ..	135
4.3	Characterization of catalysts prepared using H – Beta - 25 zeolites as support.....	143
4.3.1	Introduction.....	143
4.3.2	Surface structure and topology study by High resolution transmission microscopy	144
4.3.3	Crystalline phases study by X-ray diffraction spectroscopy.....	145
4.3.4	Surface area and pore size distribution study by N ₂ -B.E.T	148
4.3.5	Chemical bonding study of the catalysts by Fourier transformed infrared spectroscopy.....	154
5	CONCLUSIONS AND RECOMMENDATIONS.....	156
5.1	Conclusions.....	156
5.2	Recommendations for future work	159
6	REFERENCES.....	160
7	APPENDICES	169
7.1	Loading calculations	169
7.2	ANNEX I: Overview of techniques and analysis mode used for NO _x analysis.....	177
7.3	ANNEX II: Instrumentation list of the rig.....	182

LIST OF FIGURES

Figure 1-1: Overview of different NO _x abatement techniques	2
Figure 2-1: SCR Design options for fossil fuel coal fired power plants to install emission control systems.....	13
Figure 2-2: Low-dust catalysts design based on selected parameters and positioned options for the SCR converter	14
Figure 2-3: Single steps of SCR catalysis.....	16
Figure 2-4: Proposed catalytic SCR cycles of Bronsted acid sites and redox sites for vanadia supported on titania.	17
Figure 2-5: Dependence of the reciprocal temperature on the effective reaction velocity	19
Figure 2-6: Review of different supports used for SCR with ammonia as reducing agent	26
Figure 2-7: Schematic diagram of flame atomic adsorption spectroscopy	59
Figure 2-8: Types of diffraction patterns which arise from different specimen microstructures (a) A single perfect crystal. (b) A small number of grains. (c) A large number of randomly oriented grains.....	61
Figure 2-9: Schematic diagram of Michelson interferometer	67
Figure 3-1: Schematic of the experimental approach	71
Figure 3-2: Calculated loadings of metal during wet impregnation	76
Figure 3-3: Calculated loading of metal after ion exchange.....	78
Figure 4-1: SEM images of the support (a) and three other catalysts (wet 20, 30 and 30 %) synthesized by wet impregnation.....	91
Figure 4-2: SEM spot image of the 30 wet % loaded MCM-41 by wet impregnation. ...	92
Figure 4-3: Elemental composition of four different elements on the MCM - 41.....	93
Figure 4-4: SEM image of Ion 30 catalyst synthesized by ion exchange.....	94
Figure 4-5: EDS as well elemental mapping of three (Si, O ₂ , Fe) different elements of the Ion 30 catalyst.....	95
Figure 4-6: Summary of the loading procedure of wet impregnation samples.....	102
Figure 4-7: Overview of the Fe and Mn loading obtained on MCM - 41 samples using the ion exchange procedure.	107

LIST OF FIGURES

Figure 4-8: HRTEM images of the carrier (MCM – 41) at 10 nm (a) and 20 nm (b) magnification.	108
Figure 4-9: HRTEM images of a Wet 30 catalyst at two different magnifications.	109
Figure 4-10: Selected area electron diffraction of the carrier (MCM – 41).....	111
Figure 4-11: SAED images of the Wet 30 catalyst on two different spots.....	112
Figure 4-12: Low 2 θ angle XRD of the carrier (MCM – 41).	113
Figure 4-13: Wide 2 θ angle XRD of carrier (MCM – 41).....	114
Figure 4-14: Low angle XRD of catalysts synthesized by wet impregnation and calcined at 400 °C.	115
Figure 4-15: Low angle XRD of catalysts synthesized by ion exchange and calcined at 400 °C.	116
Figure 4-16: Wide angle XRD of catalysts synthesized by ions exchange and calcined at 400 °C.	117
Figure 4-17: Wide angle XRD of catalysts synthesized by wet impregnation and calcined at 400 °C.	118
Figure 4-18: Surface area after loading of MCM-41 support by wet impregnation.	120
Figure 4-19: Surface areas after loading of MCM-41 support by ion exchange.	121
Figure 4-20: Pore size distribution of calcined carrier and wet 30 catalyst (BJH adsorption curves).....	122
Figure 4-21: Nitrogen adsorption/desorption isotherms at 77 K of different catalysts synthesized by wet impregnation in comparison with the of the carrier’s isotherm.	123
Figure 4-22: Pore size distribution of the ion 30 catalyst in comparison with the calcined carrier (BJH adsorption curves).....	124
Figure 4-23: Nitrogen adsorption/desorption isotherm at 77 K of different catalysts synthesized by ion exchange in comparison with the carrier’s isotherm.....	125
Figure 4-24: FT-IR spectra of the carrier (MCM-41) in comparison with six catalysts synthesized by wet impregnation.....	127
Figure 4-25: FT-IR spectra of the carrier (MCM-41) in comparison with six catalysts synthesized by wet impregnation in the scan range from 500 to 1000 cm ⁻¹	128

LIST OF FIGURES

Figure 4-26: FT-IR spectra of the carrier (MCM-41) in comparison with six catalysts synthesized by wet impregnation in the scan range of 1000 to 1800 cm^{-1}	129
Figure 4-27: FT-IR spectra of the carrier (MCM-41) in comparison with six catalysts synthesized by ion exchange in the scan range of 1000 to 1900 cm^{-1}	130
Figure 4-28: FT-IR spectra of the carrier (MCM-41) in comparison with six catalysts synthesized by ion exchange in the scan range of 1100 to 1900 cm^{-1}	131
Figure 4-29: FT-IR spectra of the carrier (MCM-41) in comparison with six catalysts synthesized by ion exchange in the scan range of 1100 to 1900 cm^{-1}	132
Figure 4-30: TGA graph of a carrier (MCM-41)	133
Figure 4-31: TGA graphs of two different catalysts (wet 20 and wet 30) in comparison with the TGA graph of the carrier	134
Figure 4-32: H_2 - TRP profiles of wet impregnated samples of Fe and Mn at different loadings	137
Figure 4-33: TRP profiles of ion exchanged samples of Fe/Mn in comparison with an ion exchanged sample of Mn.	139
Figure 4-34: HRTEM of the Fe-Beta-25 catalyst loaded by ion exchange	144
Figure 4-35: XRD profile of a pure H-Beta zeolite	145
Figure 4-36: XRD profile of a pure H-Beta zeolite in comparison with two Fe-Beta catalysts synthesized by wet impregnation	146
Figure 4-37: XRD profile of a pure H-Beta zeolite in comparison with four Fe-Beta catalysts synthesized by ion exchange	147
Figure 4-38: Nitrogen adsorption/desorption isotherm at 77 K of the calcined support (H-Beta) in comparison with two catalysts synthesized by wet impregnation (5 %-Fe-Beta-25 and 10 % Fe-Beta-25)	150
Figure 4-39: Pore size distribution of support (H-beta-25) in comparison with the pore size distribution of two catalysts (5 %Fe-Beta-25 and 10 %Fe-Beta-25)	152
Figure 4-40: Hysteresis of the support (H-Beta-25) in comparison with the hysteresis of three catalysts synthesized by wet impregnation	153
Figure 4-41: Pore size distribution of support (H-beta-25) in comparison with the pore size distribution of three catalysts (0.1Fe-Beta-25, 0.05Fe-Beta-25, 0.01-Fe-Beta-25)	154

LIST OF FIGURES

Figure 4-42: FT-IR spectra of the support (H-Beta-25) and two catalysts taken in the range of 500 to 2100 cm^{-1}	155
Figure 4-43: FT-IR spectra of the support (H-Beta-25) and two catalysts taken in the range of 500 to 2100 cm^{-1}	156



LIST OF TABLES

Table 1.1: Overview of main and undesired side reactions	3
Table 2.1: Properties of the examined supports.....	27
Table 2.2: Characteristics of the activated carbon fibers.....	29
Table 2.3: Textural and mechanical properties of the monolithic catalysts	33
Table 2.4: Composition of the monolithic catalysts	33
Table 2.5: Preparation and chemical analyses of the Cu-OFF solids	40
Table 2.6: Preparation conditions and characterization of catalysts impregnated with FeCl ₂	43
Table 2.7: Different suggestions in term of gas analysis and carrier.....	68
Table 3.1: Nomenclature and short description of the catalysts using MCM-41 as support.	75
Table 3.2: Calculated metal loading used for wet impregnation	76
Table 3.3: Calculated metal loading used for ion exchange	78
Table 3.4: Nomenclature and short description of different catalysts using H-Beta as support.....	80
Table 3.5: Instrument details for SEM and EDS	81
Table 3.6: Instrument details of HR-TEM.....	81
Table 3.7: XRD instrumental set up conditions (low angle)	83
Table 3.8: Instrument details for TGA.....	86
Table 3.9: Instrumental set up conditions for TPR.....	87
Table 3.10: Typical flue gas composition analysis on a vol/vol dry basis for ESKOM power stations	89
Table 3.11: DeNO _x feed gas composition for screening tests.....	89
Table 4-1: Electron Dispersive Spectroscopy results of wet impregnated samples	97
Table 4.2: Electron dispersive results of the ion exchanged samples.....	98
Table 4.3: Inductive coupled plasma results of the wet impregnated samples.....	100
Table 4.4: Atomic adsorption spectroscopy results of the wet impregnated samples	101
Table 4.5: Inductive coupled plasma of ion exchanged catalysts.....	103
Table 4.6: Atomic Adsorption Spectroscopy of ion exchanged catalysts	104
Table 4.7: Filtrate concentration results after washing of the catalysts.....	105

LIST OF TABLES

Table 4.8: Mass balance results of catalysts after ions exchange	106
Table 4.9: Nitrogen BET surface areas and pore size of catalysts synthesized from MCM – 41 as support	119
Table 4.10: Nitrogen BET areas and mesopore diameter of catalysts synthesized from H-Beta-25 zeolites.....	149



CHAPTER 1

1 INTRODUCTION

In this chapter, concerns with regard to the pollution aspect of nitrogen oxide are underlined and ways of dealing with denitrification using the selective catalytic reduction for abatement purposes are also underlined. Further down, the key questions, the aims and objectives of the research are outlined, followed by the hypothesis and the research approach.

1.1 NO_x abatement techniques to control pollution

A major environmental issue in the generation of electric power for fossil driven power plants beside SO₂ is the emission of nitrogen oxides, collectively referred to as NO_x. Nitrogen oxides (NO, NO₂ and N₂O) remain the major source for air pollution, its removal from outgases is one of the most challenging problems of the 21st century (Grzybek et al., 2007). Nitrogen oxides contribute to photochemical smog, acid rain, ozone depletion and greenhouse effects (Gongshin et al., 2004). It is assumed by the authors (Gongshin et al.), that more than 95 % NO_x derives from transportation (49 %) and power plants (46 %). The use of catalytic systems for pollution abatement has grown in the last decades from virtually non-existing to a multi-billion-dollar word-wide business due to the adoption of strict environmental regulations for both mobile and stationary sources (Forzatti et al., 2000). In recent years, many methods have been tested and applied to reduce the emission of nitrogen oxides in the atmosphere (Gongshin et al., 2004). However, none of these findings offer a complete commercial solution all around irrespective of important notes in detail (Hums, 1998).

In term of NO_x abatement techniques, Figure 1-1 gives an overview of the different techniques, which are mainly divided into primary (where the abatement takes place during the combustion process) and secondary measures (where the reduction takes place

after the combustion process), where wet processes should be distinguished from dry processes. Selective catalytic reduction falls under the dry processes category.

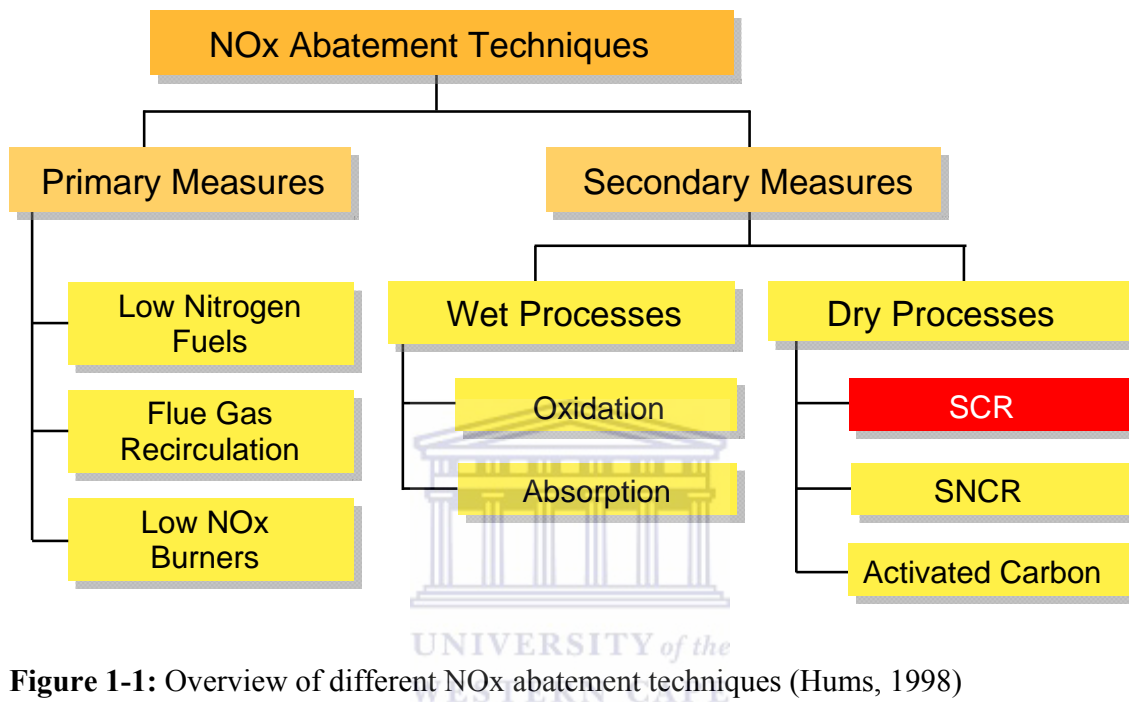


Figure 1-1: Overview of different NO_x abatement techniques (Hums, 1998)

Among the methods mentioned in the literature for nitrogen removal in stationary sources so far, selective catalytic reduction (SCR) has emerged as a major technology for nitrogen oxides reduction in the presence of ammonia as a reducing agent (Gongshin et al., 2004; Huang et al., 2008; Krishna et al., 2004). Catalytic technologies are attractive because of low cost and high efficiency (Gongshin et al., 2004). However, the degree of removal is still far from being ideal, and new catalytic materials are required to improve the following properties: high activity at either low (< 250 °C) or high (> 450 °C) temperature ranges, to broaden the temperature window, high resistance to water and sulfur dioxides (SO₂) and last, but not least, the possibility of using reductants other than ammonia-derivates, preferably hydrocarbons such as methane, propane and propylene (Grzybek et al., 2007).

The chemistry of the SCR process using ammonia as reducing agent is summarized by the following reactions shown in Table 1.1.

Table 1.1: Overview of main and undesired side reactions (Thomas et al., 2005)

$4 \text{ NO} + 4 \text{ NH}_3 + \text{O}_2 \rightarrow 4 \text{ N}_2 + 6 \text{ H}_2\text{O}$ (Main reactions)	(1)
$2 \text{ NO}_2 + 4 \text{ NH}_3 + \text{O}_2 \rightarrow 3 \text{ N}_2 + 6 \text{ H}_2\text{O}$	(2)
Undesired side reactions	
$\text{SO}_2 + \frac{1}{2} \text{ O}_2 \rightarrow \text{SO}_3$	(3)
$2 \text{ NH}_3 + \text{SO}_3 + \text{H}_2\text{O} \rightarrow (\text{NH}_4)_2\text{SO}_4$ (Ammonium sulfate)	(4)
$\text{NH}_3 + \text{SO}_3 + \text{H}_2\text{O} \rightarrow \text{NH}_4\text{HSO}_4$ (Ammonium bisulfate)	(5)

In the SCR process as applied to stationary coal-fired power plant operation, NO_x is converted to nitrogen and water by reaction with ammonia in the presence of the catalyst. The process is termed “selective reduction” because the process ideally is not suppressed by side reactions. But in practice it can be of significant importance to avoid side reactions which are resulting in undesirable by-products, primarily ammonium sulfate, $(\text{NH}_4)_2\text{SO}_4$, and ammonium bisulfate, NH_4HSO_4 if SO_2 is present in the flue gas. These by-products can cause fouling and corrosion of downstream equipment, most notably the combustion air pre-heater. Sulfur present in the coal is oxidized to SO_2 in the boiler. In turn, a small fraction of the SO_2 is oxidized to sulfur trioxide (SO_3) over the SCR catalyst, an undesirable side reaction. Major operating variables include inlet NO_x concentration, NH_3/NO_x ratio, inlet dust loading, reactor temperature, and system pressure drop.

Selective catalytic reduction (SCR) process of NO_x with ammonia has been commercialized decades ago for applications in the temperature range 300 – 420 °C using $\text{V}_2\text{O}_5/\text{TiO}_2$ as catalyst, mostly with WO_3 as a promoting agent. The above mentioned catalyst performs in a narrow range of temperatures (Richter et al., 2002) but does not

perform effectively at low temperatures, i.e. $< 200\text{ }^{\circ}\text{C}$. Although the SCR technology based on $\text{V}_2\text{O}_5/\text{TiO}_2$ catalysts has been commercialized, problems still remain, e.g., high activity for oxidation of SO_2 to SO_3 , formation of N_2O at high temperatures and the discussion about the toxicity of $\text{V}_2\text{O}_5/\text{TiO}_2$. Hence, there are continuing efforts to develop new catalysts. Currently, there are two different approaches to the study of the ammonia SCR reaction; one is focused on the high temperature range and the second one is focused on the low temperature range (Thomas et al., 2005). These low temperature catalysts will for economic reasons be able to work downstream of the back filter equipment and the desulfuration device of flue gases without the need for re-heating the gas, which will have an impact on the overall cost of the power stations (Valdés-Solís et al., 2001).

1.2 Overview of the selective catalytic reduction process

Selective catalytic reduction of NO_x using ammonia as the reducing agent was developed in the United States by Engelhard Corporation and patented in 1957. The original catalysts, consisting of platinum group metals, were unsatisfactory because of the need to operate in a temperature range in which explosive ammonium nitrate formed ($\sim 350\text{ }^{\circ}\text{C}$). Other base metal catalysts were found to have low activity. Research conducted in Japan in the 1960s in response to severe environmental regulations in that country, led to the development of vanadium/titanium catalysts, which performed successfully. Ongoing catalysts development has been instrumental in promoting continued growth in SCR applications worldwide (Thomas et al., 2005).

1.3 Problem statement

There is a great need to develop new materials that will perform SCR at low temperatures for applications such as: fossil driven power plants, cogeneration systems, shaft furnace and waste incinerator more cost effectively. Therefore, there is a need to reduce NO_x from flue gas, where the temperature falls below $200\text{ }^{\circ}\text{C}$ (Yoshikawa et al., 1998).

Many catalysts have been developed and tested for low temperatures, and up to date, catalysts such metal oxides supported on zeolites, metal oxides supported on active carbon fibers, metals supported on mesoporous silica and other compounds have shown good results for the SCR of NO_x at low temperatures (Gongshin et al., 2002; Marbán et al., 2001; Huang et al., 2008). The only aspect when working at low temperatures that one should expect is a degree of ammonia slip during the process. Other constraints that should be taken into account are the sub-reactions where products such as ammonium bisulphate can be expected, because the remaining sulfur dioxides react with ammonia. (Thomas et al., 2005).

1.4 Research questions

In light of the low temperature SCR, the present work would like to provide answers to the following questions developed below:

1. Is it possible to incorporate two different metals oxides within the structure of the MCM-41 as a substrate?
2. Can both ion exchange as well as wet impregnation of iron and manganese oxides together lead to the same results after their incorporation on the substrate in terms of active sites dispersion?
3. What is the optimum loading capacity that the substrate can incorporate within its structure compared to the theoretical loading predictions?
4. What is the direct impact of the synthesis methods followed during catalyst preparation upon the obtained metal ratio, surface area of the catalyst and oxidation state of the supported metal oxides on the substrate?
5. What are the correct analytical methods to use for identification of active sites on the mesoporous and H-Beta-25 substrate?
6. Can a microporous substrate such as H-Beta be a suitable support for a DeNO_x catalyst support?

7. What is the best way for the preparation of such a catalyst? Is it wet impregnation or ion exchange the right procedure to follow?
8. Can the metal content on both substrates lead to same metal content, same type of dispersion when wet impregnation and ion exchange are used as preparation methods?

1.5 Hypothesis

In order to answer these questions, a number of hypotheses based on the literature review were developed and investigated in this thesis. These include:

1. Mesoporous silica with its high surface area and large pore diameter can easily be used as a support for two metal oxides.
2. Metal loading will be similar when metals are simultaneously loaded by either of two different preparation procedures.
3. The ratio between the two loaded metals (iron and manganese) used during the synthesis approach has an impact on the activity of the synthesized catalysts.
4. The preparation route by either iron exchange or wet impregnation will result in a favorable catalyst for NO_x reduction based upon obtained characteristics.

1.6 Aims and objectives of the study

After giving a brief overview and a short background of the SCR, the purpose for which the technique was invented and the questions of the study, the present paragraph intends to highlight the aims behind the present research and mention some objectives that we intend to achieve at the end of the present work.

Eskom is the main power producer in South Africa and most of its electricity is generated by fossil driven power plants. A drawback of the process is the release of harmful gas such as carbon dioxide, nitrogen oxide, nitrogen dioxide and sulfur oxide and particulates including fly ash as by product of the combustion of coal. Currently studies are conducted in order to valorize the fly ash into products that will commercially be used for

environmental purposes. An example is the transformation of fly ash into zeolites which can be used for water treatment or as a possible support for low temperature DeNOx catalysts. The present work falls in the second category where the zeolite from fly ash is intended to be used as a support for low temperature DeNOx catalysts. Preparation of zeolites from fly ash zeolites is still under investigation. For the process to be viable at low temperature, the catalysts synthesized from fly ash will be compared to two other low temperature DeNOx catalysts, one published in the academic sector (Huang et al., 2008) and a second one used at the industrial scale as highlighted in the research approach further down.

1.7 Research approach

The research objectives of the present work will be achieved by carrying out several experiments, which involve the synthesis of catalysts using two porous commercial support materials (mesoporous silica material from Sigma Aldright and an H – Beta – 25 zeolite from SÜD Chemie. The reason for using mesoporous material and zeolite beta as supports is the fact that the family of M41S material is often referred to as “mesoporous zeolites”. Zeolites in general have a pore diameter below one nanometer ($< 1 \text{ nm}$), on the other hand, mesoporous materials have pore diameters in the range of two to five nanometers ($2 \text{ nm} < d < 5 \text{ nm}$). Indeed materials such as MCM-41 resemble zeolites with respect to their regular system of pores with uniform pore width. However, one difference, namely, the noncrystallinity of the silica or silica-alumina pore walls in MCM – 41 (Weitkamp, 2000).

The process of loading the two supports with metals will either be done by wet impregnation and ion exchange processes. The two methods as identified are very simple and are expected to give active and selective catalytic DeNOx results when it comes to the amount of metal needed for the synthesis. It is reported to be quite easy to load a certain percentage with either ion exchange and wet impregnation methods and expect to achieve that concentration; the only difference between the two methods is expected to be the dispersion of metal on the support, and it is expected that between the two methods

ion exchange will give better results than wet impregnation because during wet impregnation an agglomeration of metal on the surface of the support may result.

The first set of catalysts is a combination of iron and manganese oxides supported upon mesoporous silica materials synthesized by either ion exchange or wet impregnation, studies done by other authors (Pantazis et al., 2006) have demonstrated that metallic species such as copper, cerium, iron and manganese can successfully be incorporated in the structure of mesoporous silica support without alteration of the silica framework due to the fact that their respective diameters are below the diameter of the silica support; the second set of catalysts, is a single metal (Fe), either impregnated or ion exchanged onto zeolite H – beta and calcined in a nitrogen atmosphere. It has been demonstrated by companies such as Udhe and SÜD Chemie that zeolite beta with iron immobilized on its matrix can be used as NO_x catalyst. Both companies have developed two different materials, EnviNO_x and EnvCAT respectively and the developed materials have successfully been used for nitrogen oxides abatement in acid nitric plants (Meinhard et al., 2005).

The synthesized catalysts will be characterized by a number of physico-chemical analyses. Characterization by BET on both impregnated and ion exchanged materials will be done before and after the loading test. The aim of doing BET is to determine the surface area of both materials as well as the pore diameter and pore volume; these two parameters will show how the loading of metals may affect the porosity of the support. A second characterization of the catalysts will be the X-ray diffraction both by low angle XRD and wide angle X-ray to see if the supports maintain their integrity during processing, and also see if there is any particular catalytic mineral phase that has been formed on the surface of the support after metal loading and calcination. ICP MS and AAS will be done to establish the amount of catalytic metals deposited on the mesoporous or microporous silica supports after digestion of the catalysts in aqua regia solution; EDS will be performed to determine the qualitative amount of metals deposited on the support. TEM and HRTEM are used to determine the morphology of the

specimens; TPR as well as TGA will also be part of the characterization of the catalysts to determine thermal stability and regenerability (Baiker et al., 1987). This first phase of the research objectives, which mainly consist of synthesis and physicochemical characterization of the prepared catalysts will be achieved after a complete characterization of the catalysts synthesized using the two supports mentioned above, using two different metal loading procedures and investigating the percentage metal loaded.

After the first phase, the second phase of the study consisting mainly of screening tests in a stainless steel reactor using an test mixture of the following gases: NH₃, NO, O₂, CO₂, H₂O vapour and He as the carrier gas will be conducted according to an experimental set-up that will be presented further on in this study.

1.8 Scope and delimitation of the thesis

The present study intends to address the problem of SCR at low temperatures, by conducting a comparative study between prepared and commercially available catalysts chosen from catalysts among existing materials on the market as well as in the open literature.

This work will only address the problematic of the loading bimetallic oxides on the support such as MCM-41 with limitation to few available characterization techniques, the work will also look at the H-Beta-25 zeolite as commercial substrate.

1.9 Thesis structure

Apart from the introduction which constitutes the first chapter, the following overview presents the structure of the present thesis and some attached annexes which will constitute a final point of the study.

The second chapter of the present work will cover the literature review of the thesis which will start by giving examples of catalysts that have been studied for NO_x reduction

in the presence of ammonia as a reducing agent on one hand, and on the other hand, hydrocarbons as reducing agents. Papers have been studied and their findings and results are presented here. The next few paragraphs that constitute the literature review will cover points such as the introduction to the SCR process, an overview of the mechanism and kinetics of the SCR process, the impact of parameters triggering the SCR process, and some requirements for low temperature SCR applications. The chapter will also highlight the current state of the art of low temperature SCR.

The third chapter describes the loading techniques of catalysts and characterization methodology and deposition techniques of catalytic ions on support substrates are discussed in general. Different loading techniques used for catalyst loading and theories covering each as well as background to characterization techniques are also presented in this chapter.

The fourth chapter, namely experimental approach, gives step by step detail of how the catalysts have been synthesized from a theoretical point of view and the detail of experiment itself. Each technique is described at this stage in full detail with regard to the methodology applied as well as the experimental details. The SCR reaction experimental approach is also described in full detail at this stage, details about the reactor set up are presented, and the gas mixtures for the laboratory scale activity tests are also presented.

The fifth chapter presents the results and discussion of each physicochemical preparation step and results of characterization of materials prepared from the synthesis, including XRD, BET, SEM, AAS, ICP, TPR etc, with a short discussion of each analysis and the results obtained. Screening tests for catalytic are then presented.

The final chapter will summarize the work and draw conclusions and offer recommendations for future work.

Appendices include different calculations used in order to achieve the loading ratio of one to one on the support, an attached list which covers different instruments used in

terms of NO_x analysis by different authors at lab-scale, which is presented at the end of the thesis to showing the readers the advantages and disadvantages of one technique of analysis over another.



CHAPTER 2

2 LITERATURE REVIEW

The reviewed literature will differentiate between catalytic materials that have been used for SCR, the techniques used for the physico-chemical characterization of the catalysts and the reducing agents used for the SCR. The reviewed literature will also cover the operating conditions and techniques for measuring the efficiency of NO_x removal with an emphasis on lower temperature SCR operating conditions. The reducing agents used for DeNO_x will be reviewed as well, including ammonia, ammonia derivatives or hydrocarbons, CO and hydrogen. Before discussing the NO_x abatement techniques, it is important at this stage to look at the mechanism and kinetics of the SCR applied to coal fired power station and its place in the flow sheet.

2.1 Mechanism and kinetics of the SCR process applied to coal fired power stations

In this part of the literature review, the SCR mechanism is reviewed with an emphasis on the coal fired application; first the place of the SCR in the flow sheet of a normal power plant is reviewed by distinguishing a low dust environment from a high dust environment, secondly, the kinetics study has also been reviewed here, with the impact of parameters affecting the SCR mechanism and the requirements in terms of the SCR.

2.2 Place of the SCR in the flow sheet

For coal, gas and oil fired power plants the position of the SCR reactor strongly influences the decision as to what catalyst composition and physical support structure should be used (Hums, 2008). For a high amount of ash and high-sulfur containing exhausts typical of coal fired power stations there are three possible SCR arrangements for the catalytic converter, namely the high dust, low dust, and tail end configuration (Figure 2-1).

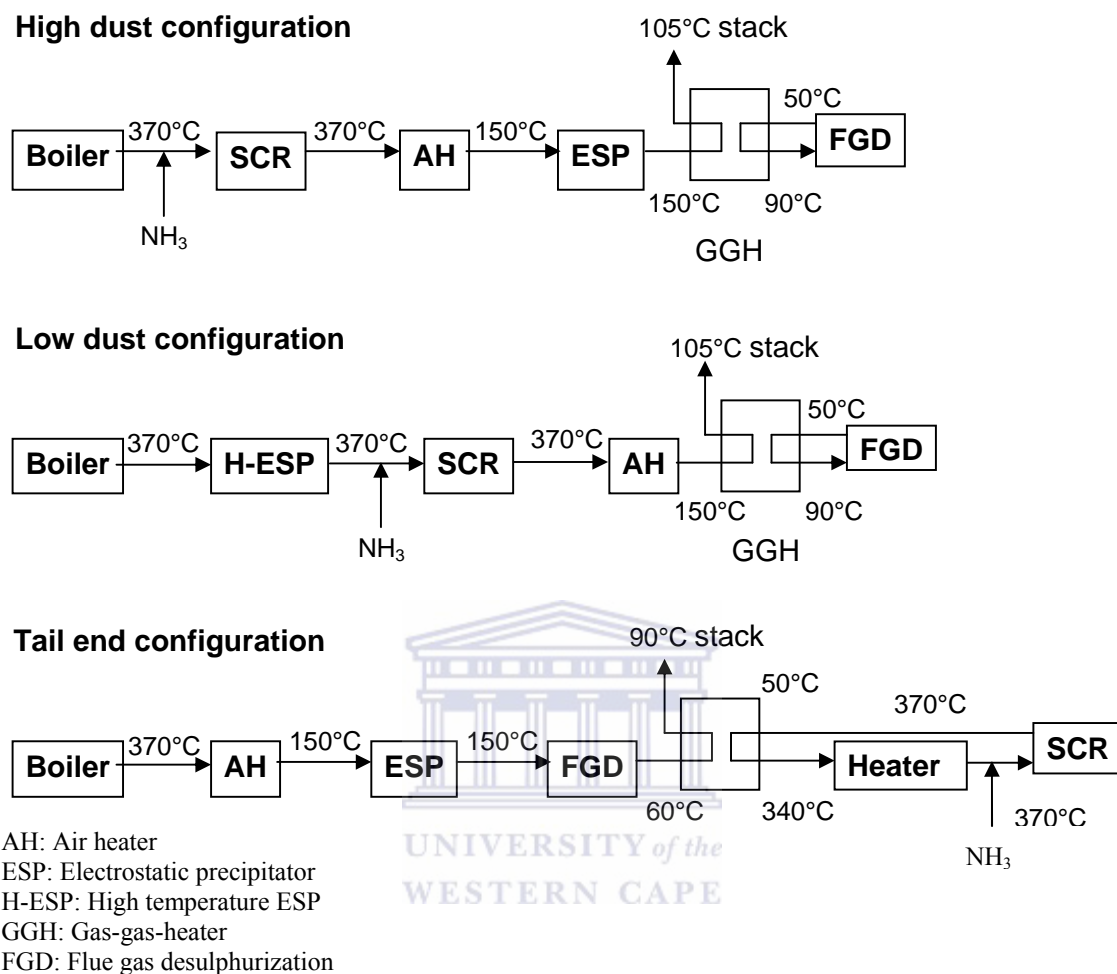


Figure 2-1: SCR Design options for fossil fuel coal fired power plants to install emission control systems.

The flue gas conditions in high dust and tail end positions have variable impact on the volume of the catalyst. The catalysts that are used can have different chemical compositions as well as geometrical design. The types of catalysts that are currently in operation on coal fired power station exhaust gases and their working temperatures are:

- Titanium oxide based (270-450 °C)
- Zeolite based (300-550 °C)
- Iron oxides based (380-430 °C)
- Activated coal/coke (100-150 °C)

The volume of catalyst required depends on the characteristics of the catalysts (activity, deactivation rate etc.) and on the operating conditions such as flue gas volume, the required NO_x reduction, gas composition and velocity (sulphur dioxide concentration, amount of ingredients affecting the catalyst etc.), and flue gas temperature. The volume of catalyst should be increased if the flow distribution is not uniform, including adjustment of the reducing agent concentration. The primary advantages of the low-dust configuration are the spatial and operational separation of the boiler and the flue gas, which is relatively free of ash and catalyst poisons downstream of the flue-gas plant. For this reason, it is generally possible to do without flow straighteners and soot blowers in this type of configuration, and a catalyst with higher specific surface area can be used.

Despite the cost savings from reducing the contained catalyst volume, the primary disadvantage of the low dust configuration lies in the high investment costs for the additional regenerative preheater and the continuing operational costs for the use of expensive fuels such as gas or oil. From this point of view it is tempting to use a catalytic system which can be operated after the bag filter (BF) as shown in Figure 2-2.

ESP → SCR

(~ 350 °C)

BF → SCR

~ 200°C

Minimum SCR temperature

Maximum SO₂ content

Figure 2-2: Low-dust catalysts design based on selected parameters and positioned options for the SCR converter (Hums, 2008)

When the position of the SCR converter is located after the bag filter (BF) the catalyst volume necessary to meet 80 % NO_x reduction at the lower temperature is about 1.7 times higher compared to that of a catalytic converter placed at 350 °C. Nevertheless running a catalytic converter located after the BF is obviously at lower cost but it is still a

technical challenge for developing a highly active catalyst to compensate for the disadvantage of high catalyst volume. The thesis therefore is focussed upon developing a highly active low temperature catalyst at lab-scale and studying its potential for NH₃-SCR to develop this option.

2.2.1 Mechanism and kinetics

The catalyst in its simplest term is used to increase the rate (molecules converted over unit time) of the chemical reaction while the material itself is theoretically not undergoing any permanent change. While the real chemical reaction rate (micro kinetics) is dependent upon the concentration of the reactants, temperature and quality of the catalyst, the macro kinetics has to consider additionally issues such as mass and heat transfer phenomena in the reactor system. The adsorption of the reductant onto the catalyst provides a shortcut in which the reactants are converted to products more rapidly than if no catalytic material were present. For the DeNO_x process, ammonia and NO_x were studied for the necessary adsorption steps, it was found that ammonia adsorption is dominating over a weak NO adsorption on the catalytic sites (Hums, 2008). Figure 2-3 gives an overview of the SCR catalysis mechanism.

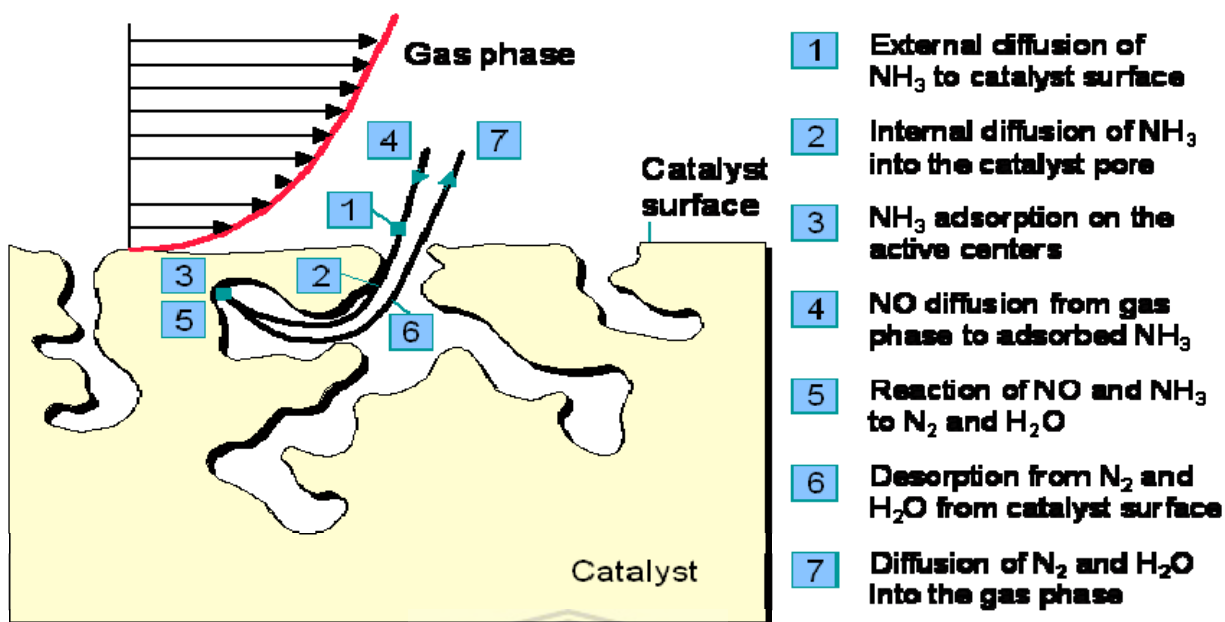


Figure 2-3: Single steps of SCR catalysis (Hums, 2008)

The desirable ability to enhance the reaction rates and direct reactants to specific products such as water and nitrogen is challenging with regard to finding the most suitable catalytic material and the necessary parameters required in optimizing the technical process. To maximize reaction rates, it is essential to ensure accessibility of all reactants to the active catalytic sites dispersed within the internal pore network of the carrier. Step 1 and 7 (Figure 2-3) represent bulk mass transfer, which is a function of the specific molecules, the dynamics of the flow conditions and the geometric external surface area of the catalytic support material. Pore diffusion, illustrated in step 2 and 6 (Figure 2-3) depends primarily on the size and shape of both the pore and the diffusing reactants and products respectively. Step 3, 4 and 5 (Figure 2-3) are related to the chemical interactions of reactants and products at the catalytic active sites. Any of the seven steps can be rate-limiting and may control the overall rate reaction. In the chemical kinetic control region, the reaction of adsorbed NH_3 with NO_x is slow relative to diffusion and thus is rate limiting. As the temperature is further increased to the higher activation energy, the chemical steps with exponential dependence increase the fastest, and control of the overall rate will shift to pore diffusion. Here the rate of conversion of NH_3 and NO_x is

faster than the rate at which they can be supplied and a decreasing concentration gradient exists within the particle (Hums, 2008). This is referred to as intraparticle diffusion in which the dispersed catalytic sites deep within the carrier are not being completely utilized. At higher temperatures the rate of diffusion of NH_3 and NO_x from the bulk gas to the catalytic sites in the pores is slow relative to the other processes and the rate becomes controlled by bulk mass transfer. In this regime NH_3 and NO_x are converted to water and nitrogen as soon as they arrive at the external surface of the catalytic material resulting in a lower conversion rate. For low temperature NH_3 -SCR catalysis this step has to be considered when running the reaction. The NH_3 -SCR is thus based on a redox reaction system corresponding to both the reactants/products and catalytic sites (Hums, 2008).

The interplay of Brønsted acid sites and redox sites for vanadia supported on titania was proposed by (Dumesic et al., 1996) is shown in Fig. 2-4 and gives an example of the adsorption character of the catalytic sites responsible for NH_3 .

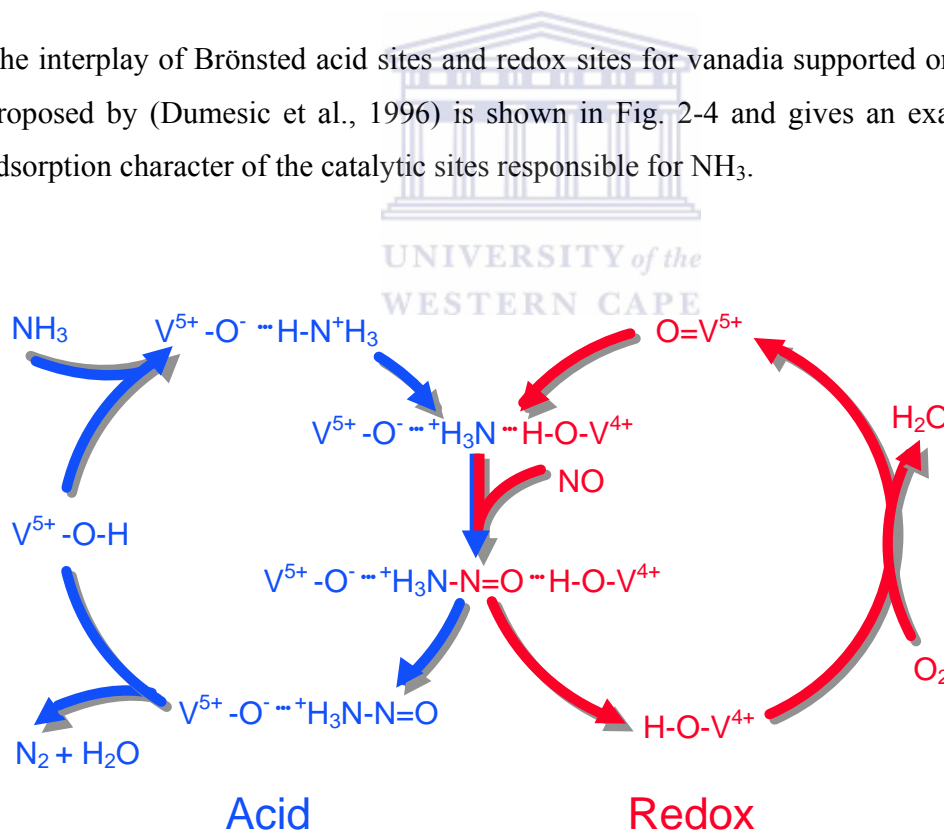


Figure 2-4: Proposed catalytic SCR cycles of Brønsted acid sites and redox sites for vanadia supported on titania. (Dumesic et al., 1975)

Many catalytic processes in the industry, where selectivity is important, operate under conditions that give maximum yield of the desired products and may be specifically designed to operate under chemical or pore diffusion control. Knowledge of all the rate-controlling steps throughout the entire process is essential in designing the catalyst and the reactor not only when scale-up parameters are required. In the laboratory, when screening a large number of catalyst candidates, it is important to measure activity at low conversion levels to ensure that the catalyst is evaluated in the intrinsic or chemical rate-controlling regime (Dumesic et al., 1975). The optimized intrinsic activity of the catalyst is essential even when operated for the industrial application under mass transfer control. Mass transfer control occurs only when the intrinsic activity is higher than transport effects. At low conversion levels, heating effects due to exothermic or endothermic reactions are small and temperatures within the reactor bed are essentially equal to that of the bulk gas entering the reactor.

By taking the Arrhenius equation (1) the linear expression results in a series of straight lines whose slopes are directly related to the activation energy of the rate controlling steps. The Arrhenius equation connects rate constant k to the pre-exponential factor k_0 , which is a mechanistic term, but also proportional to the number of catalytic active sites, E is the activation energy representing the slowest of all steps involved in converting reactants into the products, R is the universal gas constant and T the absolute temperature.

$$\ln k = \ln k_0 - \frac{E}{R} \frac{1}{T} \quad (1)$$

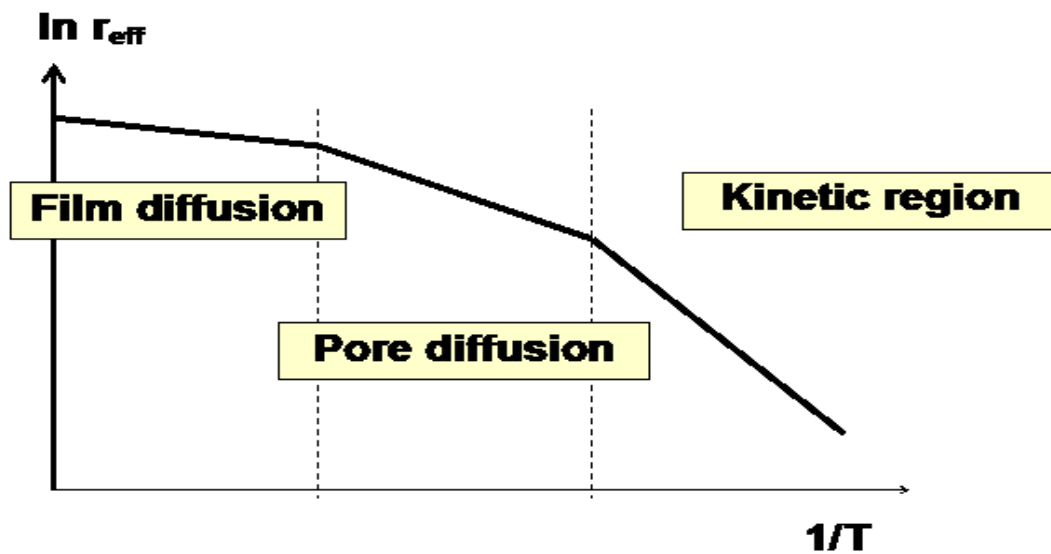


Figure 2-5: Dependence of the reciprocal temperature on the effective reaction velocity (Thomas et al., 1997)

The largest slope (Figure 2-5) is related to chemical, the intermediate slope to pore diffusion and the smallest slope to bulk mass transfer. When the reaction is controlled by one of the chemical steps, bulk transfer and pore diffusion of the reactants to the active sites including the reverse process is fast. With pore diffusion control, the concentration of reactants decreases from the outer periphery of catalyst surface towards the porous system. Finally, with mass transfer limitations, the concentration of reactants approaches zero at the outside surface of the catalysts including the reverse processes (Thomas et al., 1997).

2.3 Impact of parameters triggering the SCR reactions

Whereas studies done by academia are often confined to more or less ideal conditions, industrial applications have to withstand the rigour of a complex SCR reaction regime which is triggered by multiple parameters. This section will give an overview of the relevant parameters which have been considered when reviewing both the literature critically and will be applied during the evaluation of the test results.

When the catalyst is exposed to a test gas containing NH_3 but no NO_x , adsorption of ammonia will take place at all acidic sites. If the measured concentration of NH_3 before and after the reactor bed filled with catalysts is at the same level, the surface is saturated. Parameters which are necessary to be considered in the SCR reaction include the following (Larry et al., 1999):

- ❖ Concentration of ammonia and NO_x
- ❖ Storage of ammonia, conversion rate depending on the stoichiometry
- ❖ Oxygen and water concentration
- ❖ SO_2 concentration
- ❖ Gas velocity and mass transfer
- ❖ Temperature
- ❖ Deactivation phenomena

2.4 Requirement for low temperature SCR system

Surface area, pore size distribution, pore structure and pore volume of the carrier are among the most fundamentally important properties in catalysis because the active sites are dispersed throughout the internal surface through which reactants and products are transported depending on the space velocity of the gas flow in the reactor. The size and number of pores which determine the internal surface area are very essential especially for low temperature SCR systems and have to be adjusted if possible. In the case of adjustment, it is usually advantageous to have a high surface area (large number of small pores) to maximize the dispersion of catalytic components. However, if on the other hand the pore size is too small, diffusional resistance becomes a problem. From this view for example geometrically regular mesoporous silica such as MCM-41 with pore diameters ranging from 1.5 to 5 nm come up to the required expectations (Hartmann et al., 1999). In order to achieve a better DeNO_x process in the presence of ammonia, the following requirements must be taken into account.

- ❖ High activity for SCR catalyst operation
- ❖ High selectivity for desired reaction
- ❖ Low SO₂/SO₃ oxidation rate
- ❖ Chemical resistance to operation conditions
- ❖ Thermal resistance to operation conditions
- ❖ Tolerable deactivation behavior of the catalytic active sites
- ❖ Low pressure drop agreeing to the operation condition of the plant
- ❖ High reactive surface
- ❖ No disposal problems of spent catalysts
- ❖ Low cost

2.5 Overview of the different NO_x abatement techniques

In the context of the scope and delimitation of the thesis, the present literature review covers some of the most recent works published on numerous catalysts for NO_x abatement at low temperature in the presence of either ammonia or hydrocarbons as reducing agents. The present survey will be divided into two main sub groups; the first part deals with the reduction of NO_x in the presence of ammonia as reductant, and the second part deals with the reduction of NO_x in the presence of hydrocarbon as reductant; each part will be sub-divided in groups in terms of the catalyst nature, whether it is a metal, metal oxide, or zeolite supported metals and noble metals.

Among the methods that have been investigated to clean exhaust gas streams for NO_x removal (Figure 1-1), some methods were previously investigated and due to their inefficiency and economic cost, they have been abandoned or have not received much attention, among these techniques can be mentioned:

- ❖ Injection of methanol into flue gases to convert NO to NO₂ via radicals formed (potential by-products are CO and CH₂O), which is removed in a 'liquid-modified' wet limestone SO₂ scrubber. Various configurations of the latter step

include using a spray dryer with aqueous slurried lime with NaOH as an additive, where the NO_x removal rate is 35–50 % (Lyon et al., 1990).

- ❖ Enhanced NO_x removal in wet scrubbers using Fe²⁺ chelates has been demonstrated at the Miami Fort Pilot Plant (Ohio), achieving 75 % NO_x removal (≈50 % in the first stage burner and an additional 50 % in the chelate stage) (Ramachandran et al., 2000)
- ❖ Use of adsorbents, e.g. utilizing γ-alumina impregnated with sodium carbonate in a fluidized bed, where it was found that SO₂ must be present for efficient NO_x removal; when SO₂/NO_x > 4 in the flue gas, the NO_x removal efficiency attained was 70–75 % (Ramachandran et al., 2000).
- ❖ Selective non-catalytic reduction (SNCR), using aqueous urea or ammonia injection into the furnace at ≈ 875–1150 °C, can be used to reduce NO_x level by 30–75 %. However, >90 % NO_x reduction was reported for the NO_x OUT[®] process under particular conditions, e.g. at 980 °C at refineries and petrochemical plants (Ramachandran et al., 2000).
- ❖ Concentration of NO followed by SNCR, such as adsorption of NO on supported MgO that is subsequently heated in a regeneration cycle in a reducing atmosphere to reduce NO to N₂, which has attained ≈30 % NO_x removal under steady-state operation (Ramachandran et al., 2000).
- ❖ Selective catalytic reduction (SCR) of NO using ammonia (or other compounds such as hydrocarbons) as the reductant to form nitrogen and water. The principal types of catalysts that have been investigated for SCR are: (a) metal oxides based catalysts, e.g. those containing vanadia etc., (b) metal ion exchanged zeolites, e.g. Cu-ZSM-5, and (c) supported noble metal catalysts, e.g. Pd/Al₂O₃ (Ramachandran et al., 2000).

The first five processes as described are still expensive in terms of high running costs and poor efficiency; contrary to the last process, namely SCR, which presents advantages such as low cost and high efficiency (Gongshin et al., 2004). Process number six, SCR, will be the focus of this dissertation.

The selective catalytic reduction (SCR) of NO/NO₂ (NO_x) by NH₃ as reductant has been defined as the state-of-the-art technology for the abatement of nitrogen oxides from exhaust gases of stationary plants (Richter et al., 2002). This process has received much attention over the last past two decades and that can be seen by the number of papers and patents published by both industrials and academics (Pârvulescu et al., 1998). SCR based on V₂O₅/TiO₂ removes at maximum 60 – 85 % of NO_x using between 0.6 and 0.9 mol NO and leaves 1- 5 ppm of NH₃ unreacted. The addition of large amounts of ammonia increases the NO_x removal efficiency but the slip of unreacted ammonia is not desirable. The major components required for SCR technology include a suitable reactor system, an NH₃ injector system, and NH₃ storage. The main problems encountered at an early stage in the development of SCR technology were: The poisoning of catalysts by SO_x present in the flue gas, the plugging of catalyst by dust using high dust arrangement, the deposition of ammonium hydrogen sulfate on the catalysts below 300 °C, the deposition of ammonium hydrogen sulfate in the air pre-heater below 250 °C using a high-dust arrangements, the enhancement by the catalysts of SO₃ formation from SO₂, the erosion of the catalysts by fly ash particulates in the gas stream.

2.5.1 Selective catalytic reduction using ammonia as reducing agent

The reduction of NO_x in the presence of ammonia is a common method that has seen immense applications at the industrial scale. Despite the fact that the application has been commercialized, everyone agrees on the fact that when used as a reductant, ammonia presents some disadvantages. These include, firstly: Large quantities of ammonia must be stored either as liquid ammonia or ammonium hydroxide, raising the risk of release of a toxic compound (Amiridis et al., 1996). Secondly: the introduction of ammonia to the SCR process must be carefully controlled to avoid ammonia slippage into the effluent

gases leaving the converter (Amiridis et al., 1996). Thirdly: Ammonia in the reactor effluent can react with water and sulfur trioxide to produce ammonium sulfate which can deposit onto the surfaces of the heat exchanger thereby causing a reduction in heat transfer efficiency (Amiridis et al., 1996).

It is important at this stage to underline a complete literature review done by Parvulescu on NO_x reduction in the presence of ammonia as a reductant, the work was published in 1998, but 10 years later, the review is still a powerful tool in order to get an insightful view of the DeNO_x process where ammonia is used as a reductant. Among the catalysts studied so far, a long list of base oxide catalysts were studied by Bosch and Janssen, as quoted by Parvulescu; vanadia (V₂O₅) supported titania (TiO₂) is described as the catalyst that performs well for NO_x reduction and thus was recommended for technical applications because of its good stability over time. Metal zeolites have also been another group of catalysts investigated so far, Seiyama et al. quoted by Parvulescu, first investigated the SCR of NO with ammonia over a large number of M-Y zeolites. In mono-exchanged catalysts, the activity order of these different materials studied follows this trend: Co (II)-Y > Cu (II)-Y > Pt (II)-Y > Pd (II)-Y > Fe (III)-Y > Ni (II) > Co (III)-Y.

The best solution for the removal of NO has still not been found, as Parvulescu et al. (1998) pointed out. Although SCR using ammonia as reductant is an effective process and already industrialized, this process involves the use of an expensive and furthermore polluting product as reductant. In time, these catalysts are also deactivated by sulphur or heavy metal compounds. For the reduction of NO both with CO or H₂, the best catalysts are those containing Rh. However, these catalysts are also sensitive to different poisons. On the other hand, Rh is the most expensive noble metal, an identification of some substitutes for it could offer very promising catalysts. For the reduction of NO with hydrocarbons as well as for NO decomposition, the best catalysts are metal zeolites, namely Cu, Co, Ce or even Pt. However, these catalysts exhibit catalytic activity only in a very limited range of temperature, and in addition are extremely sensitive to water and

different poisons, sulphur again being the principal one. The active components are now more or less known. Substitution of some of these, like rhodium for platinum, with non-expensive bi or multi component systems could be a possible solution. However, the most important work should be directed in designing a new support. This new material should present a high stability against water or sulphur compounds, should exhibit oxygen storage properties and should achieve an extremely high dispersion of the active components, similar to those determined in the metal zeolite (Pârvulescu et al., 1998).

Activated carbon has been investigated as a potential catalyst for the DeNO_x process in the presence of ammonia, and one important advantage mentioned is that, activated carbons are very cheap. It has been reported by Moulijn et al. (Singoredjo et al., 1990) quoted once again by Parvulescu that, activated carbon exhibits good performance which was dependent on a number of factors such as: the preparation procedure of the catalyst, a porous texture and surface chemistry.

Other investigated catalysts in the presence of ammonia are catalysts such as: M_xMo₆S_{8-y} and M_xMoS_{8-y}O_z, where M = Ni, Fe, Mn, Cu, Zr, Cr; and Al₂O₃-supported coordinative complexes of the type: M'' (M''(CN)₆Fe), M = Mn, Fe, Ce, Ni, Cu or M-sulphophthalocynines, M = Cu, Ni, Co (Pârvulescu et al., 1998). Honeycomb catalysts have also been reported to be effective in the reduction of NO_x in the presence of ammonia (Pârvulescu et al., 1998).

Ten years after Parvulescu published his review on catalytic removal of NO, Hevia (2008). On the other hand showed that many studies have been done on DeNO_x processes in order to find new materials that can be able to reduce NO_x at low temperatures, and recent published papers have shown good results in terms of new materials developed by both academic, and industry (Hevia et al., 2008) Some of these studies will be reviewed here.

For the rest of this literature review, attention will be given to substrates given in Figure 2-6. The mentioned Figure (2-6) shows different supports that will be reviewed here one by one.

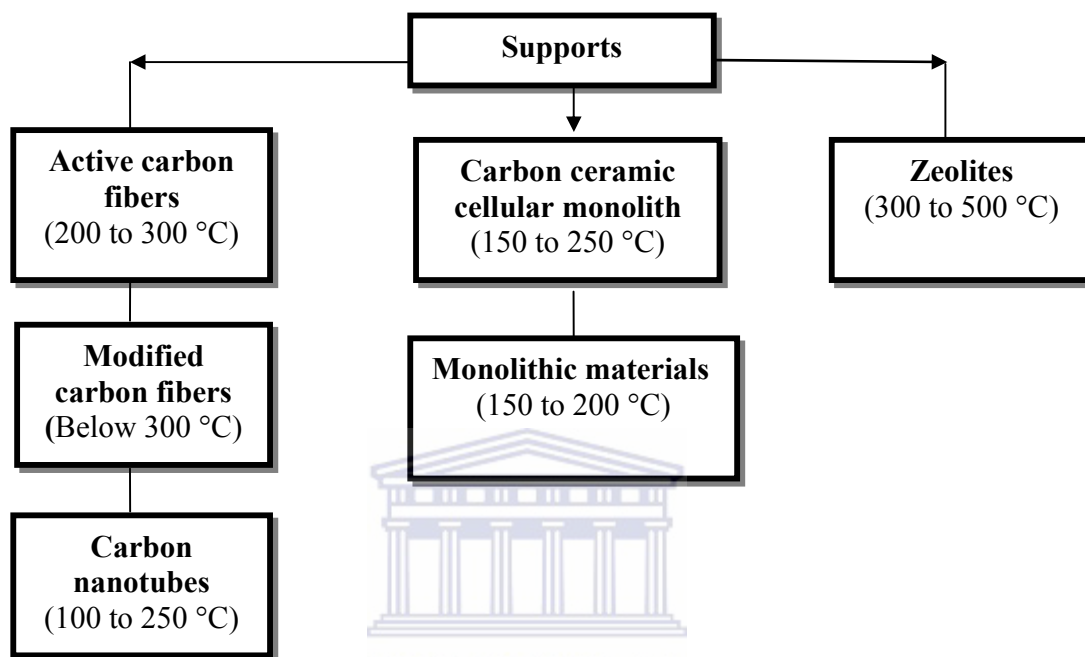


Figure 2-6: Review of different supports used for SCR with ammonia as reducing agent.

2.5.1.1 Low temperature catalysts

An interesting paper published by Masaaki Yoshikawa et al. in 1998 (Yoshikawa, M. 1998), reports the results of a study done on three metal oxides supported on active carbon fibers; it was discovered that between Fe_2O_3 , Co_2O_3 and Mn_2O_3 ; Mn_2O_3 gave good results in the reduction process in the presence of ammonia at temperatures around 50 °C and 150 °C. The experiment was conducted in a fixed bed flow reactor, flowing 400 ml/min of 200 ppm NO, 200 ppm NH_3 , 10.5 % O_2 , and 8 % H_2O in N_2 over 2 g of catalyst to adjust W/F where W is the weight of the catalyst and F the feed weight rate of NO as 5×10^{-3} g min/ml. NO and NO_2 concentrations were analyzed continuously at the inlet and outlet of the reactor by a chemical luminescence NO_x meter.

The effect of the support was firstly studied. Activated carbon fibers (ACF) were compared to granular active carbons (GAC) and Al_2O_3 as supports. It was found that, ACF had a good surface area ($740 \text{ m}^2/\text{g}$), good pore volume (0.342 ml/g) and good physical surface area ($0.5\text{-}1$) compared to granular active carbons (GAC) and Al_2O_3 which had respectively (831 and $197 \text{ m}^2/\text{g}$) as surface area and ($0.01\text{-}0.03$ and $0.00166 \text{ m}^2/\text{g}$) as physical surface area. The Table 2.1 below shows the properties of the examined supports.

Table 2.1: Properties of the examined supports (Yoshikawa et al., 1998)

Material	BET surface area (m^2/g)	Pore volume Cm^3/g	Pore size mm
ACF	740	0.342	D1 = 20 mm L = over 50mm
GAC	831	0.414	D2 = 1mm
Al_2O_3	197	0.084	D2 = 2.3 mm

D₁: Mean diameter of active carbon fibers

D₂: Mean diameter of particles

L: Mean length of active carbon fibers

The second aspect studied was the loading capacity of the metal on the activated carbon fibers, 10 % of three different metals Co, Fe and Mn loaded on the same support (ACF) were tested under the same conditions in the presence of ammonia as the reductant. It was found that 10 % of Mn on the ACF had a good catalytic activity. A third aspect investigated was the loading capacity of the metal on other supports (TiO_2 , Al_2O_3 and granular active carbon); it was found that 15 % of Mn on the support yielded a good effect in terms of NO_x reduction. The next aspect investigated was the heat treatment of the catalyst. Two temperatures were investigated, $200 \text{ }^\circ\text{C}$ and $300 \text{ }^\circ\text{C}$, in both cases, it was found that 15 % Mn/ACF compared to 10 and 5 % Mn on ACF gave good results, and finally the 15 % Mn/ACF was compared to some standard catalysts such as V_2O_5 , 15

% Mn/GAC and 15 % Al₂O₃, the 15 % Mn/ACF once again proved to be a good catalyst compared to standard catalysts used in their study.

To sum up, it was found that low-temperature SCR could be carried out by Mn₂O₃/ACF material at 150 °C, at which temperature the conventional catalysts could not work effectively, Mn₂O₃ supported onto ACF showed a higher activity for low-temperature SCR than other transition metal oxides, such as Fe₂O₃ and Co₂O₃, and catalysts made using the ACF as support had the highest activity compared to other supports, such as GAC and Al₂O₃. The contribution of ACF is considered to allow high dispersion of Mn₂O₃ particles in its micro-pores and thus large gas contact surface areas through the analysis of surface atoms and surface areas.

A second group of catalysts that has been reported for low temperature activity (Yoshikawa et al., 1998), these are modified activated carbon fibers in the presence of ammonia as a reductant. Activated carbon fibers with small diameter guarantee fast adsorption kinetics and their fibrous shape permits their use in forms that allow easy handling (i.e. felt, fabrics and monoliths). Due to these properties, ACFs are excellent adsorbents to be used in flue gas cleaning. First to report the activity of carbon as catalysts are Bergbau-Forschung quoted by Muniz (Muñiz et al., 2000), who showed that activated carbons exhibit a high catalytic activity for NO reduction with ammonia at temperatures below 300 °C, and secondly Juntgen quoted once again by (Muñiz et al., 2000) reported data on active coke and activated carbons used as catalysts for the removal of NO_x with ammonia. These authors concluded that the observed activity was influenced by the presence of hetero-atoms and functional groups on the carbon surface.

In 2000, Muniz conducted a study on three different commercial activated carbon fibers (ACFs) coming from different sources and a sample activated in their laboratory. The results are reported here. First, the characteristics of the three samples are reported in Table 2.2

Table 2.2: Characteristics of the activated carbon fibers (Muñiz et al., 2000)

Type	Supplier	Precursor	Diameter (μm)	Surface area	Pore volume
FN-100PS15	Osaka Gas	Coal pitch	13	1500	0.8
FE-400	Toho Rayon	PAN (polyacrylonitrile)	7-15	1100	0.6
Ft300-15	Kuraray	Phenolic resin	8-10	1500	0.5
PK		Petroleum pitch	15	-	-

In order to enhance the NO_x removal capacity of the ACFs, different treatments were examined:

Heat treatment at 800 °C (HT/800) in which the original fibers were heated in N₂ at 10 °C/min from ambient temperature to 800 °C, maintained at this temperature for 1 h and cooled down in nitrogen. Then, the treated fibers were exposed to air at ambient temperature. Reaction with ammonia in which the ACFs were treated in an ammonia stream for 15 min at 800 °C. Then, the fibres were heat-treated in N₂ at the same temperature for 30 minutes and cooled down in nitrogen to ambient temperature. Ammination of ACFs (ONA) in which the fibers were oxidized with HNO₃ (40 wt. %, in reflux, 4 hours) and then treated with an ammonia stream at 250 °C for 2 hours. Finally, the fibres were heat-treated in N₂ at 800 °C as described previously. Ammoxidation of ACF (AO) in which the ACFs were treated in a mixture of air–ammonia at 450 °C for 2 hours. Finally, the ammoxidized fibers were heat-treated at 800 °C as described previously. This treatment was also performed on the carbon fiber composites. After each treatment, all samples were oxidized in a stream of 3 vol. % O₂ and He (balance) at a temperature of 400 °C for a period of 2 h (Muñiz et al., 2000).

Two aspects were studied (Muñiz et al., 2000), firstly, the effect of ACF oxidation on NO reduction and secondly, the influence of porous pre-treatments of the carbon on NO

reduction activity. It was found that, the enhancement of DeNO_x activity obtained by applying different treatments to the ACFs evidenced the role of surface chemistry in the SCR process. Thus, by means of mild air oxidation of the ACFs, an activity increase was observed as a consequence of enhanced NH₃ adsorption linked to the formation of superficial acid groups. Additionally, the chemical treatments (AM, AO, ONA) improved the fibers activity by incorporating nitrogen functionalities of basic character that can act either as adsorption sites for reactant species at low temperatures (< 200 °C) or as true catalytic active centers at higher temperatures (200 – 400 °C). The ammination treatment (ONA) was shown to be the most effective treatment to enhance the NO reduction activity of the fibers. Among the different ACFs treated so far, polyacrylonitrile PAN-based ACFs exhibit the highest NO reduction activity in the whole temperature range. The effect of water was also studied; the results suggest that the presence of H₂O inhibits NO reduction at low temperatures (< 200 °C). This effect was ascribed to a competing mechanism for adsorption sites.

An active carbon ceramic supported manganese-based monolithic catalyst has also been investigated for low temperatures selective catalytic reduction in the presence of ammonia as reductant. The study case was conducted by Tang et al., (2007), during which they studied a series of metals loaded on activated carbons (AC/C) that were compared and tested under the same conditions. The work showed that MnO_x-based monolithic catalysts were more active than other metal oxide catalysts for low-temperature SCR reactions of NO with NH₃ in the presence of excess oxygen. More than 90 % NO_x conversion was obtained over the range of 150 - 250 °C under the condition of GHSV = 10600 h⁻¹. It was also observed that during the catalyst preparation, the use of ultrasonic treatment could promote the dispersion of metal oxides on the surface of the AC, and improve a high catalytic activity at low temperature, especially at 150 °C. The investigation of O₂ effect and the oxidation of NO to NO₂ on monolithic catalysts both indicated that NO oxidation is one of the essential factors of low-temperature SCR reaction. Doping with Ce and Pd could improve the MnO_x-based catalysts which also could be improved by doping with Fe and V, and more than 50 % of the catalytic activity

could remain under conditions of 100 ppm SO₂ in the flue gas. The SO₂ deactivation of the catalyst might have two causes. On one hand, the metal oxides on the supports, acting as active sites of the monolithic catalyst, were sulfated by SO₂ and lost activity. Alternatively, the reductant (NH₃) reacted with SO₂ and produced (NH₄)₂SO₄. Along with the reaction, more and more (NH₄)₂SO₄ particles formed and deposited on the catalyst's surface, covering many active sites, which resulted in a blocking of the SCR reaction. The first effect of SO₂ is irreversible, but subsequent impacts could be eliminated by washing to remove the deposited (NH₄)₂SO₄ or heating at relative high temperature to decompose it. In another publication by Valdés-Solís (2001), the results indicated that the deactivation of SO₂ was weak with increasing temperature, and interestingly, adding SO₂ also showed the effect that the SCR reaction above 300 °C was improved.

In 2003, Valdes-Solis et al. reported a new method for preparing vanadium oxide supported on carbon ceramic cellular monoliths. The reported method included four different steps for the support synthesis: (i) impregnating the honeycomb in a polymeric solution; (ii) removing the excess solution by fast spinning; (iii) curing in air (150 °C); and (iv) carbonizing in N₂ (700 °C). Vanadia was impregnated on the support by using an aqueous solution of VO²⁺ (0.034 M) prepared from ammonium metavanadate and oxalic acid. Two impregnation procedures were tested: (i) equilibrium adsorption impregnation followed by washing and drying at 120 °C for 1 h and (ii) consecutive cycles of dip-impregnation, removal of the excess solution by fast spinning and drying at 120 °C for 1 h. The synthesized catalyst was tested in the presence of water as well as in the presence of SO₂, and temperature programmed desorption experiments (TPD) and ageing of catalyst tests were also performed to study the catalyst at the industrial scale. It was found from the results that, firstly, the method developed for the preparation of the support provided a uniform distribution of carbon over the monoliths. Secondly, the results of the two methods mentioned earlier for impregnation were as follow: a loading capacity of 2.42 wt % on carbon weight basis was obtained after 5 cycles of dip-impregnations. Increasing the number of impregnation cycles led to a decrease in the vanadium content.

The second method which consisted of an equilibrium adsorption in a diluted VO^{2+} solution followed by washing and drying led to a lower vanadium content. However, a higher catalytic activity, represented by the kinetic constants k_v and k_m was displayed by the material prepared by equilibrium adsorption. It has been suggested that, the increasing in activity must be caused by a higher dispersion degree of these catalysts. Thirdly, the effect of both SO_2 and water were studied, and it was found that SO_2 produced only a little deactivation in the V-catalysts (~20 %) when the SCR reaction was carried out at lab scale at 150 °C. Water also caused a decrease in catalytic activity (~45 % at 125 °C). The inhibitory effect of water vapour is parallel to the competitive adsorption of NO and NH_3 which suggest that NO and NH_3 react from the adsorbed state. Finally, when the catalyst was subjected to the exit gases of a coal fired power plant for ageing tests, it was discovered that the catalytic activity of the catalyst underwent considerable deactivation even after a short period of time of exposure with an approximate constant value of about 13 % of the initial conversion. In conclusion, the loss in catalytic activity was ascribed to be caused predominantly by arsenic (As) poisoning and surface sulphates.

Valdes-Solis and his co-workers conducted another study in order to improve the selective catalytic reduction in the presence of ammonia, (Valdés-Solís et al., 2001), The authors studied the reduction of nitrogen oxide over carbon-ceramic cellular monolith-supported manganese oxides; these monolith supported materials combined the properties of ceramics, such as high mechanical strength and low pressure drop, with those of carbonaceous materials (i.e. adjustable surface properties). The studied materials are also known to be more abrasion resistant than the non-coated material, with a high axial crushing strength, a lower pressure drop in the system and a high textural development. Consequently, carbon–ceramic monoliths are materials with wide possibilities of application. The catalytic activity tests were conducted under isothermal conditions at temperatures between 100 °C and 300 °C. In each test, a cellular catalyst containing ~300 mg of carbon was placed in a quartz reactor heated by a vertical Carbolite furnace. The effect of textural development on the catalytic performance was studied from carbon–ceramic monoliths with different activation degrees (burnoff). The effect of reaction

temperature on catalytic activity was also evaluated. The prepared catalyst displayed a good catalytic activity for the reduction of NO_x with NH₃ at low temperatures (Reduction of NO_x in the range of 60–70 % at around 150 °C and space velocities of ~ 4000 h⁻¹). An increasing in temperature led to an increase in catalytic conversion consequently coming with a loss of selectivity. For temperature above 200 °C an existence of diffusional limitations was confirmed. The activation of the support led at the same time to an increase in the micropore volume and manganese loading that promoted NO_x reduction. An acidic carbon surface was created by oxidation of the support which in turn enhanced the loading of Mn during the impregnation process, therefore, improving the catalytic activity of the impregnated material. Using a carbon–ceramic monoliths as a catalyst support with a burnoff degree of 40 wt.% led to the best results during the experiment, oxidized with nitric acid at 90 °C for 4 h and Na-exchanged prior to impregnation with Mn (NO_x reduction: 73 % at 150 °C and GHSV of 4000 h⁻¹).

Another interesting series of catalysts for low temperatures published by Blanco in 2000 (Blanco et al., 2000) are alumina and titania based monolithic materials, their properties and compositions are presented in Table 2.3 and Table 2.4 respectively.

Table 2.3: Textural and mechanical properties of the monolithic catalysts

Name	Area BET (m ² /g)	Pore volume (cm ³ /g)	Mean pore diameter (nm)	Axial crushing strength (kg cm ⁻²)
CuNiAl	157	0.61	10	95
VAl	135	0.56	10	95
CuNiTi	108	0.60	68	108
VTi	55	0.47	72	108

Table 2.4: Composition of the monolithic catalysts

Name	Active phase	Content (wt. %)	Support
CuNiAl	CuO/NiO	6.4/0.6	Al ₂ O ₃
VAl	V ₂ O ₅	5.5	Al ₂ O ₃
CuNiTi	CuO/NiO	1.7/0.2	TiO ₂
VTi	V ₂ O ₅	5.1	TiO ₂

The catalytic activity in terms of nitrogen oxide conversion was studied on the four catalysts as a function of three parameters: $[\text{NH}_3]/[\text{NO}_x]$ feed ratio, operating temperature and $[\text{NO}]/[\text{NO}_x]$ feed ratio. Three additional relevant aspects related to the catalysts were studied; namely the ammonia slip, the formation of undesired nitrous oxides and the ammonia oxidation by oxygen. The performance of the selected catalyst was further studied by analyzing the evolution of the reaction products as a function of feed composition and programmed temperature increase. It was found that, the vanadium-titania monolithic system showed the best performance amongst the four studied systems, at operating conditions similar to those used in industrial scale units. The catalytic activity of vanadium-titania system was higher in the presence of both NO and NO+NO₂ gas mixtures. With this catalyst, the ammonia slip was lower when NO₂ was present in the feed. On this catalyst, the presence of NO₂ as only nitrogen oxide increased the quantity of adsorbed species. These species seem to be responsible for the NO₂ formation. When NO is also present, it effectively competes with this NO₂ reaction path, and N₂O formation was not observed.

Other catalysts report so far in the open literature for NO_x reduction in the presence of ammonia at low temperature are carbon nanotube supported vanadium oxides, these materials were studied by Huang et al. (2007). Carbon nanotubes (CNTs) have attracted much attention due to their unique electric, mechanical and structural characteristics for a variety of future applications. With the tunable pore structure and surface properties and large specific surface area, carbon nanotubes have been regarded as perfect supporting materials for catalysts. The evaluation of the catalyst activity was performed in a quartz fixed-bed continuous flow reactor, operating at a pressure of 0.1 MPa. The performance of non-impregnated carbon nanotubes at low temperatures was first reported, it was observed that NO conversion over non-impregnated CNTs decreased as the temperature increased. The activities of the CNTs were quite low in the range tested, with NO conversions less than 6 %. The NO conversion mechanism over CNTs at low temperature has been proposed by Valdes-Solis et al. (2001). This involves the physical adsorption of NO on the carbon surface. Increasing temperature caused a decrease in physical

adsorption and consequently a decrease in NO removal. When V_2O_5 was added on the catalyst, the addition led to a significant increase in catalytic activity. NO conversion increased with increasing reaction temperature in the range of 70-190 °C, which corresponds to an activated process. The NO conversion reached a maximum at 190 °C, and then decreased in the temperature range greater than 190 °C. The decline of NO conversion over 190 °C might be caused by ammonia oxidation. The loading capacity of V_2O_5 was also studied, 2.35 % in terms of V_2O_5 was observed as the best capacity of loading with a conversion of NO reaching 83 % which decreased to 76 % when the loading capacity reached 2.82 %. The effect of CNTs diameter on the catalyst activity was also investigated by the same group (Huang et al., 2007), and it was found that the activity of V_2O_5 /CNT catalyst increased with increasing CNTs diameter, which resulted in NO conversion of 92 % with the outer diameter of 60-100 nm. When the results were correlated with the data of surface areas of catalysts with different CNTs diameters, this indicated that the surface area was not a crucial factor for the catalytic activity in the case of V_2O_5 /CNT, and a higher V_2O_5 coverage was favored for NO conversion at low temperatures. It could be associated with the available oxygenated surface groups for CNTs with different diameters in the process of HNO_3 pretreatment, and the dispersion of vanadium particles on the surface of CNTs.

To sum up, the prepared catalysts showed a good catalytic activity at a temperature range of 100-250 °C. The Lewis acid sites on the vanadium species were the active sites for the catalytic reduction of NO. It was proposed that the reaction path might involve the adsorbed NH_3 species reacting with NO from the gaseous phase and the adsorbed NO_2 species simultaneously. The best NO conversion of 92 % was obtained by using CNTs with 60-100 nm (outer diameter) as support, with a V_2O_5 loading of 2.35 wt % under the reaction conditions of 190 °C, 0.1 MPa and GHSV of 35000 h^{-1} .

Gongshin et al. (2003) conducted a study on low temperature SCR over an iron and manganese oxides supported on titania for tests in a fixed-bed reactor. Four different aspects were studied, firstly the effect of manganese loading of MnO_x/TiO_2 ; secondly,

the promoting effect of iron oxide; thirdly, the effect of oxygen; and lastly, the simultaneous effect of H₂O and SO₂. It was observed that the addition of manganese on TiO₂ caused enhancement of the catalytic activity. Increasing the manganese loading increased the NO conversion until the manganese loading reached 10 %. A further increase of manganese loading did not increase the activity. The effect of loading on the selectivity was quite significant. The higher the loading, the more N₂O was formed. With increasing temperature, the selectivity decreased considerably for all samples. The results obtained when studying the promoting effect of iron oxide showed that, the addition of Fe increased NO conversion significantly, although the 10 % Fe/TiO₂ catalyst had a low activity for low-temperature SCR. Among the catalysts studied, the Mn–Fe/TiO₂ with Mn/Fe = 1 was the most active catalyst; the selectivity for N₂ increased significantly upon the addition of Fe. The selectivity for N₂ on Fe–Mn/TiO₂ was nearly 100 %. When the effect of oxygen was conducted, it was discovered that 10 % Mn –10 % Fe/TiO₂ showed a low activity for the reduction of NO by NH₃ at 150 °C in the absence of oxygen. However, when small concentrations of O₂ were introduced to the reactants, NO_x conversion showed approximately no change compared to the previous activity without oxygen. The importance of O₂ was also verified by another experiment. The transient behavior of the catalyst was tested by turning the oxygen off and on in the gas phase. The NO conversion declined steadily to 10 % after O₂ was turned off. The first steady decline was relatively fast, followed by a slower decline. Switching O₂ back on resulted in an immediate increase in NO conversion, and the original conversion was restored quickly. This indicated that O₂ played a significant promoting role in the SCR reaction. The results obtained when studying the effect of H₂O and SO₂ showed that, when 100 ppm SO₂ and 2.5 % H₂O were added to the reaction gas and the reaction temperature and space velocity were kept at 150 °C and 15,000 h⁻¹, respectively, the NO conversion on Fe – Mn oxides was decreased to 85 % at 150 °C in 5 h. For 10 % MnO_x/TiO₂ catalyst, NO conversion was decreased to 48 % at 150 °C in 5 h. However, the NO conversion was only decreased to 90 % on 10 % Fe – 10 % Mn/TiO₂ catalyst and then stabilized in 5 h. The decrease in activity is consistent with the previous observation that MnO_x catalysts were deactivated by SO₂. SO₂ is oxidized to SO₃ by O₂. The SO_x compounds (SO₂ +

SO₃) are adsorbed on the transition metal oxides and they are difficult to desorb at low temperatures. The occupation of the active sites by metal sulfates and ammonium sulfates would consequently decrease the SCR activity. To sum up, it has been shown that, the TiO₂ supported manganese iron mixed oxide catalysts were highly active for the low temperature SCR of NO with NH₃ in the presence of excess oxygen. More than 99 % of NO conversion was obtained on the 10 % Mn–10 % Fe/TiO₂ at 120 °C under the condition of GHSV = 15, 000 h⁻¹. These catalysts are substantially more active than all other catalysts reported in the literature. SO₂ and H₂O had slight effects on the SCR activity.

Another interesting catalyst reviewed for NO_x reduction in the presence of ammonia as reductant is iron and manganese oxides supported on mesoporous silica studied by Huang et al. (2008). Mesoporous silica holds high specific surface area ranging 500-1400 m²/g and nanopores of several nm in diameter even after the hydrothermal treatment; they are also known to be resistant to sulfur poisoning. The stability of sulfates on the mesoporous silica is weaker than on other metal oxides.

The results of Huang et al, (2008) showed that mesoporous silica supported iron-manganese oxide catalysts (Mn-Fe/MPS) were highly active for the low-temperature SCR of NO with NH₃ in the presence of excess oxygen. The Mn-Fe/MPS with Mn/Fe = 1 prepared and calcined at 400 °C showed the highest activity and this catalyst yielded 99.1 % NO conversion at 160 °C at a space velocity of 20000 h⁻¹. H₂O had no adverse impact on the activity. When the SCR reaction proceeded in the presence of H₂O and SO₂, an excess amount of sulfate salts was formed resulting in gradual catalyst deactivation and the activity could almost recover to the initial level after heat treatment. The catalyst is substantially superior to any reported catalyst in terms of integrated performance.

Long et al. (2002) has conducted a study on a series of mixed metal oxide catalysts such as Fe – Mn, Fe – Mn – Zr and Fe – Mn – Ti for low temperature SCR, but before that step, he discovered that the three oxides could be used as sorbents for NO (Long et al., 2002). The three oxides showed very high activity for NO oxidation of NO to NO₂ at

room temperature with 63 – 76 % NO conversion at GHSV of 6000 h⁻¹. When studied as catalysts at 80 °C for SCR, the catalysts showed a conversion of 63 to 75 % at a GHSV of 6000 h⁻¹, with an increase in temperature to 120 °C, the conversion reached 100%. The catalysts were also studied in the presence of water and sulfur. When studied in the presence of water at 80 °C the effect of water was very high with a sharp decrease in activity but when the temperature was increased to 140 °C the activity of catalysts reached 100% conversion once again. The influence of sulfur dioxide was also studied and the formation of compounds such as ammonium ions and sulfates species that occupied the active sites were the main causes of the low activity of the metal oxides in the presence of sulfur dioxide.

Other metal oxides mentioned in the open literature for low-temperature SCR are catalysts such as MnO_x-CeO₂ mixed prepared by co-precipitation (Landong et al., 2004), and sulphated vanadia supported carbon coated monoliths are also an example of low-temperature SCR catalysts (García-Bordejé, 2006). Activated carbon fiber composite supported manganese oxides have also been study for SCR at low temperature (Marbán et al., 2001). Fe-Mn based catalysts and Cu/Ce mesoporous silica have been reported as low temperature catalysts by Richard et al. (2002) and Constantious et al. (2006) respectively.

2.5.1.2 High temperature catalysts

Metal supported zeolites have been in general studied for high temperature selective catalytic reduction in the presence of ammonia as a reducing agent. Below are few catalysts studied for NO_x reduction in the presence of ammonia.

In terms of metal supported zeolite in the presence of ammonia as reductant, few zeolites have been tested; reported results by Rahkamaa et al. (2005) on a series of zeolites prepared by ion-exchange showed interesting NO_x reduction. The studied catalysts include: Cu-ZSM-5, Cu-beta, Cu-MOR, Cu-FER, Cu-Y, Ag-beta, Fe-ZSM-5 and Fe-beta. The activity and hydrothermal stability of these materials have been studied in the NH₃-

SCR reaction with excess of oxygen. The results suggest that based on the hydrothermal stability, the best zeolite-based catalysts for NH₃-SCR are Fe-beta, Cu-FER, Cu-MOR, and Fe-ZSM-5. These catalysts had the highest NO_x conversions (85 %) and widest temperature windows (350 to 600 °C). Hydrothermal aging modified the acid properties of zeolites. The higher the activity retained, the better the hydrothermal stability for the SCR activity. The results of this study also reveal that the presence of NO₂ in the feed gas mixture enhanced the SCR reactions. The highest increase in the activity by NO₂ was observed on H and metal promoted zeolites at low temperatures. One important fact that should be considered when metal-based zeolites are used for NO_x reduction is the fact that, the conversion temperature is still higher than what industry would like to achieve.

Arous et al. (2007) reported the influence of the preparation method on the activity of Cu-offretite as a catalyst on the NO-SCR by ammonia. The properties and the presence of metals in the synthesized material were confirmed by XRD, Al NMR techniques, UV visible spectroscopy and the reducibility of the metal species forming the catalysts have also been confirmed by temperature programmed reduction (TPR). The catalytic activity of the Cu-offretite catalyst was performed in a micro-flow reactor in the presence of a feed mixture of NO, NH₃ (2000 ppm each) and O₂ (3 %) in He at a space velocity of 332.000 h⁻¹. Seven Cu-OFF catalysts were prepared by different methods and tested in the same condition; Table 2.5 shows the results of different synthesized materials.

Table 2.5: Preparation and chemical analyses of the Cu-OFF solids (Arous, W. 2007)

Catalysts	Preparation method	Al (wt %)	K	K/Al (mol/mol)	Cu/Al (mol/mol)
Cu(3.23)-K(8.07)OFF _{Acac}	Exchange+	6.30	8.0	0.88	0.44
	evaporation		7		
Cu(2.65)-K(2.31)OFF _{Acac}	Exchange+	6.82	2.3	0.23	0.33
	evaporation		1		
Cu(3.92)-K(2.54)OFF _{Acac}	Exchange+	6.86	2.5	0.25	0.49
	evaporation		4		
Cu(2.81)-K(2.59)OFF _{Impr}	Impregnation	5.67	2.5	0.31	0.42
			9		
Cu(2.88)-K(2.32)OFF _{Acet}	Exchange+	6.98	2.3	0.23	0.35
	evaporation		2		
Cu(2.49)-K(2.04)OFF _{SSIE}	Solid-state ion	5.45	1.9	0.24	0.41
	exchange		3		
Cu(2.89)-K(4.53)OFF _{IES}	Ion exchange	6.22	4.5	0.50	0.38
			3		

Cu-OFF: copper-exchanged offretite zeolite

Cu-KOFF: copper-exchanged K-offretite zeolite form

H-KOFF: H-form of K-offretite zeolite

The results obtained by Arous et al. (2009) after treatment of seven different catalysts tested for activity under the same conditions clearly showed that, whatever the preparation method, Cu-KOFF solid is more active than the H-KOFF zeolites. The comparison of NO conversion of all catalysts shows that Cu (2.89)–K(4.53) OFF_{IES} prepared by ion exchange from Cu(NO₃)₂ was the most active catalyst (100 %). Cu(2.88)–K(2.32) OFF_{Acetyl} prepared in acetylacetone from Cu (acac)₂, is the least active (90 %). On the other hand, Cu(2.65)–K(2.31) OFF_{Acac} and Cu(3.92)–K(2.54) OFF_{Acac} prepared by the same method exhibited nearly the same activity in nitric reduction (90

%). It seems that, an increase of the copper content did not modify the NO reduction. Moreover, the NO conversion on the Cu(2.88)–K(2.32) OFF_{Acety1} and Cu(2.81)–K(2.59) OFF_{Imp} catalysts is the approximately the same as on the two last catalysts. To sum up Arous's study, Cu-offretite catalyst prepared by Ion – Exchange in Solution (IES) in aqueous medium was the most active in the NO-SCR by NH₃. This catalyst mainly contained isolated Cu²⁺ species at charge compensation sites in the zeolite structure. The catalyst prepared by Solid – State - Ion - Exchange (SSIE) could be also considered very efficient if one takes into account the environmental advantages of this preparation method. This latter catalyst exhibited a copper species distribution close to the catalysts prepared by IES. On the other hand, in the least efficient catalyst, the very weak amount of protons and the large amount of copper oxide aggregates can be put forward to explain the weak catalytic behaviour observed. It is well known that the activity of the NO SCR by NH₃ reaction depends on both the acidic and redox properties of the catalysts, i.e. a good balance between Brønsted acidity and the facility to oxidize NO. Finally, the other catalysts prepared from Cu (acac)₂ and H-KOFF developed these two properties but, probably, with a weaker facility to oxidize NO.

Another case of low temperature zeolite based catalysts studied in the presence of ammonia has been reported by Gongshin et al. (2002). The work investigated an ultra-stable Y zeolite (USY) supported manganese synthesized by incipient wetness and promoted by different metals at different loading capacities. The promoting effects of metals studied were cerium and iron. The catalyst's activity was conducted in a fixed bed quartz reactor in the presence of a mixture of nitrogen oxide and ammonia and excess of oxygen, water and sulfur dioxide were used when needed. The catalysts as synthesized were characterized by different techniques such as BET, XRD. The BET results showed that, when the second metal was added to the Mn/USY catalyst, the surface seemed to increase; the XRD result suggested a non-crystalline phase of the three metals. In addition to the catalytic activity, the order of the reaction was also investigated by Gongshin in 2003. In conclusion, it was reported by the author that the 14 % Ce – 6 % Mn/USY nearly had a conversion of 100 % and a high selectivity toward nitrogen at high

space velocity ($30.000 \text{ cm g}^{-1} \text{ h}^{-1}$), while the MnOx/USY and Fe/USY had low conversions of nitrogen oxide. It is important for this study since combining two metals to understand the promoting effect of one toward another is one of the aims of this study.

Another interesting catalyst for SCR in the presence of ammonia as a reducing agent at high temperature this time, reported by Gongshin et al. (2005), is an ultra-active Fe/ZSM-5 catalyst synthesized according to a simple impregnation technique which is quite interesting for this project, because the same procedure might be used as a standard technique for metal incorporation on zeolites. The catalyst was synthesized according to the following procedure: FeOx/FeZSM-5 catalysts were prepared using NH₄-ZSM-5 (Si/Al = 10 from Alsi-Penta) by incipient wetness impregnation with FeCl₂ or Fe (NO₃)₃ solutions and then dried at 110 °C overnight. The samples were calcined in air at 500 °C for 6 h. This method was a one-step method. It is reported that by this method, a minimum amount of water was evaporated and no excess solution was needed. Also, no washing is required as in the aqueous ion exchange method. So this method is simpler and should be less costly than the ion-exchange method using aqueous solution.

Table 2.6 gives an overview about the catalysts synthesized under different conditions by Gongshin et al., (2003).

Table 2.6: Preparation conditions and characterization of catalysts impregnated with FeCl₂

Sample	Fe content (wt %)	Preparation conditions	Surface area (m ² /g)	Pore volume (cm ³ /g)
FeZ-1	2.5	Calcined in air at 500 °C for 6 hours	325	0.186
FeZ-2	2.5	Calcined in He at 500 °C for 6 h and then calcined in air for 6 hours	337	0.190
FeZ-3	1.0	Calcined in air at 500 °C for 6 hours	346	0.198
FeZ-4	5.0	Calcined in air at 500 °C for 6 hours	277	0.164
FeZ-5	7.5	Calcined in air at 500 °C for 6 hours	237	0.147
FeZ-6	1.6	Exchanging NH ₄ -ZSM-5 with FeCl ₂ solution for 24 h at room temperature	340	0.197
FeZ-7	1.0	Calcined in He at 500 °C for 6 h and then calcined in air for 6 hours	354	0.200
FeZ-8	5.0	Calcined in He at 500 °C for 6 h and then calcined in air for 6 hours	297	0.171
FeZ-9	7.5	Calcined in He at 500 °C for 6 h and then calcined in air for 6 hours	267	0.158

Activity tests on the catalyst were performed in a fixed bed quartz reactor in the presence of an excess of oxygen; it was found that the catalyst had superior activities for SCR of

NO with ammonia in the presence of excess oxygen. The activities of the catalysts prepared by wet impregnation with FeCl₂ (97 % maximum) were reported to be much higher than that of Fe-ZSM-5 prepared by an aqueous ion exchange method (maximum 90 %). Another process in which the Fe/ZSM-5 sample was first calcined in an inert gas (He) instead of air and then calcined in air was also investigated, and the activities of the catalysts prepared by these two processes were very similar, which indicated that even if the exchange between NH₄⁺ and Fe²⁺ took place as evidenced by the Electron-spin resonance (ESR) and XRD, it was found that the exchange was incomplete. Such incomplete exchange should lead to Brønsted type acid sites in the catalysts after the decomposition of NH₄-ZSM-5, which is considered as the active site for ammonia adsorption. Based on the reported catalytic activity and characterization results, it was concluded that the Fe²⁺, Fe³⁺ species as well as highly dispersed iron oxide species may contribute to the high activities.

2.5.1.3 Partial summary

From the above reviewed papers, the following conclusions that drive the choice of the catalyst can be made; first of all, the surface area of the support is an important aspect to look at, because a high surface area support results in good dispersion of the active metal sites. Secondly, the type of treatment that the support can go through before being used is also an important factor that needs to be considered, especially when dealing with activated carbon fibers in general or monolithic materials. In terms of experimental conditions, one needs to understand that there is no standard operating conditions that can be followed for SCR activity screening tests, all these reported catalysts have been tested in different conditions in terms of gas mixture, gas hourly space velocity, temperature and other parameters that can be varied. Thus, it is difficult to compare the results obtained in each case against one another. One thing in common with all these catalysts is the fact that they all were tested for the SCR in the lower range of temperatures and they all used ammonia as a reducing reagent. Experimental conditions and analytical method and type of equipment have been put in an attachment (see appendixes 7.4). One

interesting catalyst was considered as the most interesting among the reviewed catalysts for low temperature, because of its structure (large pores and surface area) and the temperature at which nitrogen oxide as well sulfur dioxide were reduced (180-200 °C), this catalyst is known as Fe-Mn/MCM-41 (iron-manganese supported mesoporous silica) and is easy to synthesized (Huang et al., 2008). The mentioned catalyst Fe-Mn/MCM-41 will be the focus of the following dissertation, because few people have looked at the incorporation of iron and manganese on the MCM-41 and to our knowledge, Huang and his group has been the first to report the use of this catalyst as a DeNO_x catalyst in the presence of ammonia. Being able to approve or disapprove the findings of Huang in terms of ratio obtained during the synthesis procedure is very crucial for this study; using diverse physicochemical analysis techniques to identify the nature of the active sites on the support and prove that they exist will attract industries to use the Fe-Mn/MCM-41 as a catalyst of choice for NO_x reduction. Discussion of the synthesis and characterization of the catalysts are presented further down in this thesis. H-Beta-25 incorporated with iron as a second catalyst of choice has been chosen for so many reasons; currently only two catalysts using the Beta-25 as a support have been reported to work for low temperature selective catalytic reduction (EnviNO_x and EnvCAT). It is important to us to conduct a comparative study of what is working already at the industrial scale and compare its synthesis approach with a new catalyst (Fe-Mn/MCM-41) using the same methods of preparation.

2.5.2 Selective catalytic reduction using hydrocarbons as reducing agent (High temperature)

As mentioned earlier in the introduction, the second section of this chapter will discuss the reduction of nitrogen oxides in the presence of hydrocarbons as reducing agents due to the fact that ammonia as a reducing agent presents some disadvantages such as storage, transportation and handling of unreacted ammonia, but this will not be a thorough literature review since hydrocarbons are mainly used for the three way catalysts (mobile system) in general which is not of huge interest for this study as the purpose of this study

is stationary systems for the flue gas detoxification, but a look at a few examples is necessary for a conclusive literature review.

A comprehensive review of catalysts and their behaviour in the presence of some hydrocarbons have been published by Amiridis et al. (1996) and Parvulescu et al. (1998). The first catalyst to be reviewed by Parvulescu was Cu-ZSM-5 in the presence of a series of hydrocarbons; it was observed that NO could selectively be reduced over Cu-ZSM-5 in the presence of O₂ by a variety of hydrocarbons including C₂H₆, C₃H₆ and C₃H₈. Oxygen was also found to enhance the rate of the NO-hydrocarbon reaction just as in the case of SCR using of ammonia. Another similarity with NO-ammonia reaction is that the conversion rate using hydrocarbon went through a maximum depending upon the reaction temperature. In both cases the loss of activity at high temperatures was due to the onset of the oxidation of the reducing agent (NH₃ or hydrocarbon) by O₂. The temperature at which the maximum rate of NO reduction was obtained depended on the type of the hydrocarbon for a given catalyst. Over Cu-ZSM-5, for example, maxima in activity were reported at 250, 325 and 300 °C for C₂H₄, C₃H₆ and C₄H₈ respectively. Iwamoto et al. (1991) has classified the hydrocarbon reductants over Cu-ZSM-5 as selective (i.e., C₂H₄, C₃H₆, C₃H₈, and C₄H₈) and non-selective (CH₄ and C₂H₆), although more recent reports show that such classification cannot be generalized for all catalysts. Iwamoto et al., (1991) also reported the fact that the rate of NO_x reduction increased at high hydrocarbon concentrations, and that unsaturated hydrocarbons (i.e., C₃H₆) are better reducing agents than the corresponding saturated species (i.e., C₃H₈).

A second catalyst to be reported for SCR with hydrocarbons is iron (Fe)-exchanged zeolites, Iwamoto et al. (1991) studied several Fe-exchanged zeolites, and found that, similar to the Cu zeolites, the catalytic activity of the zeolites for the reduction of NO by ethylene was dependent on the type of zeolite. The activity of the Fe-mordenite zeolite increased almost linearly with the Fe-exchange level up to 60 % and became constant at higher exchange levels. Possible explanations for the effect of the zeolite structure on the catalytic activity included changes in the acidity and the pore structure of the zeolite, as

well as modifications of the redox properties, the local environment and the geometric configuration of the exchange cations.

Platinum (Pt)-containing ZSM-5 zeolites as a catalyst for SCR in the presence of hydrocarbon has also been investigated by several groups, Kharas et al. (1994) quoted by Amiridis have reported that the activity of Pt-ZSM-5 increased with Pt loading in the range investigated (0.5 - 4.67 wt. %). The temperature of maximum activity was determined to be approximately 200 °C, which is significantly lower than the corresponding temperature for Cu-containing zeolites. A comparative study of Pt-ZSM-5, Cu-ZSM-5 and Fe-mordenite for their performances in the NO reduction by ethylene conducted by Iwamoto et al, (1994 and 1995) revealed that, in agreement with the previous results, Pt-ZSM-5 was more active than the other Cu or Fe containing zeolites at low temperatures (below 227 °C). More importantly, the activity of Pt-ZSM-5 was hardly affected by addition of 8.5 % water vapour, while the other known catalysts were completely deactivated. The long term stability of Pt-ZSM-5 has been confirmed in simulated and actual diesel engine exhaust gases containing excess O₂ and water vapour.

Cobalt (Co)-exchanged zeolites have also been investigated for NO reduction in the presence of hydrocarbon. Li and Armor (Li, 1993) were the first to report that NO can be selectively reduced by methane in the presence of excess O₂ over a cobalt-exchanged ZSM-5 zeolite (Si/Al = 14). It was found that the catalytic activity of Co-ZSM-5 was low in the absence of O₂ and was significantly enhanced in the presence of excess O₂. The NO conversion increased with the methane level, although a relatively small amount of methane was needed for complete NO reduction reaction.

Gallium (Ga)-exchanged zeolites reported by Yogo and coworkers (1993) has also been found to be active for nitric oxide reduction by hydrocarbons in the presence of an excess O₂. The author first reported the results of Ga-exchanged zeolites in the presence of propane as reducing agent. The zeolite structure was found to be an important factor, with Ga-ZSM-5 and Ga-Y respectively being the most and least active catalysts tested for NO reduction, while G-ferrierite exhibited the best high temperature (above 500 °C) activity.

The H-form form of several zeolites reported by Hamada and co-workers (Hamada et al., 1990) have also been studied for the reduction of nitric oxide by hydrocarbons in the presence of hydrocarbons in excess O₂. Using propane and propylene as the reducing agents, Hamada et al. found that the H-zeolites can also be active as Ga ion exchanged zeolites studied by Yogo and co-workers. In a comparison to metal ion-exchanged zeolites for the NO reduction by ethylene in the presence of 2 % O₂, it was found that H-ZSM-5 was less active than some metal ion-exchange zeolites (i.e. Ag-, Co-, Zn- and Cu-ZSM-5), but was significantly more active than others (i.e. Mn-, Fe-, Ca-, La-, Pd and Cr-ZSM-5). The temperature of maximum NO reduction for H-ZSM-5 was found to be 400 °C, which was higher than those of Cu-ZSM-5 (250 °C) and Co-ZSM-5 (350 °C), but lower than those of Ag-ZSM-5 (450-600 °C) and Zn-ZSM-5 (600 °C). When methane was used as the reducing agent, H-ZSM-5 was reported to be significantly less active than Co-ZSM-5, Ga-ZSM-5, Ga-H-ZSM-5 (ion exchanged or impregnated). Nevertheless, the H-ZSM-5 is not expected to have any practical usage because of its high sensitivity to hydrothermal environments typical in diesel exhaust.

Base metal (metals that oxidize, tarnish or corrode relatively easily when exposed to air or moisture) ion exchanged zeolites in their current forms face severe limitations for commercial applications in diesel exhaust, primarily due to their poor hydrothermal stability and poisoning by sulfur oxides. A substantial improvement in catalyst stability and durability is obtained with Pt-containing zeolites. Characterization of these materials has indicated that in many cases platinum exists at the exterior of the zeolites as fine metallic particles, in contrast to exchanged base metal cations which are located at specific sites in the zeolites crystal and remain atomically dispersed. This observation has prompted questions regarding the role of the support in the activity of noble metal catalysts, which eventually resulted in a number of studies of Pt and other noble metals supported on non-zeolitic oxides.

To sum up, metal exchanged zeolites have been extensively studied specifically on ZSM – 5 zeolites as support, and it has been demonstrated from the results obtained out of

published papers that these catalysts are suitable for high temperatures despite their instability and poisoning by sulfur over time. For screening tests, an excess of oxygen during the experiment must always be taken into account to enhance the activity of the catalyst and a high concentration plays an important role during the reduction process. (Amiridis et al., 1996).

2.6 Loading techniques of catalysts and characterization methodology

2.6.1 Introduction

This subsection covers a review of different techniques used for the synthesis and characterization of the SCR catalysts. The section starts by reviewing the synthesis techniques giving some general deposition techniques and secondly, reviews two synthesis techniques in particular for the purpose of the study. The second part of the chapter gives in detail each characterization technique used to determine the characteristics of the SCR catalysts with principles where needed.

2.6.2 Deposition techniques on substrates

Deposition techniques on supports such as zeolites and mesoporous silica are numerous, but two depositions techniques from the exhaustive list given in the following section will be of interest for the purpose of this study. The two methods have been chosen because they are easy to follow and they are reported to give precise loading results at the end (Gongshin et al., 2005). The two methods of choice include impregnation and ion exchange. A general overview of the methods is given followed by the discussion of each method in the case of H-beta-zeolite and mesoporous silica.

2.6.2.1 Impregnation techniques in general

Impregnation consists of contacting a porous support substrate with a liquid containing the components to be deposited on the surface of the substrate. During the impregnation process, many different processes may take place at different rates (Haber et al., 1995).

These include: The selective adsorption of species (charged or not) by Coulomb forces, Van der Waals forces or H-bonds; the ion exchange between the charged surface and the electrolytes; the polymerization/deposition of the species (molecules, ions) to be attached to the surface, and the partial dissolution of the surface of the solid. The type of catalyst product depends on (i) the nature of both reactants (the liquid and the solid surface), and (ii) the deposition conditions. The main parameters affecting the liquid are the pH, the nature of the solvent, the nature and the concentrations of the dissolved substances. The first parameter (pH) affects ionization and in many cases, the nature of the ions containing the active elements. The second (nature of the solvent) and third (nature and concentrations of dissolved substances) influence solvation (Haber et al., 1995).

The main properties of the support are texture, the nature of functional groups, the presence of exchangeable ions, and the reactivity (surface dissolution in an acidic or basic solution, etc.). In the overall impregnation process the following important facts should be noted: The properties of the liquid in the pores are different from those liquid properties measured in the bulk; the equilibrium between liquid and solid is slow to establish and an even distribution of attached species inside the pores is not easy to attain in porous materials because the deposition involves many different types of interaction as described above (Haber et al., 1995).

Impregnation of the active metal onto substrate can be achieved by at least 8 different methods (Haber et al., 1995).

- ❖ Impregnation by soaking, or with an excess of solution
- ❖ Dry or pore volume impregnation
- ❖ Incipient wetness impregnation
- ❖ Deposition by selective reaction with the surface of the support
- ❖ Impregnation by percolation
- ❖ Co-impregnation
- ❖ Successive impregnation
- ❖ Precipitation-deposition

In the present study, emphasis will be placed on wet impregnation and on ion exchange of the metal species because they are easy to follow and they are reported to give precise loading of the metal of choice at the end of the process. During wet impregnation the volume of solution required is empirically determined to correspond to that beyond which the catalysts begins to look wet. The method is best suited to deposition of species which interact very weakly with the surface, and for deposition of quantities exceeding the number of adsorption sites on the surface. If the number of species which can adsorb on the surface is low, a chromatographic effect may occur, i.e. attachment of species to the mouth of the pores. Redistribution inside the pores of porous support matrices is very slow (Haber et al., 1995).

The most common commercial procedure for dispersing the catalytic active species within the carrier is by impregnating an aqueous solution containing a salt (precursor) of catalytic elements (Komiya et al., 1985; Trimm et al., 1980; Thomas and Brundrett, 1980; Stiles et al., 1983; Worstell et al., 1992). Most preparation techniques simply involve soaking the carrier in the solution and allowing capillary and electrostatic forces to distribute the salt over the internal surface of the porous network. The salt generating the cations or anions containing the catalytic element is chosen to be compatible with the surface charge of the carrier to obtain efficient adsorption or possibly also ion exchange. The isoelectric point of the carrier (charge assumed by the carrier surface) which is dependent on the pH, is useful in making decisions regarding salts and pH conditions for the preparation. The maximum water uptake by capillary impregnation of the carrier is referred to as the pore water volume. This can be achieved by slowly adding of water to the carrier until it is saturated. The precursor salt is then dissolved in an amount of water equal to the pore water volume.

2.6.2.2 Ion exchange technique in general

The ion exchange method of metal loading of a support has the advantage of producing a highly dispersed catalytic component within the carrier. Assuming that the carrier has a well-defined exchange capacity, a cation salt containing the catalytic species can

exchange with the exchangeable carrier cations. Ion exchange is the most commonly used method for metal loading zeolite catalysts. It is common practice to first treat the acid form of the support zeolite with an aqueous solution of NH_4^+ to form the ammonium exchanged zeolite. This can then be treated with a salt solution containing a catalytic cation to form the metal exchanged zeolite. The obtained metal containing exchanged zeolite is washed and dried, and the metal salt then reduced by thermal means in the presence of a gas such as nitrogen or hydrogen (Haber et al., 1995).

2.6.3 Methods for introducing catalytic active species into mesoporous silica support

In practice, metal loaded supports are often porous; the porous structure is important in controlling reactant accessibility and product selectivity, while the pore structure of a support influences the way in which a metallic phase is introduced (Anderson, 1928). In general, several methods are used for introducing metal, metal ions oxides or metal complexes into a porous material such as mesoporous silica for example, MCM – 41. These methods can be summarized as follow:

2.6.3.1 Direct hydrothermal synthetic (DHT) method

The most common known method for the introduction of active catalytic sites into mesoporous materials is the DHT method, direct addition of the ion precursors to the synthesis gel before hydrothermal synthesis. This method has been applied for the synthesis of catalysts such as Al – MCM – 41, Ti – MCM – 41 and V – MCM - 41 (Lawrence, 2005) in early studies to introduce acid and redox sites. Many other hetero-atoms such as B, Zr, Cr and Nb have also been incorporated into MCM – 41 with the DHT method.

2.6.3.2 Impregnation method

Impregnation of metal salt is the common method used for the preparation of supported catalysts and is probably the most convenient method to introduce different kinds of

active sites. Nonetheless, it cannot be assured that the active component will be located only in the mesoporous channels with this method. A part of the precursor species may uncontrollably undergo aggregation during post-treatments processes such as drying and calcination, forming large oxide particles on the external surface of the mesoporous materials. Despite this drawback, there is still a number of studies that have embraced this method to prepare metal or metal oxide containing MCM- 41 mainly because of its simplicity (Lawrence, 2005).

2.6.3.3 Grafting method

Inorganic compound such as organometallic complexes can be used as the precursors to graft the active metal onto the surface of mesoporous silica, using surface silanol groups as anchor sites under anhydrous conditions. After treatments such as calcination, metal ion or metal oxide – grafted MCM – 41 could be obtained. Ti – grafted, V - grafted and Mn – grafted mesoporous materials have been derived with this method and their applications in catalytic oxidation reactions have been demonstrated (Lawrence, 2005).

2.6.3.4 Chemical vapour deposition (vapour grafting) method

Volatile inorganic or organo-metallic precursors are deposited on the surface of mesoporous silica by vacuum sublimation under certain conditions. With this method, Ti – deposited, Mn – deposited and Pd - deposited materials have been synthesized using TiCl_4 , $\text{Mn}_2(\text{CO}_3)$ and $\text{Cp Pd}(\eta^3 - \text{C}_3\text{H}_5)$ as the corresponding precursors followed by appropriate treatments (Lawrence, 2005).

2.6.3.5 Template – ion exchange method

Mesoporous silica materials generally used do not possess ion exchange ability like aluminosilica zeolites. Nonetheless, the template cations in the $\text{S}^+ \text{X}^- \text{I}^+$ type inorganic species – surfactant composite (where, S, I, and X are surfactant, inorganic species and counter anion, respectively) may function as exchangeable sites. It is now clear that the

cationic surfactants in the as-synthesized MCM-41 after hydrothermal synthesis are mainly organized in the form of cylindrical micellar structure with hydrophilic positive ends interacting with silica pore surfaces via coulombic interaction, and can be replaced through ion-exchange by other cations such as Mn^{2+} , Fe^{3+} [$Co(en)_2Cl_2$] and other positively charged complexes (Lawrence, 2005).

2.6.4 Methods for introducing catalytic active species into zeolites

2.6.4.1 Introduction

Zeolites, in a narrow definition, are porous crystalline aluminosilicates having a uniform pore structure and exhibiting ion exchange behavior. The framework of zeolites consists of SiO_2 and AlO_4 tetrahedra sharing oxygen ions located at their apices, thus described by the general framework formula $(Al_2O)_x(SiO_2)_{(n-x)}$, where n is the number of tetrahedra per unit cell, and $x < n/2$. Since aluminium is trivalent, every AlO_2 unit carries a negative charge, which is compensated by a positive framework charge associated with a non-framework cation. Therefore, the ion exchange capacity of a zeolite depends on the chemical composition, i.e., a higher ion-exchange capacity is observed in zeolites having a low SiO_2/Al_2O_3 ratio (Weitkamp, 2000).

There are basically two procedures by which precursor metals can be introduced into zeolites, by ion exchange if the metal forms cations, and by sorbing neutral metal compounds, i.e., carbonyl complexes. A third method frequently applied to introduce catalysts is impregnation, which introduces anions as well as cations (Weitkamp, 2000).

2.6.4.2 Ion exchange with zeolites

Usually, ion exchange is performed by simply contacting the zeolites with a salt solution of the required cation at ambient temperature, or at elevated temperature if an accelerated exchange rate is desired. The exchange reaction, in which one type of cation is replaced with another, assumes an equilibrium state that is unique for the particular zeolite and the particular cations (Weitkamp, 2000).

2.6.4.3 Impregnation of zeolites

Impregnation of zeolites is employed when the quantity of metal ion to be introduced is greater than would be obtainable by ion exchange of, e/g., high silica zeolites, but the distribution is more uniform in the ion exchange sample. In order to impregnate a zeolite of low Si/Al ratio, a high concentration of the solution is required to overcome the anion-repelling effect of the negative charges around the pore mouth. A convenient method involves evaporation of the impregnating solution in contact with the zeolites (Weitkamp, 2000).

2.6.5 Characterization techniques

2.6.5.1 Introduction

A number of techniques have been used to characterize catalysts supported on mesoporous and microporous silica materials. Among these techniques, X-Ray powder diffraction, high resolution transmission electron microscopy and adsorption measurements are considered the essential techniques to identify the structure of the catalysts. Temperature Programmed reduction and Thermal Gravimetric analysis have been used in order to obtain additional information about the catalysts such as redox behavior and mass loss respectively. Brunauer-Emmett-Teller has been used for determination of surface area and pore size distribution. Selected area electron diffraction has been used in order to measure the crystallinity and symmetry of materials. Scanning electron microscopy has been used in order to determine morphology with great depth of field and high magnification. Energy dispersive spectrometry has been used for determining elemental composition or weight percentage and the results obtained could be confirmed by atomic adsorption spectroscopy and Inductive coupled plasma.

The following paragraphs discuss in detail each technique used by outlining each technique, discussing the principle, and presenting equations where needed. It will also

show examples in literature where different techniques were used to characterize a catalyst.

2.6.5.2 Morphology study by scanning electron microscopy

One technique in the field optical electron spectroscopy that is able to provide information concerning the crystal shape and the size of a powder sample. Scanning electron microscopy used in conjunction with EDS yields a great deal of information on catalysts support as well as zeolites (Szostak, 1989). In scanning electron microscopy (SEM), a finely focused electron beam is scanned across the specimen, and the interaction between the electrons and the solid generates a variety of signals, each of which can be collected and used to modulate the brightness in a cathode ray display screen, the scan of which is synchronized with the scan of the specimen (Goodhew, 2001). In normal SEM, it is the secondary electrons which are usually collected and used for image formation, but X-rays or optical photons may also be collected for this purpose. The electron beam energy is variable, typically in the range 5-50 keV, with a beam spot size at the specimen in conventional instruments down to about 10 nm.

2.6.5.3 Elemental composition study by energy dispersive spectroscopy

Elemental analysis by X-ray emission is an additional analytical technique for determining elemental composition which is frequently fitted to a scanning electron microscope, and since the exciting electron beam can be controlled to scan the specimen, the elemental distribution revealed from the emitted X-rays is readily displayed as a line scan, or as two-dimensional distribution. The practical limit of resolution obtainable in SEM is rather greater than the incident spot size because of beam spreading effects in the specimen. When used in the secondary electron emission modes a conventional instrument has a resolution limit of about 15 nm, but if the image is formed using the back-scattering X-rays the resolution is considerably poorer since the X-rays can be generated from a region in the specimen up to 1 μ m in diameter (Goodhew, 2001). In elemental analysis by EDS, a very small sample size is analyzed and which is not

representative of the entire sample; the heterogeneity of the sample may result in high variability of results. The EDS analysis has been used here as a qualitative analysis and not as a quantitative analysis. It just tells you that the metal is on the sample but not how much of it.

2.6.5.4 Composition study inductive coupled plasma mass spectroscopy

The Inductively Coupled Plasma (ICP) technique gives very high sensitivity for the determination of elements in solution. This technique has the ability to detect very low levels (parts per billion) of most elements in an aqueous sample. ICP is the technique of choice for trace element analysis of natural waters, and can be used in the analysis of minerals and rocks after digestion of the solid sample in concentrated solution such as aqua regia (HCl/HNO₃) or hydrofluoric acid.

In ICP-MS, a plasma or gas consisting of ions, electrons and neutral particles is formed from Argon gas. The plasma is a very aggressive ion source, and virtually all molecules in a sample are broken up into their component atoms because of the high temperature (7000 K) at which the ion source operates. To create the inductively-coupled plasma (ICP), a radio frequency signal is fed into a tightly wound, water-cooled coil where it generates an intense magnetic field. In the centre of this coil is a specially made glass or quartz plasma torch where the plasma is formed. The plasma is generated in the argon gas by "seeding" the argon with a spark from a Tesla unit (similar to that used on a car spark plug). When the spark passes through the argon gas, some of the argon atoms are ionized and the resultant cations and electrons are accelerated toward the magnetic field of the radio frequency coil. Through a series of inelastic collisions between the charged particles (Ar⁺ and electrons) and neutral argon atoms, a stable high temperature plasma is generated. The plasma is used to atomize and ionize the elements in a sample. When the sample aerosol passes through the plasma, it collides with free electrons, argon cations and neutral argon atoms. The result is that any molecules initially present in the aerosol are quickly and completely broken down to charged atoms. The resulting ions are then passed through a series of apertures (cones) into the high vacuum mass analyzer. The

isotopes of the elements are identified by their mass-to-charge ratio (m/e) and the intensity of a specific peak in the mass spectrum is proportional to the amount of that isotope (element) in the original sample (Jarvis et al., 1992).

2.6.5.5 Composition study by atomic absorption spectroscopy

The Atomic Absorption Spectroscopy (AAS) determines the presence of metals in liquid samples as well as solid samples after digestion of the solid (powder) in concentrated solutions such as aqua regia or hydrofluoric acid. Metals include Fe, Cu, Al, Pb, Ca, Zn, Cd and many more. It also measures the concentrations of metals in the samples. Typical concentrations range in the low mg/L range. In their elemental forms, metals will absorb ultraviolet light when they are excited by heat. Each metal has a characteristic wavelength that will be absorbed. The AAS instrument looks for a particular metal by focusing a beam of an ultra violet (uv) light at a specific wavelength through a flame and into a detector. The sample of interest is aspirated into the flame. If that metal is present in the sample, it will absorb some of the light, thus reducing its intensity. The instrument measures the change in intensity. A computer data system converts the change in intensity into an absorbance. As the concentration goes up, the absorbance goes up. A calibration curve can be constructed by running the standards of various concentrations on the AAS and observing the absorbances. The computer data system will draw the curve, and then samples can be tested and measured against this curve.

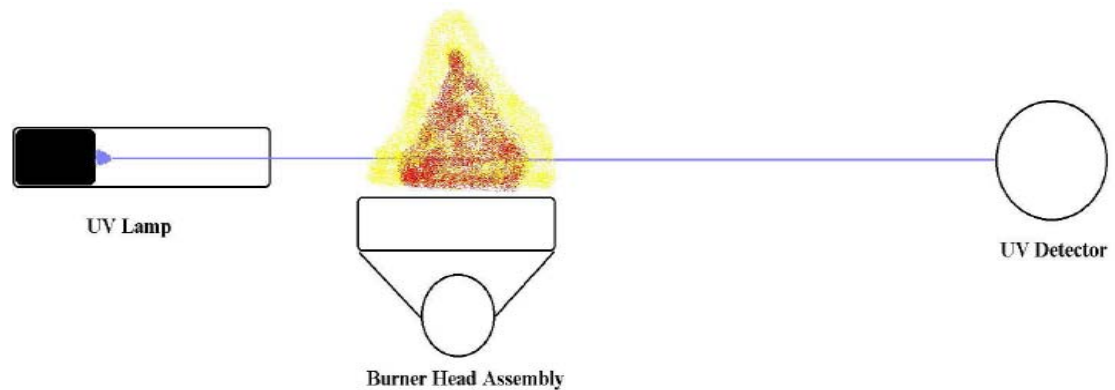


Figure 2-7: Schematic diagram of flame atomic adsorption spectroscopy (Metcalfé et al., 1987)

The Figure 2-7 shows the schematic diagram of a flame AAS. As the diagram indicates, there are four primary parts of the system: the light source, the flame apparatus, the detector, and the data system.

Each element in the periodic table has a specific ΔE that will absorb a specific wavelength of uv light. The relationship between the energy transition and the wavelength (λ) can be described by:

$$\Delta E = h / \lambda \quad (2)$$

Where:

h is the Planck's constant.

The atomic absorption uses this relationship to determine the presence of a specific element based on absorption in a specific wavelength (Metcalfé et al., 1987).

2.6.5.6 Surface structure and topology study by high resolution transmission microscopy

In order to study nano-particles in general and catalysts in particular, transmission electron microscopy is a useful technique that can be used in three different ways as described below; Firstly, when the specimen is of substantial macroscopic size so that electron beam penetration is impossible; Secondly, the direct observation of specimen morphology when the specimen is a powder or some other sort of material in a state of subdivision which lies beyond resolution by optical microscopy. Estimation of average metal particle size and particle size distribution in dispersed metal catalysts is an example of this application; Thirdly, the use of HRTEM lies in observation and interpretation of contrast features which occur within specimen images, extension contours, various sorts of phase contrast features, and lattice images, which all can give information about specimen structure (Anderson et al., 1988).

2.6.5.7 Crystalline phases study by diffraction pattern study by selected-area diffraction

A HRTEM can provide two separate kinds of information about a specimen – a magnified image showing morphology at the angstrom level and crystal habit, and a diffraction pattern.

There are many reasons for wanting to analyze a diffraction pattern. It may be necessary to accurately measure the camera constant of the microscope, or to attempt to identify an unknown material using its interplanar spacing or diffraction geometry. Or a certain diffraction condition may be needed to obtain a particular diffraction contrast image. The accuracy and the type of measurement may depend both on the specimen and the type information required (Goodhew, 2001).

Figure 2-8 is an illustration of different selected area diffraction patterns that can be obtained from the TEM microscope. Details are given below the images.

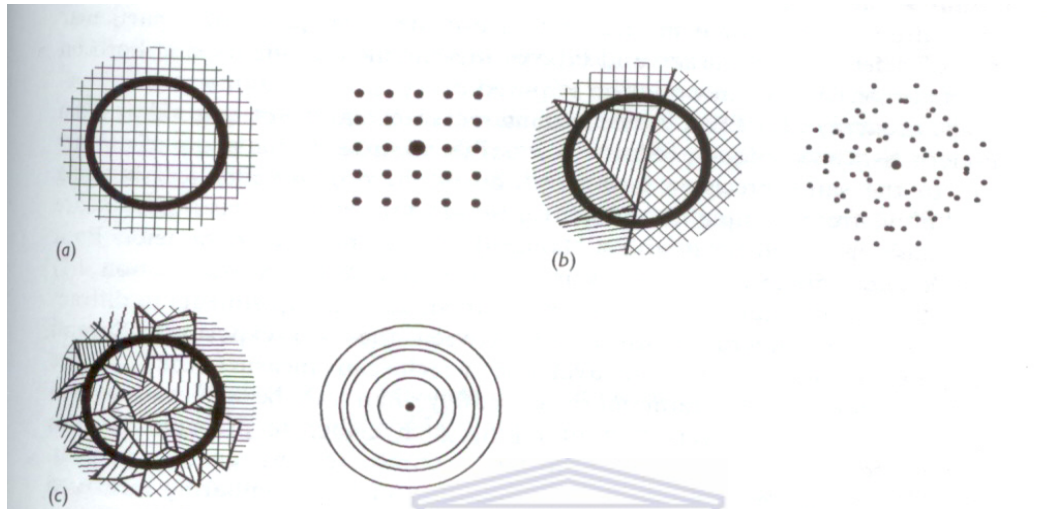


Figure 2-8: Types of diffraction patterns which arise from different specimen microstructures (a) A single perfect crystal. (b) A small number of grains. (c) A large number of randomly oriented grains (Goodhew, 2001)

2.6.5.8 Crystalline phases study by X-ray diffraction spectroscopy

Powder X-ray diffraction is used to identify the structure, degree of crystallinity, unit cell parameters and crystallite size. In X-ray diffraction technique a spectrum is produced by the diffraction of X-rays through the closely spaced lattice of atoms in a crystal. The spectrum generated is recorded and then analyzed to reveal the identity nature of the crystal lattice (Shimura, 1989). The spacing in the crystal lattice can be determined using Bragg's law.

2.6.5.8.1 Principle

During the experiment, when the X-ray penetrates the atoms, it induces an electromagnetic wave motion of the electronic cloud (Shimura et al., 1989)

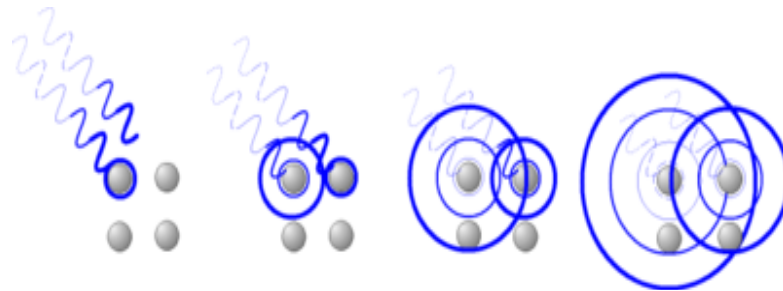


Figure 2-9: The X-ray penetration inducing Rayleigh scattering (Shimura et al., 1989)

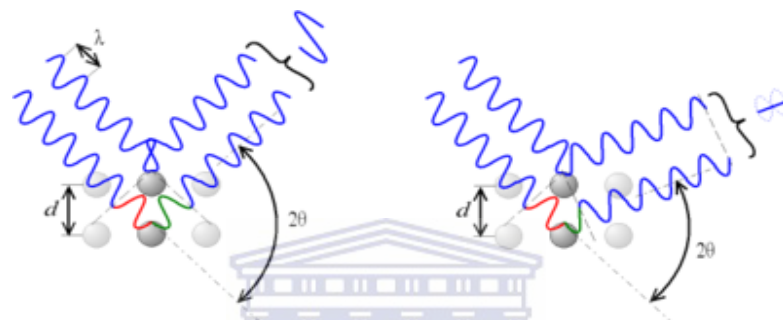


Figure 2-10: According to the 2θ deviation, the phase shift causes constructive (left Figure) or destructive (right figure) interference (Shimura et al., 1989)

The re-emitted X-ray interference gives rise to constructive and destructive interference as shown in figure 2-10, this is known as the diffraction phenomenon. Constructive interference is induced when the phase shift is proportional to 2θ , which can be expressed by Bragg's law.

$$n\lambda = 2d \sin(\theta) \quad (3)$$

Where

n : is the order of diffraction, and is an integer ($n = 1, 2, 3$, etc)

λ : is the wavelength of the X-ray, and moving electrons, protons and neutrons.

d : is the spacing between the planes in the atomic lattice

θ : is the angle between the incident ray and the scattering planes.

Determination of the crystal size of the metal centre from XRD may be calculated using the Scherrer equation. The XRD line broadening versus crystallite size effect can be exploited to determine the average size of metal crystallites on various molecular sieve supports. The full width at half maximum (FWHM), β , is related to the mean dimension of crystallites perpendicular to the hkl planes, D as given by Scherrer's equation.

$$D = 0.9 \frac{\lambda}{\beta} \cos \theta \quad (4)$$

Where

D: is the particle diameter (nm) measured at its half maximum intensity.

λ : is the wavelength of the X-ray radiation,

β : is the FWHM (radians) and

θ : is the angle of reflection.

The FWHM is strongly affected by crystal defects and distortions, which cause line broadening. Here, the variation in the FWHM (β) is used as a rough indication of the changes in crystal size as a function of radiation dose (Shimura et al., 1989). The Scherrer's equation is mainly specific to perfectly spherical particles. As a result there may be discrepancies in particle size determination for non-spherical particles.

2.6.5.9 Surface area and pore size distribution study by N₂-BET

The characterization of a catalyst ideally includes the measurement of the total surface area of a sample, together with the measurement of the surface area of each different chemical phase which may be present. Whether this idea can be achieved will depend on the composition of the catalyst sample and in particular on the number and natures of the various phases present (Anderson, 1988).

Mesoporous materials have the ability to absorb probe molecules of different sizes. Sorption capacities for probe molecules such as n-hexane, water, benzene, nitrogen and

so on, yield information about the hydrophobicity, pore dimensions and pore volume of the mesoporous materials. The Brunauer-Emmett-Teller (BET) volumetric gas adsorption technique using gases such as nitrogen or argon is a standard method for the determination of the surface areas and pore size distribution of finely divided porous samples (Shimura, 1989). The relation between the mass of gas adsorbed and the equilibrium pressure of the gas at constant temperature is defined by the adsorption isotherm. This relation is represented by the BET equation (5).

$$\frac{1}{w \left[\left(\frac{P_0}{P} \right) - 1 \right]} = \frac{1}{W_m C} + \frac{(C-1)}{W_m C} * \frac{P}{P_0} \quad (5)$$

Where

W : Weight of N_2 adsorbed at a given relative pressure (P/P_0)

W_m : Weight of N_2 producing monolayer coverage ($\theta = 1.00$ ml)

C : is the BET constant

P/P_0 is the relative pressure; P_0 the saturated vapor pressure and P the pressure of the adsorbate.

The isotherms observed in physical adsorption can vary widely. The basic types are shown in Figure 2-11. At a free surface, physical adsorption merges continuously from the sub-monolayer region to the supra-monolayer region.

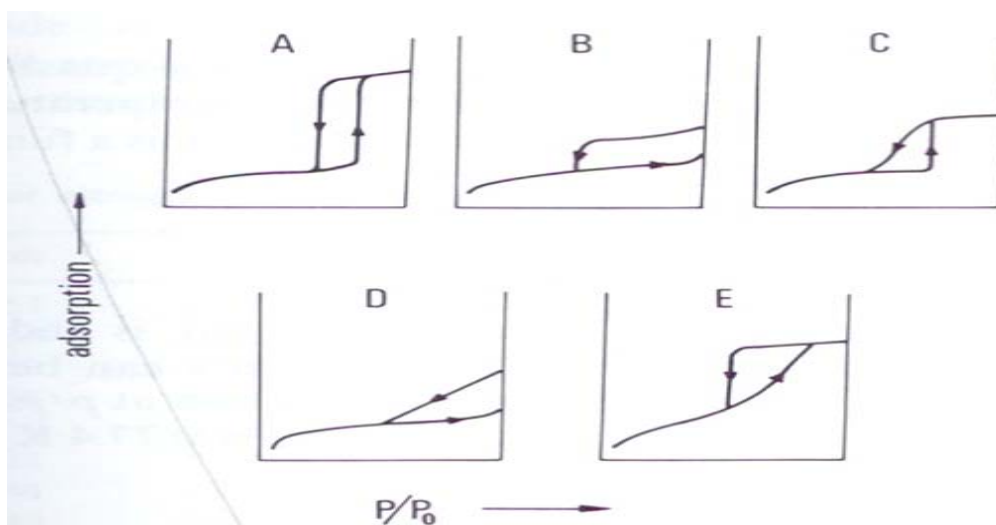


Figure 2-11: physical adsorption possibilities of isotherm shape (Goodhew, 2001)

The type A isotherm (Figure 2-11) is not found for physical adsorption at a free surface, but is characteristic of a microporous solid (pore width $\leq 2\text{nm}$) where the pore size and the size of the adsorbate molecules are not of the same order of magnitude so that a very severe limitation is put upon the number of adsorbed layers that can be formed. Isotherms of types B and C apply to multilayer physical adsorption at a free surface, or at a quasi-free surface in a macroporous solid (pore width $> 50\text{nm}$). Isotherms of type D and E refer to sorption in mesoporous solids (pore width roughly within the range 2-50 nm): capillary condensation occurring in the pores and isotherms of types D and E are always accompanied by a hysteresis loop. In practice, isotherms of types B and D are by far the most common, and these are the only ones from which reasonably reliable surface area measurements can be obtained (Goodhew, 2001).

N_2 - adsorption - desorption isotherm of MCM-41 is of type D isotherm. This implies an increase in N_2 adsorption (within the P/P_0 range between 0, 2 to 0, 4) that corresponds to capillary condensation within uniform pores. The sharpness and the height of this step (adsorption) reflect the uniformity of the pore size and the pore volume respectively.

2.6.5.10 Chemical bonding study by Fourier transformed infrared spectroscopy

Fourier Transform Infrared Spectroscopy (FTIR) is a technique that provides information about the chemical bonding or molecular structure of materials, whether organic or inorganic. FTIR analysis can be applied to minute quantities of materials, whether solid, liquid, or gaseous. When the library of FTIR spectral patterns does not provide an acceptable match, individual peaks in the FTIR plot may be used to yield partial information about the specimen (Goodhew, 2001).

The Fourier transform infrared (FTIR) technique makes use of an interferometer rather than a monochromator, and provides a number of advantages in the measurement of infrared spectra. In operation, the incident beam is split and half transmitted to a fixed mirror while the other half is transmitted to a movable mirror oscillating with a speed v (Figure 2-12). Typically, v is around 0.2 cm s^{-1} . The two beams are then recombined interfering either constructively or destructively according to the difference in path-length created by the moving mirror. If the incoming radiation is monochromatic and of wave number ν , it can be shown that the intensity of the exit beam from the interferometer is modulated according to the cosine function, with a frequency f given by

$$f = 2 \nu v \quad (6)$$

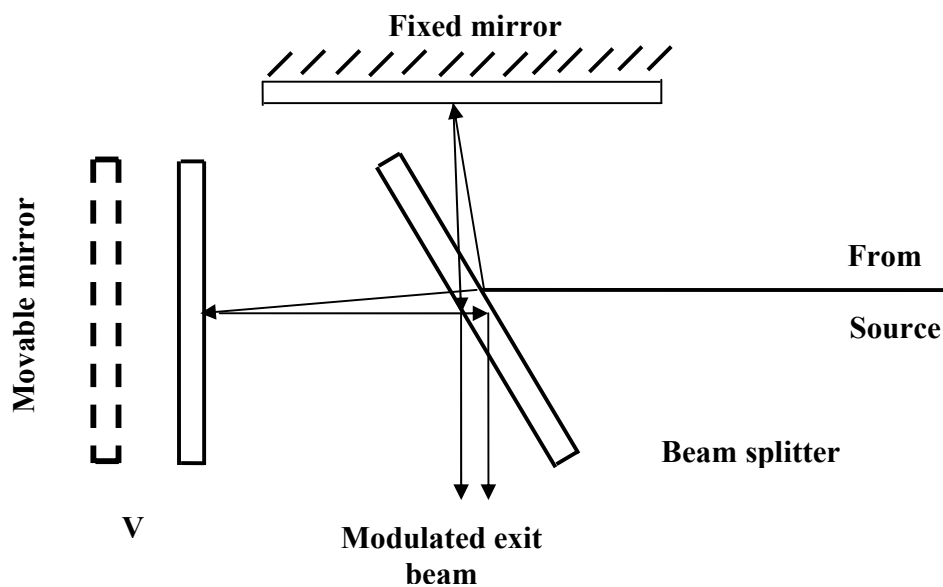


Figure 2-12: Schematic diagram of Michelson interferometer (Goodhew, 2001)

2.6.5.11 Structural stability study by thermo-gravimetric analysis

Thermal analysis is used to study the structural stability of the as-synthesized forms of catalysts or other molecular sieves such as zeolites and mesoporous materials. It provides information about the temperature required for the removal of absorbed water, decomposition of the oxides formed during the synthesis and dehydroxylation at higher temperature. This is a simple analytical technique that measures the weight loss (or weight gain) of a material as a function of temperature. As materials are heated, they can lose weight from a simple process such as drying, or from chemical reactions that liberate gasses. Some materials can gain weight by reacting with the atmosphere in the testing environment. Since weight loss and gain are disruptive processes to the sample material or batch, knowledge of the magnitude and temperature range of those reactions are necessary in order to design adequate thermal ramps and holds during those critical reaction periods (Orton, 2002).

2.6.5.12 Reducibility study by temperature programmed reduction

Temperature programmed reduction (TPR) is most commonly used to determine the “ease of reducibility” of a metal oxide or oxygen containing metal compound. For this purpose, hydrogen diluted with an inert gas (nitrogen or argon if the undesirable formation of nitride is anticipated) is used (Baiker et al., 1987).

The interaction of reactants with the catalyst surface is a key parameter in heterogeneous reaction systems. For example, the temperature at which species are desorbed from a surface is indicative of the strength of the surface bond: the higher the temperature, the stronger the bond. Therefore the adsorption of a probe molecule at low temperature, and subsequent monitoring of its desorption/reaction characteristics with temperature, is a simple way to characterize surface properties of catalysts and adsorbents (Baiker et al., 1987).

In term of gas, consideration regarding purity of gases should be given as for vacuum volumetric measurement. The carrier gas is of particular importance since it is constantly flowing over the sample. Even a very small amount of undesirable reactant can very quickly de-activate the sample. According to analysis type, the present table has been suggested by (Baiker, 1987).

Table 2.7: Different suggestions in term of gas analysis and carrier

Analysis type	Carrier gas	Reactive gas
H ₂ pulse titration	100 % N ₂ or Ar	100 % H ₂
CO pulse titration	100 % He	100 % CO
TPR	95 % N ₂ or Ar	5 % H ₂
TPO	98 % He	2 % O ₂
TPD (H ₂)	100% N ₂ or Ar	n/a
TPD (NH ₃)	100 % He	n/a
TPD (CO ₂)	100 % He	n/a

2.7 General summary

The papers reviewed in the present thesis have been informative in terms of operating conditions, requirements for low temperature SCR; they have also has been informative in terms of support (substrate) choice that can be used for DeNO_x catalyst and different preparation techniques for incorporation of active sites onto the support. Two simple methods such as ion exchange and wet impregnation where identified for the synthesis of the new catalysts. A clear distinction in the choice of the reducing agent must be made between the two commonly reducing agents currently in use. The first part of the literature review as summarized in section 2.5.1.3 has highlighted the choice of the two supports that are going to be used during the experimental part of the thesis. The second part of the literature review which covers different methods for catalyst's characterization has been more revealing in terms of information. The paper published by Huang and his group (2008) on the Fe:Mn/MCM-41 has only looked at the XRD and BET as ways of characterization of the synthesized catalysts. These two methods by themselves are not sufficient to draw valuable conclusions on the nature of the catalyst active sites or pores size distribution of the catalysts. Papers published by others scientists have shown that it was possible by other methods to go deep down in terms of catalysts characterization. In this regards, The EDS was used by Pantazis et al. (2005) as a qualitative analysis; he was able to synthesize the Cu/Ce mesoporous silica catalyst and give evidence by EDS that the two metals were present on the support. Xiang et al. (2006) synthesized the mesoporous silica supported CuO, he was able by means of ICP and AAS as quantitative analysis to determine with precision the amount of the loaded metal onto the support. Xiang and coworkers also used other technique such FT-IR, TEM, TPR and XRD to characterize the synthesized CuO mesoporous silica. FT-IR was for instance used to say something on the vibrational groups present on the support and see whether or not there were new bands formed on the support due to the presence of CuO. TEM in combination with SAED were used to say something of the nature of the support and see if the basic structure of the support did not collapse after incorporation of the metal and secondly, say

something on the particles distribution formed on the support, whether they amorphous or just randomly distributed on the support. XRD has been the most common tool for phase's identification on the support; for the mesoporous silica, low angle and wide angle XRD need to be distinguished, the low angle XRD will give you the characteristic peaks of the support before and after incorporation of active sites. The decrease in intensity is the most important factor to look at when analyzing different catalysts; the wide XRD angle is used for crystalline phase's identification after synthesis of new catalyst, this technique will tell you if the new synthesized material is still amorphous after calcination or crystalline phases have been formed on the support. TRP and TGA as complementary techniques have been used by Xiang et al., (2006); Velu et al., (2002) and Köhn et al., (2001) to characterize catalysts. Velu was for example able to relate the copper content to the hydrogen consumption, the hydrogen consumption was proportional to the amount of Cu^{2+} ; Xiang on the other hand was able by means of TPR to say something on the CuO particles size supported on mesoporous silica, he was able to distinguish large particles from small particles by means of TRP. Large CuO have broad peaks compared to small CuO with sharp peaks. Köhn used the TGA to study the redox stability of transition metal oxide and compared the behaviour of the metal oxide with their bulk phases. The bulk phase of CuO showed a one-step reduction starting from high temperatures (800 K) while the CuO dispersed of the mesoporous material showed different reduction stages of CuO to elemental copper, proving a good dispersion of the nanoparticles on the mesoporous support.

CHAPTER 3

3 EXPERIMENTAL APPROACH

3.1 Introduction

In this chapter, the catalysts used for the selective catalytic reduction of nitrogen oxides will be firstly described, in terms of the support materials used prior to the loading of metal oxides and secondly, in terms of the synthesis procedures used to prepare the final metal oxide loaded product (catalysts). An overview of the set up and sample preparation of the various characterization techniques used in the analysis of the catalysts are given, followed by the SCR experimental reactor set up for screening tests.

Figure 3-1 shows step by step the procedures followed to achieve the goal of the synthesis of the catalysts prior to characterization and the screening tests

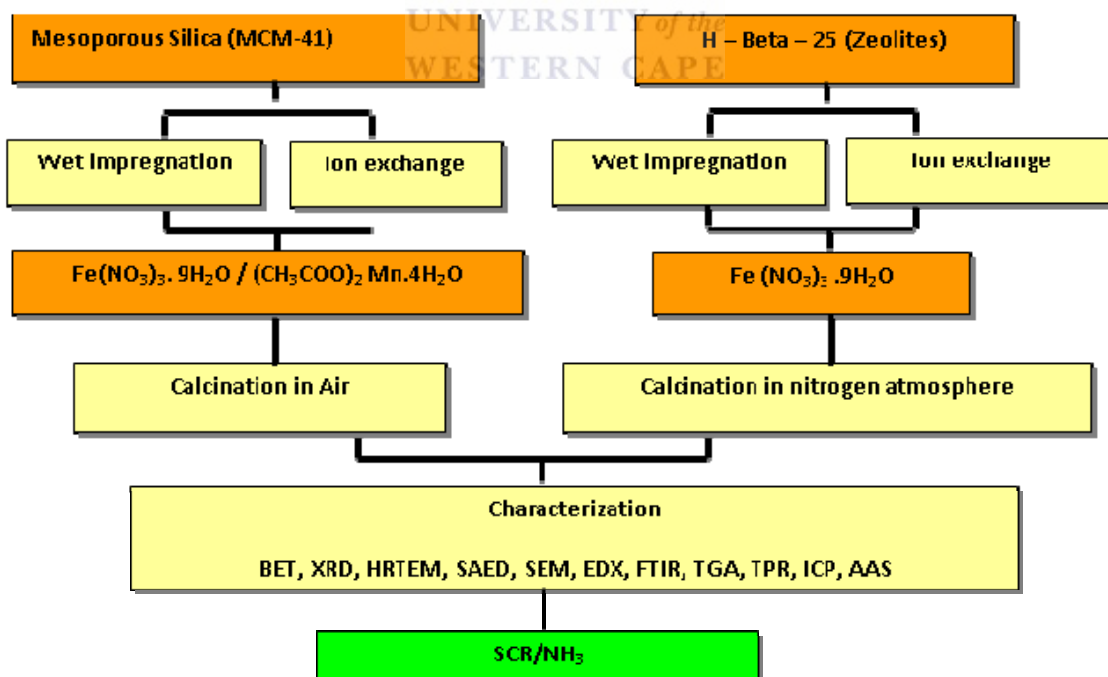


Figure 3-1: Schematic of the experimental approach.

3.2 Carrier description

3.2.1 Introduction

Two different supports have been used in the present study; details describing the two supports such as manufacturer's specifications supplied, characteristic and chemical composition are provided in the following.

3.2.2 Mesoporous silica ($\text{SiO}_2/\text{Al}_2\text{O}_3$)

3.2.2.1 Description

Supplier: Sigma Aldrich

Catalogue number: 643645

Application: Absorbent, catalysts support, nanoscale template

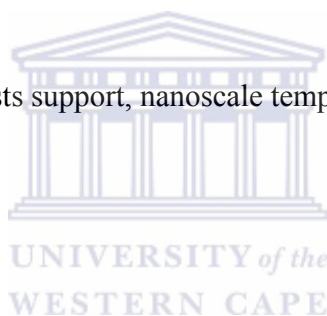
3.2.2.2 Properties

Form: powder

Unit cell size: 4.6 – 4.8 nm

Pore size: 0.98 cm^3/g ; pore volume; 2.3 – 2.7 nm pore size.

Bulk density: 0.34 g/ mL



3.2.3 H-Beta-25 zeolite ($\text{SiO}_2/\text{Al}_2\text{O}_3$: 11)

3.2.3.1 Description

Supplier: Sud Chemie

Synthetically manufactured using organic templates

Application: Catalytic alkylation of aromatics, adsorption of hydrocarbons from exhaust gas emission, NO_x reduction

3.2.3.2 Properties

Form: powder

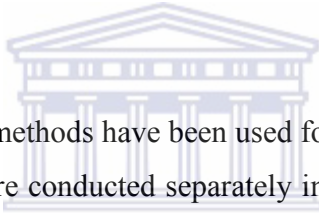
Tetragonal crystal structure with straight 12-membered ring channels (7.6 x 6.4 Å) with crossed 10-membered ring channels (5.5 x 6.5 Å)

Carrier treatment

A calcined carrier is the parent material (MCM-41 or H-Beta-25 zeolite) stirred in ultra-pure water for 24 hours, dried for 10 minutes before being calcined in air at 400 °C for 4 hours.

3.3 Synthesis of SCR metal loaded catalysts

3.3.1 Introduction



For comparison purposes, two methods have been used for the loading of oxide metals on MCM-41; the two methods were conducted separately in order to establish the optimum amount of metal oxides that the support (MCM – 41) can incorporate into its porous structure. The first method used is called wet impregnation and the second method, ion exchange. In the first method, the mixture of Fe and Mn salts were dissolved together in a small volume of ultra-pure water sufficient to fill up the pores of the support (MCM – 41) which results in 7 mL of water corresponding to 2 g of support. In the second method, the mixture of Fe and Mn salts were dissolved together in a small volume of ultra-pure water enough to make the mixture completely wet, 10 ml of ultra-pure water is enough to make the mixture wet.

3.3.2 Catalysts prepared by wet impregnation using MCM - 41 as support

3.3.2.1 Methodology

Before wet impregnation was done, the maximum amount of water that can be absorbed by the support (MCM-41) was first determined empirically. As the result 2g of MCM-41

required 7 mL of de-ionised water. Then the specific amount of $\text{Fe}(\text{NO}_3)_3 \cdot 8\text{H}_2\text{O}$ and $(\text{CH}_3\text{COO})_2 \cdot \text{Mn} \cdot 4\text{H}_2\text{O}$ were weighed out according to their calculated loadings at an atomic ratio (Fe: Mn) of 1/1 and were dissolved in 7 ml de-ionised water (see Table 3.1). The obtained water salt mixture was stirred for a few minutes to become homogeneous, mixed with the 2g MCM-41 and stirred until reaching dryness. The obtained powder was dried in an oven at 100 °C for 10 minutes and then placed in a muffle furnace for calcination in air for 4 hours at 400 °C at a heating ramp of 2 °C per minute.

3.3.2.2 Equipment

Magnetic stirrer plate

Porcelain dishes

Magnetic bar

Oven: Scientific, Series 2000

Muffle furnace: Gallenkamp

Purelab UHQ de-ionizer: ELGA



3.3.2.3 Chemicals

Mesoporous Silica hexagonal framework, MCM – 41 type, Sigma Aldrich

Iron (III) nitrate hydrate 98 % $[\text{Fe}(\text{NO}_3)_3 \cdot 9\text{H}_2\text{O}]$, Sigma Aldrich

Manganese (II) acetate tetra hydrate > 99% $(\text{CH}_3\text{COO})_2 \cdot \text{Mn} \cdot 4\text{H}_2\text{O}$, Sigma Aldrich

Ultra-pure water

The following Table (Table 3.1) provides the names and a short description of different prepared catalysts that were used throughout thesis. Here the support used is the MCM-41 and the loaded metals are iron and manganese for the wet impregnation and ion exchange.

Table 3.1: Nomenclature and short description of the catalysts using MCM-41 as support.

Catalyst names	Description	Catalyst names	Description
Wet 15	Synthesis by wet impregnation at 15 Wt% of Fe/Mn	Ion 15	Synthesis by ion exchange at 15 Wt% of Fe/Mn
Wet 20	Synthesis by wet impregnation at 20 Wt% of Fe/Mn	Ion 20	Synthesis by ion exchange at 20 Wt% of Fe/Mn
Wet 25	Synthesis by wet impregnation at 25 Wt% of Fe/Mn	Ion 25	Synthesis by ion exchange at 25 Wt% of Fe/Mn
Wet 30	Synthesis by wet impregnation at 30 Wt% of Fe/Mn	Ion 30	Synthesis by ion exchange at 30 Wt% of Fe/Mn
Wet 35	Synthesis by wet impregnation at 35 Wt% of Fe/Mn	Ion 35	Synthesis by ion exchange at 35 Wt% of Fe/Mn
Wet 40	Synthesis by wet impregnation at 40 Wt% of Fe/Mn	Ion 40	Synthesis by ion exchange at 40 Wt% of Fe/Mn
MCM-41	Dried and calcined support		

3.3.2.4 Calculated metal loading results

Table 3.2 summarizes the metal loading that ideally the support can theoretically take up by wet impregnation, these results were subjected to a comparison with the results obtained by Electron Dispersive Spectroscopy (EDS), Inductive Coupled Plasma (ICP) and Atomic Adsorption Spectroscopy (AAS), and the results are presented in chapter 4, section 4.2.1.

Table 3.2: Calculated metal loading used for wet impregnation

Samples	Aimed loading of Fe and Mn (Wt %)	Mass of $\text{Fe}(\text{NO}_3)_3 \cdot 9\text{H}_2\text{O}$ (g) per 2 g support *	Mass of $\text{Mn}(\text{CH}_3\text{COO})_2 \cdot 4\text{H}_2\text{O}$ (g) per 2 g of support *	Mol of Fe per L of solution per g support **	Mol of Mn per L of solution per g support **	Fe:Mn calculated ratio	Calculated total loading
Wet 15	15	1.092	0.555	0.191	0.194	1:1	0.385
Wet 20	20	1.454	0.739	0.255	0.258	1:1	0.513
Wet 25	25	1.822	0.925	0.319	0.323	1:1	0.641
Wet 30	30	2.184	1.112	0.383	0.386	1:1	0.769
Wet 35	35	2.553	1.295	0.446	0.451	1:1	0.898
Wet 40	40	2.914	1.481	0.510	0.515	1:1	1.026

*Mass (g) of salt per 7 mL of de-ionized water

* Mol of Fe and Mn metal per 7 mL of de-ionized water

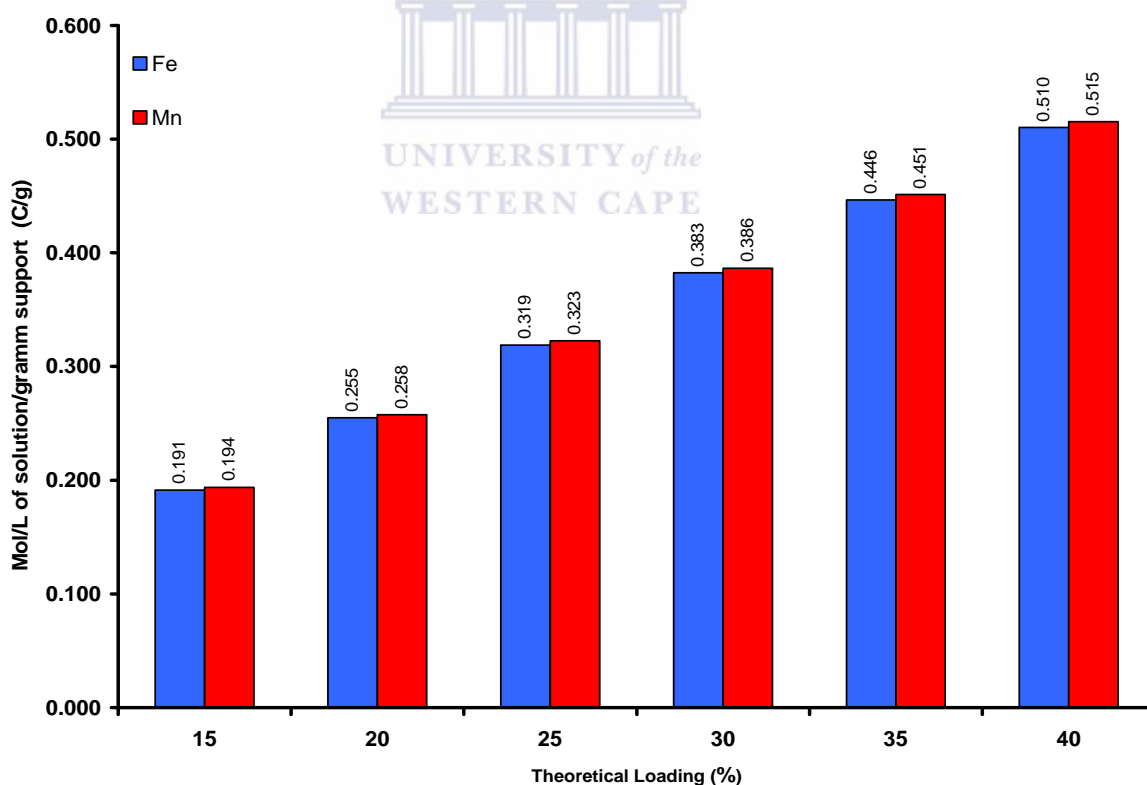


Figure 3-2: Calculated loadings of metal during wet impregnation

The graph as presented here (Figure 3-2), gives the calculated loading based upon the summary of columns 5 and 6 (Table 3.2) showing the equal ratio between iron and manganese which can be seen in column 7.

3.3.3 Catalysts prepared by ion exchange using MCM - 41 as support

3.3.3.1 Methodology

2 grams of MCM-41 were weighed and placed in a small dish. $\text{Fe}(\text{NO}_3)_3 \cdot 9\text{H}_2\text{O}$ and $(\text{CH}_3\text{COO})_2 \cdot \text{Mn} \cdot 4\text{H}_2\text{O}$ in an atomic ratio (Fe: Mn) of 1/1 were weighed as calculated and both dissolved in 7 mL ultra-pure water (see Table 4.2). The mixture was poured into the porcelain dish and stirred together with the amount of MCM-41 previously placed in the dish for 24 hours. After stirring for 24 hours, the mixture was washed with 30 ml of de-ionized water and filtered under suction. The powder obtained was dried in the oven at 100 °C for 10 minutes and finally placed inside a muffle furnace for calcination at 400 °C for 4 hours at a temperature ramp of 2 °C per minute.

3.3.3.2 Calculated metal loading results

Table 3.3 summarizes what loading ideally the support could take up by ion exchange; these calculated amounts were compared with the actual loading results obtained by Electron Dispersive Spectroscopy (EDS), Inductive Coupled Plasma (ICP) and Atomic Adsorption Spectroscopy (AAS), and are presented in chapter 4, section 4.2.2

Table 3.3: Calculated metal loading used for ion exchange

Samples	Aimed Fe and Mn loading (Wt %)	Mass of $\text{Fe}(\text{NO}_3)_3 \cdot 9\text{H}_2\text{O}$ per 2 g of support (g) *	Mass of $\text{Mn}(\text{CH}_3\text{COO})_2 \cdot 4\text{H}_2\text{O}$ per 2 g of support (g) *	Mol of Fe per L of solution per g support **	Mol of Mn per L of solution per g support **	Fe:Mn actual ratio	Obtained total loading
Ion 15	15	1.092	0.555	0.036	0.037	1:1	0.073
Ion 20	20	1.454	0.739	0.048	0.049	1:1	0.097
Ion 25	25	1.822	0.925	0.060	0.061	1:1	0.121
Ion 30	30	2.184	1.112	0.072	0.073	1:1	0.145
Ion 35	35	2.553	1.295	0.084	0.085	1:1	0.170
Ion 40	40	2.914	1.481	0.097	0.097	1:1	0.194

*Mass (g) of salt per 7 mL of de-ionized water before washing with 30 ml of water

**Mol of metal per 7 mL of de-ionized water before washing with 30 ml of water

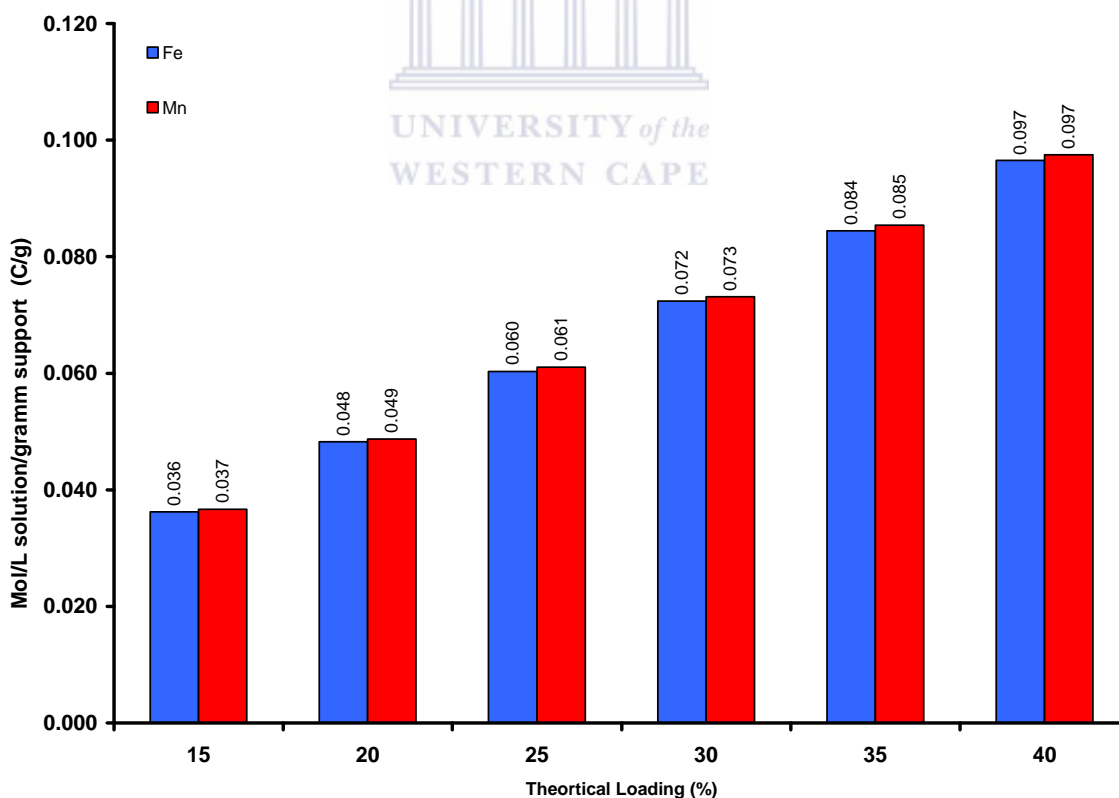


Figure 3-3: Calculated loading of metal after ion exchange.

The above graph (Figure 3-3), shows the calculated loading ratio of one to one between iron and manganese (column 7) showing the equal ratio between iron and manganese which can be obtained by dividing column 5 by 6 in Table 3.2.

3.3.4 Catalysts synthesized by wet and ion exchange using H-Beta-25 as support

3.3.4.1 Ion exchange

The H-Beta zeolite (mass: 2g) was added to aliquots of 20 mL $\text{Fe}(\text{NO}_3)_3 \cdot 9\text{H}_2\text{O}$ aqueous solutions of different concentrations (0.05; 0.01; 0.1 and 0.2 M). The mixture was adjusted to pH 7 with a solution of ammonium hydroxide (NH_4OH) and kept under agitation at room temperature for 24 hours. Next, the suspension was filtered and washed with de-ionized water in order to completely remove any occluded salt, and the solid was then air dried at 100 °C for 10 minutes and then calcined under nitrogen atmosphere at 400 °C for 4 hours at a temperature ramp of 2 °C per minute in order to reduce the oxide into its metal form.

3.3.4.2 Wet impregnation

Iron was incorporated into H-Beta-25 (mass: 5 g) through impregnation; this was achieved by dissolving 0.25 g and 0.2 g of $\text{Fe}(\text{NO}_3)_3 \cdot 9\text{H}_2\text{O}$ in 7 mL of de-ionized water to achieve the aimed loading capacity of 5 and 10 Wet % respectively. The volume of water used for the experiment is the optimum amount of water required to just wet the porous solid. After vigorously stirring the mixture at room temperature, the sample was kept under vacuum at room temperature for a few hours in order to remove the remaining amount of water. The final product was dried at 100 °C for 10 minutes and then calcined under nitrogen atmosphere at 400 °C for 4 hours at a temperature ramp of 2 °C per minute in order to reduce the oxide into its metal form.

The following table (Table 3.4) provides the names and a short description of different zeolites supported catalysts that are going to be used throughout the thesis. Here the support used is the H-Beta-25 zeolite.

Table 3.4: Nomenclature and short description of different catalysts using H-Beta as support

Catalyst names	Description	Catalyst names	Description
0.01/Fe-Beta-25	Synthesis by ion exchanged with a 0.01 M solution of $\text{Fe}(\text{NO}_3)_3 \cdot 9\text{H}_2\text{O}$	5 %-Fe-Beta-25	Synthesis by wet impregnated with 5 wt% of $\text{Fe}(\text{NO}_3)_3 \cdot 9\text{H}_2\text{O}$
0.05/Fe-Beta-25	Synthesis ion exchanged with a 0.05 M solution of $\text{Fe}(\text{NO}_3)_3 \cdot 9\text{H}_2\text{O}$	10 %-Fe-Beta-25	Synthesis by wet impregnated with 10 wt% of $\text{Fe}(\text{NO}_3)_3 \cdot 9\text{H}_2\text{O}$
0.1/Fe-Beta-25	Synthesis by ion exchanged with a 0.2 M solution of $\text{Fe}(\text{NO}_3)_3 \cdot 9\text{H}_2\text{O}$	H-Beta-25	Dried and calcined support
0.2/Fe-Beta-25	Synthesis by ion exchanged with a 0.1 M solution of $\text{Fe}(\text{NO}_3)_3 \cdot 9\text{H}_2\text{O}$		

3.4 Characterization and set up conditions details

3.4.1 Scanning electron microscopy and electron dispersive spectroscopy (Elemental mapping)

3.4.1.1 Sample preparation

A carbon tape is placed on top of a specimen holder and a small representative amount of fine powder is dusted on the tape, and the specimen is introduced into the SEM instrument. The SEM is coupled with an EDS detector using GENESIS software for elemental analysis.

3.4.1.2 Set up conditions

The experimental set conditions of the SEM instrument are presented in Table 3.5

Table 3.5: Instrument details for SEM and EDS

Name of the instrument	Hitachi X 650 Scanning electron microscope
Applied voltage	30kV
Current	1 μ A
Illumination	0.1mrad
Magnification	0.35x to 1Kx
Resolution	Depending on the experiment
Working distance	15 nm

3.4.2 High resolution transmission electron microscopy

3.4.2.1 Sample preparation

A small amount of the respective powder samples were diluted in 5 ml of methanol; the suspensions were vigorously shaken for few seconds and placed in an ultrasonic vessel for 5 minutes. A drop of the suspension was deposited on a copper grid and dried at room temperature. Set up conditions are shown in Table 3.6

3.4.2.2 Instrumental set up conditions

The experimental set conditions of the HRTEM instrument are presented in Table 3.6

Table 3.6: Instrument details of HR-TEM

Name of the instrument	Technai G ² F 20 X-Twin MAT
Applied voltage	200Kv
Emission current	48 μ A
Illumination angle	15°
Magnification	Depending upon the experiment
Resolution	0.24 nm
Exposure time	Depending upon the experiment

3.4.3 Selected area electron diffraction

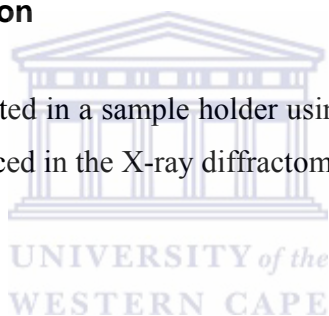
Sample grids from the transmission electron microscopy (TEM) study were retained for SAED analysis. The SAED pattern was obtained using the same instrument used for HR-TEM and the patterns were recorded using the same instrumental set up conditions.

3.4.4 X-ray diffraction spectroscopy

The X-ray diffraction experiments were performed on two different machines, one for low angle and a second one for wide angle. Experimental details are shown in Table 3.9 and 3.10.

3.4.4.1 Sample preparation

The catalyst powder was mounted in a sample holder using a spatula to make the surface of the sample even and introduced in the X-ray diffractometer.



3.4.4.2 Set up conditions

The experimental set conditions of the XRD instrument are presented in Table 3.7 and 3.8

Table 3.7: XRD instrumental set up conditions (wide angle)

Name of the instrument	Phillips PW 3830/40 Generator with PW 3710 mpd
X- ray detector	X pert data collector
Generator voltage	40 kv
Generator current	25 mA
Scanning range (2θ)	2.01° to 45.99°
Scan type	Continuous
Scan speed per step	0.50 sec
Scan time	40 minutes
Step size	0.02°
Synchronous rotation	

Table 3.7: XRD instrumental set up conditions (low angle)

Name of the instrument	D8 Advance from Bruker AXS
X- ray detector	Vantec-1
Generator voltage	40 kv
Generator current	40 mA
Scanning range (2θ)	$0.4 < 2\theta < 7.99$
Scan type	Locked coupled
Scan speed per step	Enough for good statistic
Scan time	Not given
Step size	0.03°
Synchronous rotation	Copper K alpha at 1.540598

3.4.5 N₂-B.E.T (BRUNAUER- EMMET-TELLER)

3.4.5.1 Sample preparation

0.5 mg of the catalyst powder was weighed and degassed by flowing He at 90 °C for 1 hour, then held at 350 °C for 16 hour. As the temperature increased, water vapour was desorbed from the surface and pores of the sample. The sample was then cooled down and weighed again. The TriStar machine (3000 Analyser, model 060) uses physical adsorption and capillary condensation principles to obtain information about surface area and porosity of solid materials.

3.4.5.2 Set up conditions

The experimental set conditions of the N₂-BET instrument are presented in Table 3.9

Table 3.9: Instrumental set up conditions for N₂-BET

Name of the instrument	Micrometrics Tri Star 3000 Analyser
Gas	Nitrogen
Pressure table	26 points (26 adsorption and 26 desorption)
Pressure range	0 to 999 mmHg

3.4.6 Fourier transformed infrared spectroscopy

3.4.6.1 Sample preparation

The machine was first cleaned and set up to obtain a background spectrum trial before the analysis. A small amount of the catalyst powder was placed on the crystal of an attenuated total reflectance (ATR) cell where a required force is applied for the analysis to be conducted. A spectrogram was obtained depending on the characteristic of the sample.

3.4.6.2 Set up conditions

The experimental set conditions of the FTIR instrument are presented in Table 3.10

Table 3.10: Instrumental set up conditions for FTIR

Name of the instrument	Perkin Elmer® (Universal ATR)
Scan range	4000 to 380 cm^{-1}
Scan number	5
Resolution	4 cm^{-1}
Pressure gauge	140

3.4.7 Thermo-gravimetric analysis

3.4.7.1 Sample preparation and experimental conditions

100 mg of the catalyst was placed into an alumina cup that is supported on an analytical balance located outside the furnace chamber. The balance is zeroed, and the sample cup is heated at 2 °C per minute until it reaches 600 °C as the maximum temperature. The balance sends the weight signal to the computer for storage, along with the sample temperature and elapsed time. The TGA curve plots the TGA signal, converted to percent weight change on the Y-axis against the reference material temperature on the X-axis.

3.4.7.2 Set up conditions

The experimental set conditions of the TGA instrument are presented in Table 3.11

Table 3.8: Instrument details for TGA

Name of the instrument	Q500 thermogravimetric analyzer
Heating ramp	2 °C/min
Maximum temperature	600 °C
Gases	Synair as reactive gas and nitrogen as pure gas
Flow rate	Synair 30mL/ min and N ₂ 30 mL/min

3.4.8 Temperature programmed reduction

3.4.8.1 Sample preparation and experimental conditions

The catalyst (0.1 g) was placed in a quartz tubular reactor. The reactor was heated in a furnace. Prior to the temperature programmed reduction measurement, the catalysts were flushed with high purity argon at 150 °C for 30 min, and then cooled down to 50 °C. Then 5% H₂/Ar was switched on and the temperature was raised at a rate of 10 °C/min from 50 to 800 °C (held for 1 min). The gas flow rate through the reactor was controlled by three Brooks mass flow controllers and was always 50 cm³ min. The H₂ consumption (TCD signal) was recorded automatically by a PC.

3.4.8.2 Set up conditions

Table 3.12 presents the instrumental set up conditions for the TPR machine

Table 3.9: Instrumental set up conditions for TPR

Name of the instrument	Micrometrics Auto Chem
Gas flow	50 ml/minute
Heating ramp	10 °C/minute
Maximum temperature	800 °C
Gas	H ₂ /Ar

3.5 Experimental set-up for SCR

The following section is an introduction to the gas phase catalysis; it gives the necessary starting materials for screening tests at the laboratory scale in terms of gases that must be used, the rig testing design system and few recommendations. Columns and other aspects for gas identification methods are not discussed at this stage.

3.5.1 Schematic of the rig design

Due to the presence of NO, the fittings and pipeline of the NO_x catalytic testing test reactor system were coated with a Restek Sulfinert treatment. This was to prevent the organo-sulfur compounds from adsorbing and prevent them from reacting with the uncoated steel or stainless steel surfaces. The gas analysis of the product stream after the SCR reaction was investigated by use of gas chromatography for screening tests. The proposed design of the test rig for screening tests is shown in Figure 3-4.

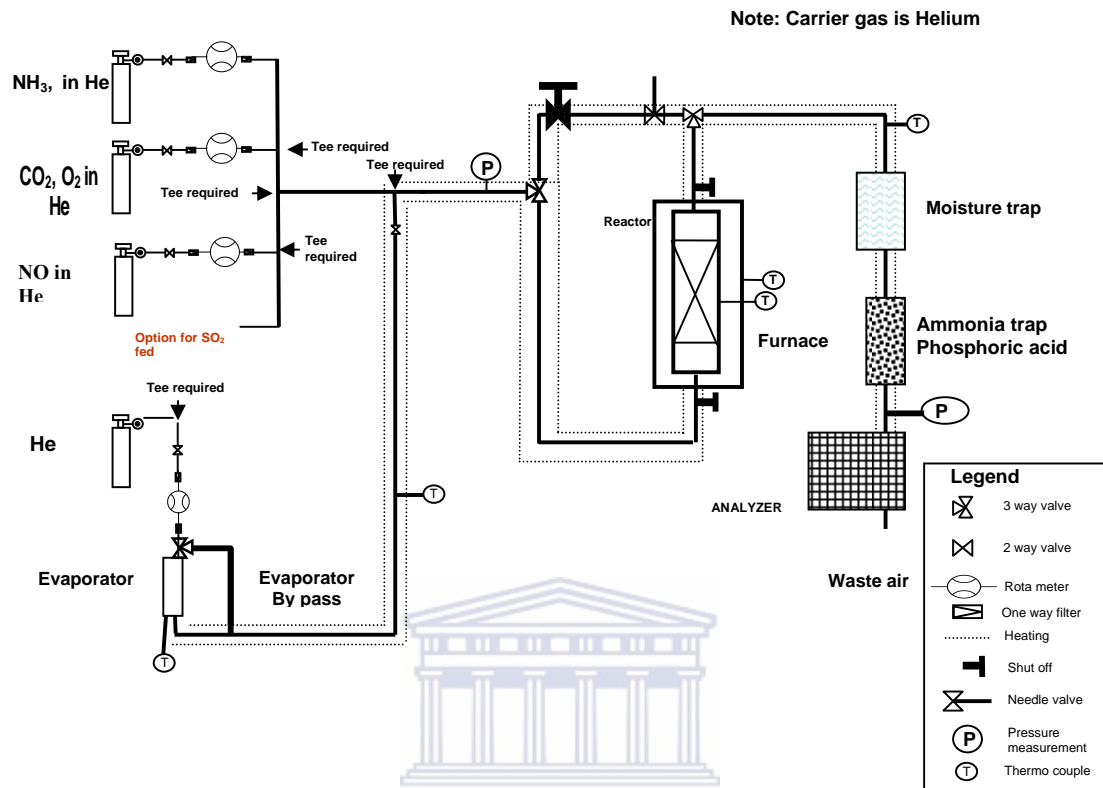


Figure 3-4: Schematic of the rig design

The DeNO_x feed gas mixture was pre-mixed to have a composition similar to the typical flue gas composition of ESKOM coal fired power plant, but due to the fact that the experiment was aimed to compare conversion of NO, few components such as: N₂, N₂O, CO and SO₂ were removed. Table 3.13 shows a typical ESKOM flue gas composition as basis of the adapted test gases and Table 3-14 shows the actual mixtures for the laboratory scale.

Table 3.10: Typical flue gas composition analysis on a vol/vol dry basis for ESKOM power stations

Compound	Amount	Unit
O ₂	8.6	%
CO ₂	9,4	%
CO	96	ppm
SO ₂	556	ppm
NO	90 % of total NO _x	
NO _x	495	ppm
N ₂ O	5 to 10	ppm
N ₂	80.7	%
H ₂ O	5.1	%

3.6 Nitrogen oxide screening tests

The following pre-mixed gas compositions were used for the screening tests. During this study, helium has been used as a carrier gas instead of nitrogen as commonly done in order to simplify the analysis of the product stream. The pre-mixed feed gas was ordered from Air Liquid Ltd and its composition is given in Table 3.14

Table 3.11: DeNO_x feed gas composition for screening tests

Compound	Amount	Unit
NO/He	1000	ppm
NH ₃ /He	1000	ppm
CO ₂ /He	10	%
O ₂	5	%
He	100	%
H ₂ O (Moisture) when needed	5 to 8	%

CHAPTER 4

4 RESULTS AND DISCUSSION

4.1 Characterization of catalysts

4.1.1 Introduction

This chapter presents the results of metal loading procedures and different physico-chemical characterization techniques used for characterization of the catalysts including the carriers used for the synthesis of the final catalysts. Carriers used for the synthesis of the catalysts include MCM-41 (mesoporous silica) and zeolites H-Beta-25 both loaded by wet impregnation and ion exchange. In the case of MCM-41, iron nitrate combined with manganese acetate were used as metal sources; in the case of H-Beta-25 zeolites only iron nitrate was used as metal source. The chapter will start by outlining the preparation procedures used and calculations done for the synthesis of each catalyst and the obtained loading of each catalyst are summarized in different tables after analysis of the digested catalyst by atomic adsorption (AAS) and inductive coupled plasma (ICP). Physico-chemical techniques used for a better understanding of the synthesized catalysts include in the present case: nitrogen adsorption BET for pore size distribution and surface area information; low and wide angle XRD for phase identification on the support after calcination; high resolution transmission electron microscopy to assess the presence of metal particles inside the pores of the support. FTIR, TGA, SEM, TPR, and elemental mapping techniques were used to support some of the techniques mentioned above to provide adequate conclusions on the catalyst characteristics.

4.1.2 Morphological study by scanning electron microscopy and electron dispersive spectroscopy (Elemental mapping)

The scanning electron microscopy was conducted on a Hitachi X 650 Scanning electron microscope according to the procedure described in section 3.4.1.1.

Figure 4-1 presents the SEM images of the support (a) and three different catalysts synthesized by wet impregnation and loaded at 20 wet % (b), 30 wet % (c) and 40 wet % (d).

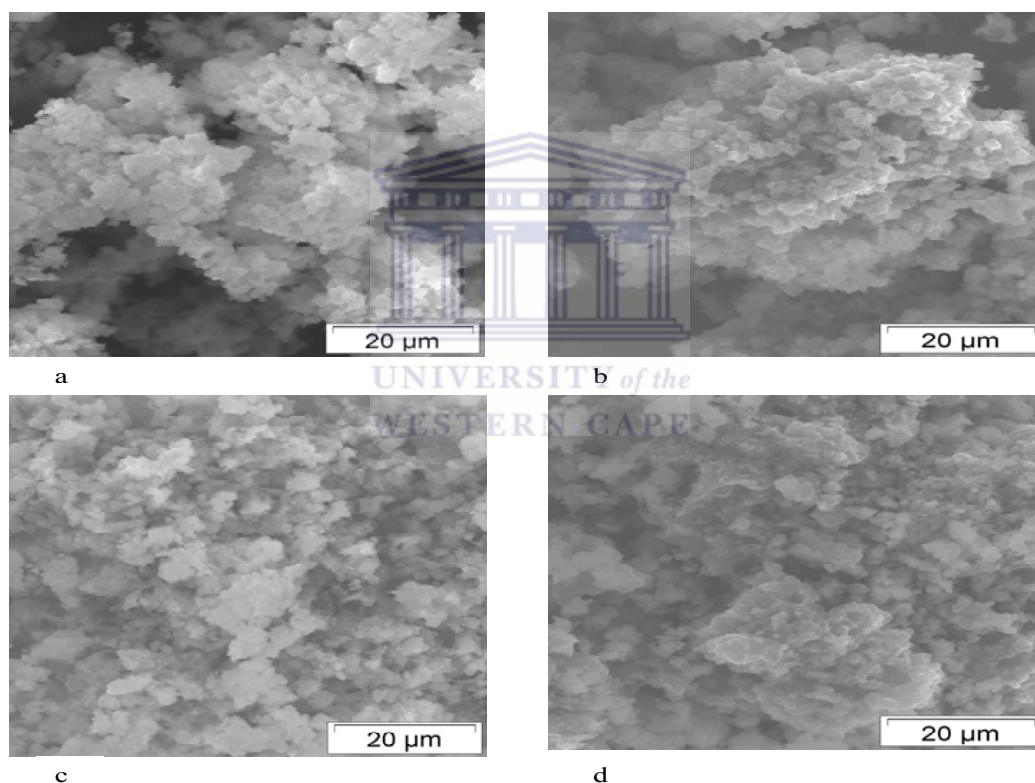


Figure 4-1: SEM images of the support (a) and three other catalysts (wet 20, 30 and 30 %) synthesized by wet impregnation.

The SEM pictures of the support (Figure 4-1 a) represents the small nearly submicron agglomerated somewhat spherical particles of the host silica (MCM-41) and the supported bimetallic catalysts (Figure 4-1 b, c and d) show a similar morphology. Similar

observations were made by Ajaikumar when analyzing the images of the $\text{ZrO}_2/\text{Al}_2\text{O}_3$ supported MCM-41 (Ajaikumar et al., 2009). At this scale it is impossible to see the metal crystallites which are in the Angstrom size range 10^{-10} m. The SEM technique only shows the particulate structure of the MCM-41; in order to confirm the presence of the sub-micron spherical agglomerations seen with the SEM technique, the elemental mapping distribution accompanied with electron dispersive spectroscopy of the same catalysts was conducted to assess the distribution of metals on the catalysts.

Figure 4-2 shows an HR-SEM image of a single spot on a wet 30 catalyst (see Table 3.1) where the magnification cannot be seen on the photo because of the mapping, this image is completely different from an image taken for SEM, see Figure 4-1.

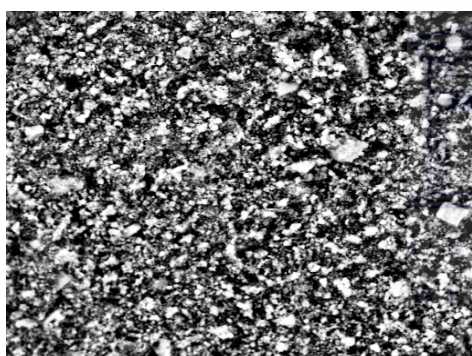
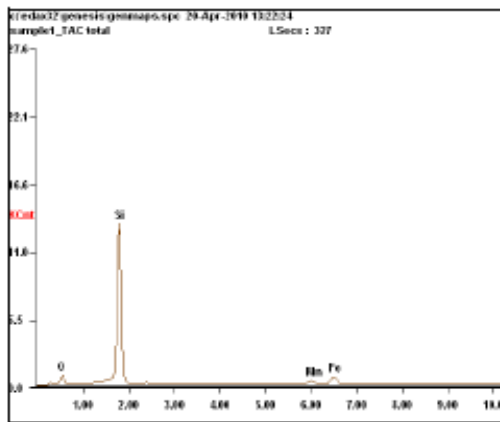
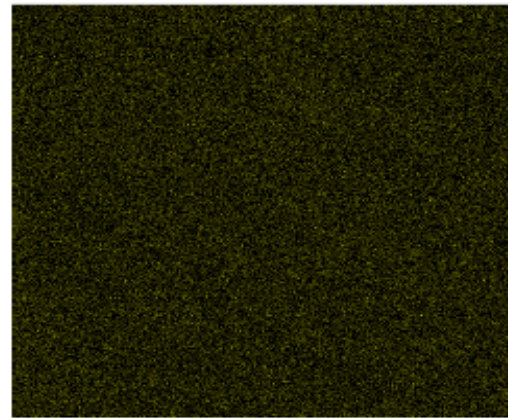


Figure 4-2: SEM spot image of the 30 wet % loaded MCM-41 by wet impregnation. (Live image on the machine without magnification)

Figure 4-3 shows the mapping distribution of the four elements present on the catalyst, the EDS graph of the catalyst is also shown as well as the over-layer image of the four elements put together.



a. EDS spectra of the wet 30



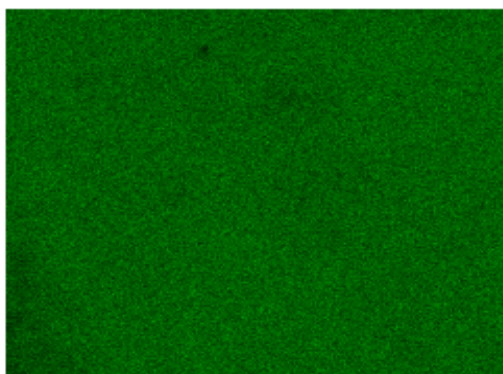
b. Fe distribution



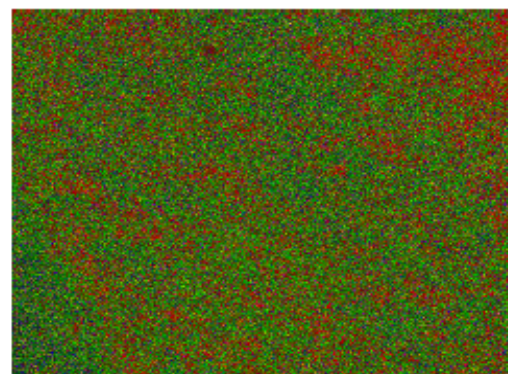
c. Mn distribution



d. Oxygen distribution



e. Silica distribution



f. Overlay of all elements

Figure 4-3: Elemental composition of four different elements on the MCM – 41.

The EDS graphs of the four elements of sample Wet 30 (Figure 4-3) shows that silica is the most abundant element on the catalyst (Figure 4.3 a). This is normal since the parent material MCM-41 used is mainly composed of silica and oxygen. The yellow image (Figure 4-3 b) shows the distribution of Fe on the support; the image reveals a well-dispersed iron phase on the catalyst. The blue image (Figure 4-3 c) shows the distribution of Mn phase on the support; the image also reveals well-dispersed manganese on the substrate. The red image (Figure 4-3 d) shows the distribution of O₂ on the substrate, since O₂ is part of the support, it is normal to see a very well dispersion on the support. (Figure 4-3 e) shows the distribution of silica on the support; with silica being part of the support, it is normal to see a high dispersion of this ion. The last image (Figure 4-3 f) shows the over-layer of the four images put together. At this resolution the mapping merely indicates the relative abundance of each element and its global distribution.

Figure 4-4 shows an HRSEM image taken for elemental mapping; this image does not have a well-defined magnification because it was used for mapping analysis. The catalyst analyzed here is an Ion 30 % (see Table 3.1).

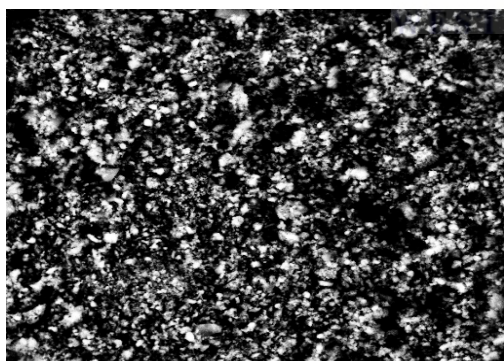


Figure 4-4: SEM image of Ion 30 catalyst synthesized by ion exchange (Live image on the machine without magnification).

Figure 4-5 shows the EDS spectra as well as the mapping of three elements present on the Ion 30 catalyst.

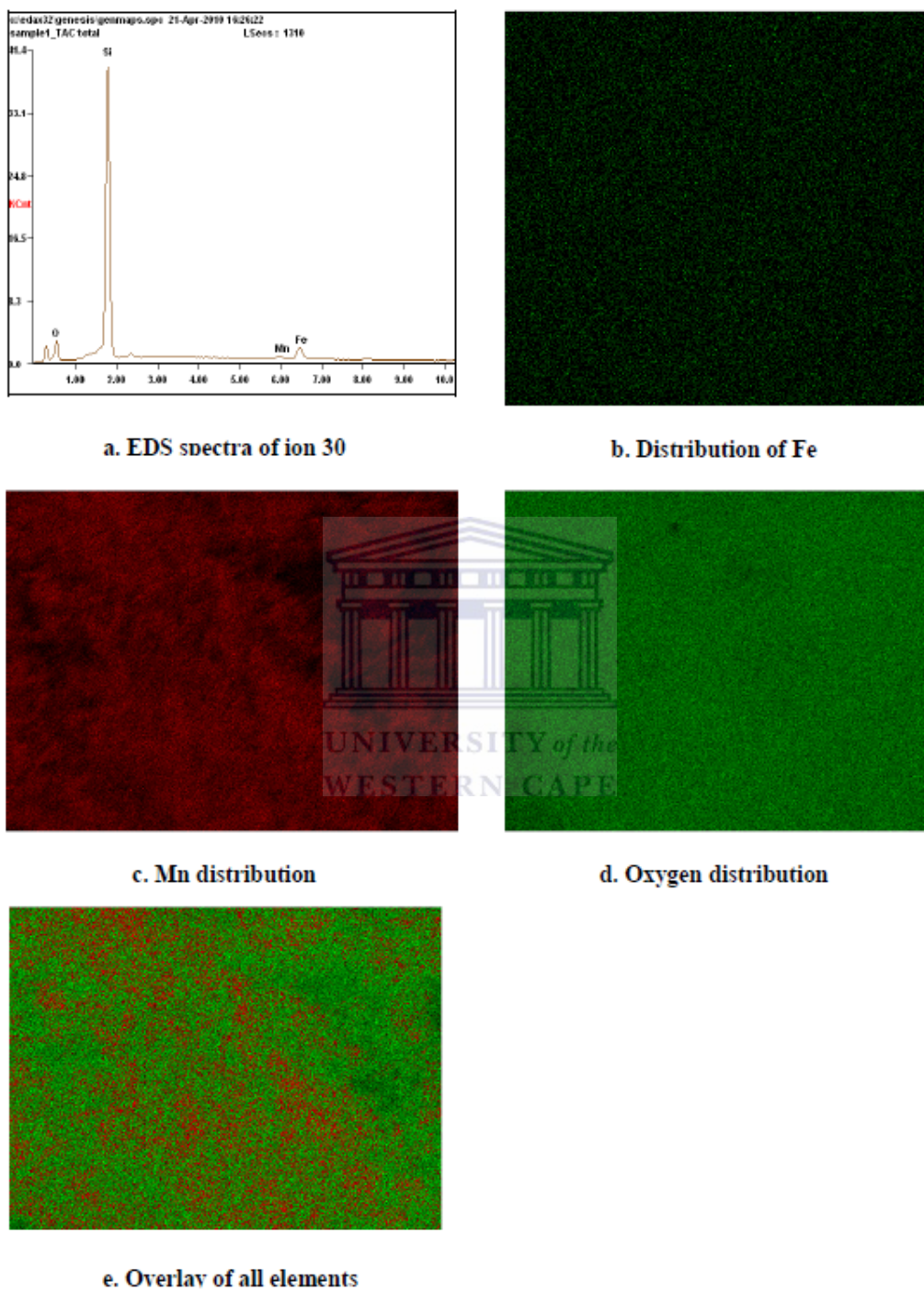


Figure 4-5: EDS as well elemental mapping of three (Si, O₂, Fe) different elements of the Ion 30 catalyst.

The EDS signal of the ion 30 catalyst (Figure 4-4 a) shows four elements (Si, O₂, Mn and Fe) on the catalyst with a very weak signal of manganese that needs to be confirmed by elemental analysis to see if the element really exist on the catalyst. Figure 4-4 b shows the iron distribution on the support; Fe still well dispersed on the support despite the change of the loading method. Figure 4-4 c and d show well distributed ions of O₂ and Silica respectively. These two signals are very strong since they are the two main components of the support. The SEM results are followed by the EDS to confirm the presence of the two metals on the support; the wet impregnated catalysts were first studied, followed by the ion exchange catalysts.

The EDS and the elemental mapping results have shown that, it was possible to synthesis two well dispersed catalysts by both iron exchange and wet impregnation; the elemental mapping results of the ion exchange catalysts have confirmed the absence of manganese of the substrate while the elemental mapping results of the wet impregnated catalysts have confirmed the presence of both iron and manganese on the catalyst. The results obtained at this stage need to be confirm by analytical technique such as EDS, ICP and AAS.

4.1.3 Elemental composition study by electron dispersive spectroscopy on wet impregnated samples

The elemental compositions of the catalysts were determined using EDS with a Hitachi X 650 Scanning electron microscope (section 3.4.1.1); details of the experimental procedure can be found in section 3.4.1.2. EDS results are much more qualitative than quantitative due to the fact that only a small fraction of the sample can be analyzed and due the fact that the analysis is done on different spots where the composition of the sample may vary, that is why up to 15 to 50 spots should be analyzed and the final result will be the average. In the present case, the results obtained were an average of 15 spots analyzed on a single sample. The inhomogeneous aspect of the catalyst must be taken into account when comparing the EDS results to the results obtained by AAS and ICP.

Columns 3 and 4 in Table 4.1 show the actual atomic loading obtained on the catalysts using EDS analysis done on wet impregnated samples prepared as is described in section 3.3.2.

Table 4.1: Electron Dispersive Spectroscopy results of wet impregnated samples

Samples	Aimed loading of Fe and Mn (Wt %)	Atomic contribution of Fe (At %) EDS	Atomic contribution of Mn (At %) EDS	Fe:Mn actual ratio EDS **	Obtained total metal loading Fe+Mn (At %) EDS
Wet 15	15	4.03	3.27	1.23:1	7.3
Wet 20	20	4.51	3.84	1.17:1	8.35
Wet 25	25	6.07	5.82	1.04:1	11.89
Wet 30	30	7.04	6.6	1.07:1	13.64
Wet 35	35	8.27	6.87	1.20:1	15.14
Wet 40	40	8.31	6.42	1.29:1	14.72

* Atomic ratio between Fe and Mn (column 3 divided by column 4)

** Atomic ratio between Fe and Mn (column 5 divided by column 6)

The elemental compositions based on Fe and Mn loading by wet impregnation was obtained after EDS (column 3 and 4, Table 4.1) and showed the approximate ratios of Fe and Mn, with iron being the more dominant metal component than manganese in each case. These EDS results are an average of 15 EDS analysis spots analyzed on a single sample, making the analysis more qualitative than quantitative. Results obtained with this method cannot be compared with quantitative results obtained by ICP and AAS. The presence of iron and manganese on the support will be confirmed further using ICP and AAS as shown in section 4.2.1.1 and 4.2.1.2. These results as obtained mean that more iron was incorporated on the support than manganese which indicates preferential adsorption of iron during wet impregnation. Discussion on the wet impregnation and ion exchange results will be presented in sections 4.2.1 and 4.2.2.

4.1.4 Elemental composition study by electron dispersive spectroscopy on ion exchange samples

The elemental composition of ion exchange samples as determined by EDS are presented in Table 4.4 and were obtained using a Hitachi X 650 Scanning electron microscope (section 3.4.1.1); details of the experiment procedure can be found in section 3.4.2.1. The EDS results in general are much more qualitative than quantitative, that aspect should be taken into account when comparing the following EDS results to the results obtained by ICP and AAS analysis on the same sample. In the present case, the result obtained is an average of 15 spots analyzed on a single sample. The inhomogeneous aspect and the small sample size of the catalyst must be taken into account when comparing EDS results to the results obtained by AAS and ICP.

Columns 3 and 4 in Table 4.4 show the actual loading obtained after EDS on ion exchanged samples prepared as is described in section 3.3.3.

Table 4.2: Electron dispersive results of the ion exchanged samples

Samples	Aimed Fe and Mn loading (Wt %)	Atomic contribution of Fe (At %)*	Atomic contribution of Mn (At %)* EDS	Fe:Mn actual ratio** EDS	Obtained total loading (At %) EDS
Ion 15	15	1.97	0.58	3.40:1	2.55
Ion 20	20	2.34	0.73	3.21:1	3.07
Ion 25	25	2.09	0.4	5.23:1	2.49
Ion 30	30	2.31	0.42	5.50:1	2.73
Ion 35	35	0.45	1.67	1:3.71	2.12
Ion 40	40	0.08	1.59	1:19.88	1.67

*Mass (g) of element per 7mL of de-ionized water before washing with 30 mL of water

** Atomic ratio between Fe and Mn (column 5 divided by column 6)

The EDS result (column 5, Table 4.4) shows the actual ratios obtained with iron being the dominant component compared to manganese. The data obtained at this level reflects an interesting behaviour of iron to manganese when the two are competing for the same ion

exchange site on the support. Results obtained with this method cannot be compared with quantitative results obtained by ICP and AAS.

The two EDS results have revealed that the ratios of Fe and Mn on the support is closer to one by one for the wet impregnated catalysts (columns, 5 Table 4.1) and not one by one as claimed by Huang et al., (2008) and his co-workers when wet impregnation and ion exchange are used as methods of synthesis, and the ratio for the ion exchanged catalysts is above one to one for the ion exchanged catalysts (columns, 5 Table 4.4). To confirm the elemental mapping results (Figure 4-4) of the ion exchange samples, the signals obtained during the EDS (Column 4, Table 4.4) show very weak signals which confirms the finding during the elemental mapping where the signal was absent on the catalysts.

4.2 Catalyst preparation and mass balance of the synthesis procedure

The two sets of catalysts Fe/Mn-MCM-41 were prepared by wet impregnation and ion exchange as described in the experimental chapter (section 3.3.2 and 3.3.3).

4.2.1 Metal content determination of catalysts prepared by wet impregnation

For metal content determination on the support, a portion of the catalysts was digested in aqua-regia (HCl: 1 and HNO₃: 3) prepared adequately respecting the ratio of each acid. The obtained solutions after digestion were analyzed by AAS and ICP.

In order to achieve the digestion, 50 mg of the catalyst was digested in 20 mL of aqua-regia and put for few minutes in a bath sonicator, 6 mL of the solution was diluted and made up to 50 mL of de-ionized water and finally the solution was analyzed by AAS and ICP.

4.2.1.1 Elemental composition study by inductive coupled plasma of wet impregnated samples (Fe – Mn/MCM - 41)

The elemental compositions based on the actual Fe and Mn loading by wet impregnation are given in columns 3 and 4 of Table 4.3 and were obtained after digesting 50 mg of the catalysts in 20 mL of aqua regia solution. 6 mL of the obtained solution was diluted to 50 mL with de-ionized water and analyzed by ICP.

Table 4.3: Inductive coupled plasma results of the wet impregnated samples

Samples	Aimed loading of Fe and Mn (Wt %)	Mol of Fe per L of solution per g support ICP*	Mol of Mn per L of solution per g support ICP*	Fe:Mn actual ratio ** ICP	Obtained total loading Fe+Mn (Mol/g) ICP
Wet 15	15	0.167	0.164	1.02:1	0.331
Wet 20	20	0.203	0.208	0.98:1	0.412
Wet 25	25	0.280	0.281	1.0:1	0.562
Wet 30	30	0.303	0.297	1.02:1	0.600
Wet 35	35	0.402	0.408	0.98:1	0.810
Wet 40	40	0.363	0.367	0.99:1	0.780

* Mol/g of element per 7 mL of de-ionized water

** Ratio between Fe and Mn (column 3 divided by column 4)

The results obtained after ICP analysis (column 5, Table 4.3) further confirm the ratios obtained, with iron being the more dominant metal component than manganese. This was further confirmed with AAS as is given in section 4.2.1.2. Columns 3 and 4 show the obtained loading after analysis by ICP. The first step in this study was to determine the method deviation and the error that comes with it; for this purpose, two standard solutions were analyzed and the error coming from that analysis was 0.01 or 1%, this error as determined will serve as reference for the rest of the results that will be obtained from the ICP instrument. The results as obtained showed more Fe than Mn on the catalysts, achieving a ratio of nearly 1 to 1 for the first sample loaded at wet 15 and below 1 in Fe and Mn for the remaining catalysts except for the wet 25 and wet 30. These results as obtained are going to be compared to the AAS results obtained on the same

samples and a conclusion based on a comparative study between the two methods will be discussed further down for a proper conclusion on the loading of bimetallic oxides onto the mesoporous support.

4.2.1.2 Elemental composition study by atomic adsorption spectroscopy after digestion of wet impregnated samples

The elemental composition based on Fe and Mn loadings by wet impregnation are given in columns 3 and 4 of Table 4.4 and show the metal loading results obtained after digesting 50 mg of the catalysts into 20 mL of aqua regia solution. 6 mL of the obtained solution was diluted to 50 mL with de-ionized water and analyzed by AAS.

Table 4.4: Atomic adsorption spectroscopy results of the wet impregnated samples

Samples	Aimed loading of Fe and Mn (Wt %) *	Mol of Fe per L of solution per g support AAS	Mol of Mn per L of solution per g support AAS	Fe:Mn actual ratio AAS	Obtained total loading AAS
Wet 15	15	0.093	0.040	2.29:1	0.133
Wet 20	20	0.127	0.046	2.74:1	0.173
Wet 25	25	0.175	0.068	2.56:1	0.243
Wet 30	30	0.169	0.067	2.54:1	0.236
Wet 35	35	0.189	0.090	2.09:1	0.279
Wet 40	40	0.240	0.098	2.46:1	0.338

* Mol/g of element per 7 mL of de-ionized water

** Ratio between Fe and Mn (column 5 divided by column 6)

The AAS result (column 5, Table 4.4) shows the actual Fe: Mn composition with iron being the more dominant component. Achieving for all the catalysts synthesized a ratio above 2 for Fe compared to Mn in most cases.

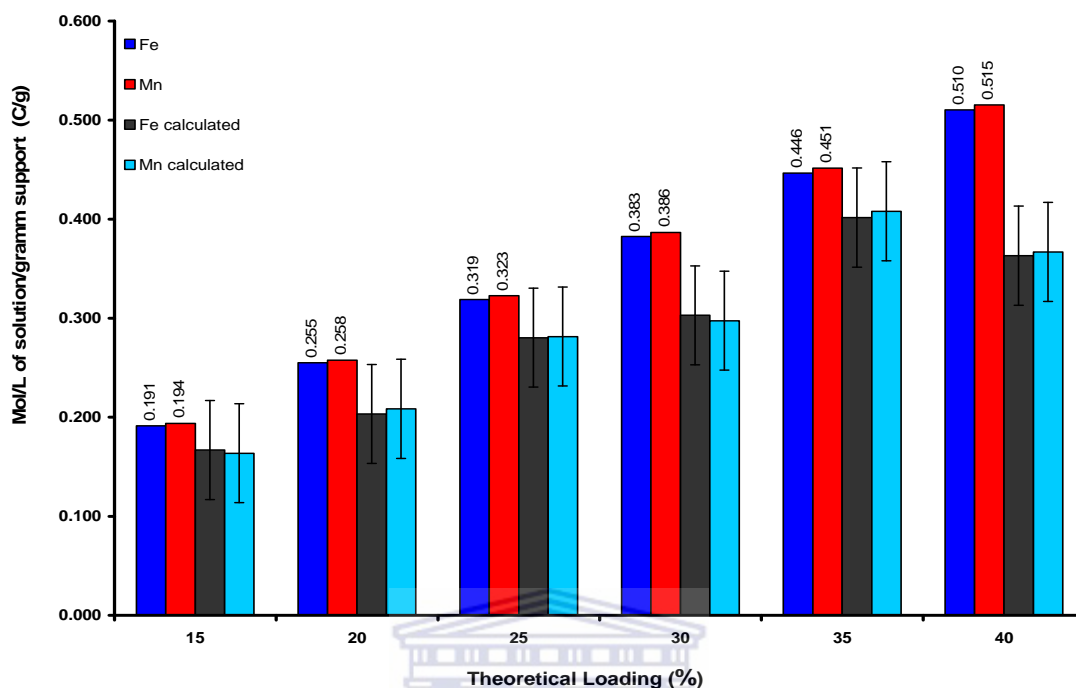


Figure 4-6: Summary of the loading procedure of wet impregnation samples.

The above graph (Figure 4-6), shows a comparison between the calculated amount loaded on the support and the actual analyzed loading (weight %) obtained after digestion of the catalyst in aqua regia; the ICP technique shows an accuracy of 1 % of deviation since two standards of Fe and Mn were run on the machine prior to the analysis of the digested catalysts. Despite the impregnation of the two metals oxides at a ratio of one over one, iron was found to be present at higher concentration than manganese, but both are below the theoretical concentration of one to one ratio showed in Figure 3-2. The difference between the theoretical results and the calculated results has been attributed to the matrix effect accompanying the ICP analysis and as a method of analysis; other factors attributed to that difference is for example the error during the preparation of the catalysts.

4.2.2 Metal content determination of ion exchange catalysts

4.2.2.1 Elemental composition study by inductive coupled plasma of ion exchanged samples (Fe – Mn/MCM - 41)

The elemental compositions of the ion exchanged samples Fe-Mn/MCM – 41 are given in columns 3 and 4 of Table 4.5 and these results were obtained after digesting 50 mg of the ion exchanged catalysts with 20 mL of aqua regia solution. 6 mL of the obtained solution was diluted to 50 mL with de-ionized water and analyzed by ICP.

Table 4.5: Inductive coupled plasma of ion exchanged catalysts

Samples	Aimed Fe and Mn loading (Wt %)	Mol of Fe per L of solution per g support ICP	Mole of Mn per L solution per g support ICP	Fe:Mn actual ratio ** ICP	Obtained total loading (Mol/g) ICP
Ion 15	15	0.033	0.012	2.75:1	0.044
Ion 20	20	0.036	0.018	2.00:1	0.054
Ion 25	25	0.046	0.023	2.04:1	0.069
Ion 30	30	0.057	0.026	2.21:1	0.083
Ion 35	35	0.063	0.031	2.02:1	0.094
Ion 40	40	0.074	0.036	2.06:1	0.109

* Mol/g of element per 7mL of de-ionized water after washing with 30 mL of water

** Ratio between Fe and Mn (column 3 divided by column 4)

The ICP results (column 5, Table 4.5) reflect the same behavior as the EDS results (Table 4.2) with a total average ratio reflecting a ratio of 4.93 Fe compared to 1 Mn. The analysis of these results (Table 4.5) in comparison with the expected results (Table 3.2) shows a small deviation in the amount of Fe obtained (0.036 Mol/g theoretical loading and 0.033 Mol/g calculated loading for the ion 15 % catalyst), while the amount in Mn has decreased compared to the theoretical loading (0.012 Mol/g calculated loading and 0.037 Mol/g theoretical loading for the ion 15 % catalyst). These differences have been observed for the remaining samples (see Table 4.5). The decrease in the amount of Mn

has been attributed to the washing of the catalyst, taking away the unattached Mn from the substrate.

The elemental compositions of the ion exchanged samples Fe-Mn/MCM – 41 are given in columns 3 and 4 of Table 4.6 and these results were obtained after digesting 50 mg of the ion exchanged catalysts with 20 mL of aqua regia solution. 6 mL of the obtained solution was diluted in 50 mL of de-ionized water and analyzed by AAS.

Table 4.6: Atomic Adsorption Spectroscopy of ion exchanged catalysts

Samples	Aimed Fe and Mn loading (Wt %)	Mol of Fe per L of solution per g support *	Mole of Mn per L of solution per g support	Fe:Mn actual ratio **	Obtained total loading (Mol/g)
Ion 15	15	0.032	0.014	2.3:1	0.046
Ion 20	20	0.035	0.017	2.1:1	0.052
Ion 25	25	0.043	0.022	1.9:1	0.064
Ion 30	30	0.053	0.032	1.7:1	0.085
Ion 35	35	0.058	0.035	1.7:1	0.093
Ion 40	40	0.063	0.039	1.6:1	0.102

* Mass (g) of element 7 mL of de-ionized water before washing with 30 mL of water.

** Atomic ratio between Fe and Mn (column 3 divided by column 4)

The AAS results (column 5, Table 4.6) show a total average ratio of 2.3 in Fe compared to 1 Mn, the obtained data in columns 3 and 4 are compared with the expected results in Table 3.2. It was observed after analysis of the above Table (4.6) that the amount of Mn has decreased compared to the amount of Fe which remains fairly stable when compared with the theoretical amount predicted in Table 3.2.

4.2.2.2 Elemental composition study by Inductive Coupled Plasma of the filtrate after washing the ion exchanged samples

The synthesis of catalysts gives way to a solution after filtration of the mixture, this solution need to be analyzed because it contains ions washed away from the catalyst, that why a mass balance is required in order to give an idea of how efficient the loading process by ion exchange with MCM-41 took place. Table 4.7 shows the filtrate concentration results obtained after washing of the catalysts as described in section 3.3.3.1

Table 4.7: Filtrate concentration results after washing of the catalysts

Samples	Aimed Fe and Mn loading (Wt %)	Mol of Fe per L solution per g support ICP filtrate	Mol of Mn Per L solution per g support ICP filtrate	Fe:Mn Actual ratio ** ICP filtrate
Ion 15	15	0.004	0.025	1: 6.8
Ion 20	20	0.013	0.031	1: 2.5
Ion 25	25	0.014	0.039	1: 2.7
Ion 30	30	0.015	0.047	1: 3.1
Ion 35	35	0.022	0.054	1: 2.5
Ion 40	40	0.023	0.062	1: 2.7

* Mass (g) of salt per 7ml of de-ionized water before rinsing and 30 ml of water used for rising

** Atomic between Fe and Mn.

The ICP results of the filtrate (Table 4.7) show that the filtrate contains more Mn than Fe which can be seen by the ratio (Fe:Mn) in column 5. The obtained results (columns 3 and 4) mean less iron than manganese in the washed solution.

4.2.2.3 Mass balance of ion exchanged catalysts

Table 4.8 presents the mass balance of the catalysts synthesized by ion exchange since the washing of the catalysts synthesized by wet impregnation has an impact on the metal content on the final dried catalysts.

Table 4.8: Mass balance results of catalysts after ions exchange

Aimed Fe and Mn loading (Wt %) *	Calculated loading (Mol/g)		Filtrate Concentration (Mol/g)		Concentration of digested Samples (Mol/g)		Filtrate + digested samples concentration	
	Fe:Mn		Fe:Mn		Fe:Mn		Fe:Mn	
Ion 15	0.036	0.037	0.004	0.025	0.033	0.012	0.037	0.037
Ion 25	0.048	0.049	0.013	0.031	0.036	0.018	0.049	0.049
Ion 30	0.060	0.061	0.014	0.039	0.046	0.023	0.06	0.062
Ion 30	0.072	0.073	0.015	0.047	0.057	0.026	0.072	0.073
Ion 35	0.084	0.085	0.022	0.054	0.063	0.031	0.085	0.085
Ion 40	0.097	0.097	0.023	0.062	0.074	0.036	0.097	0.098

Table 4.8 reveals that most of the manganese ions are found in the washed liquid or filtrate (column 5) compared to the iron ions which are found in higher concentration on the catalyst than the filtrate (column 7). The Table also reveals the competition between the two ions (Fe and Mn) to attach to the support; this competition favours the trivalent atom (Fe^{3+}) than the divalent atom (Mn^{2+}) (Lang et al., 2002).

Figure 4-7 shows the comparison between the aimed loading vs the actual loading of the ion exchange catalysts after analysis by ICP.

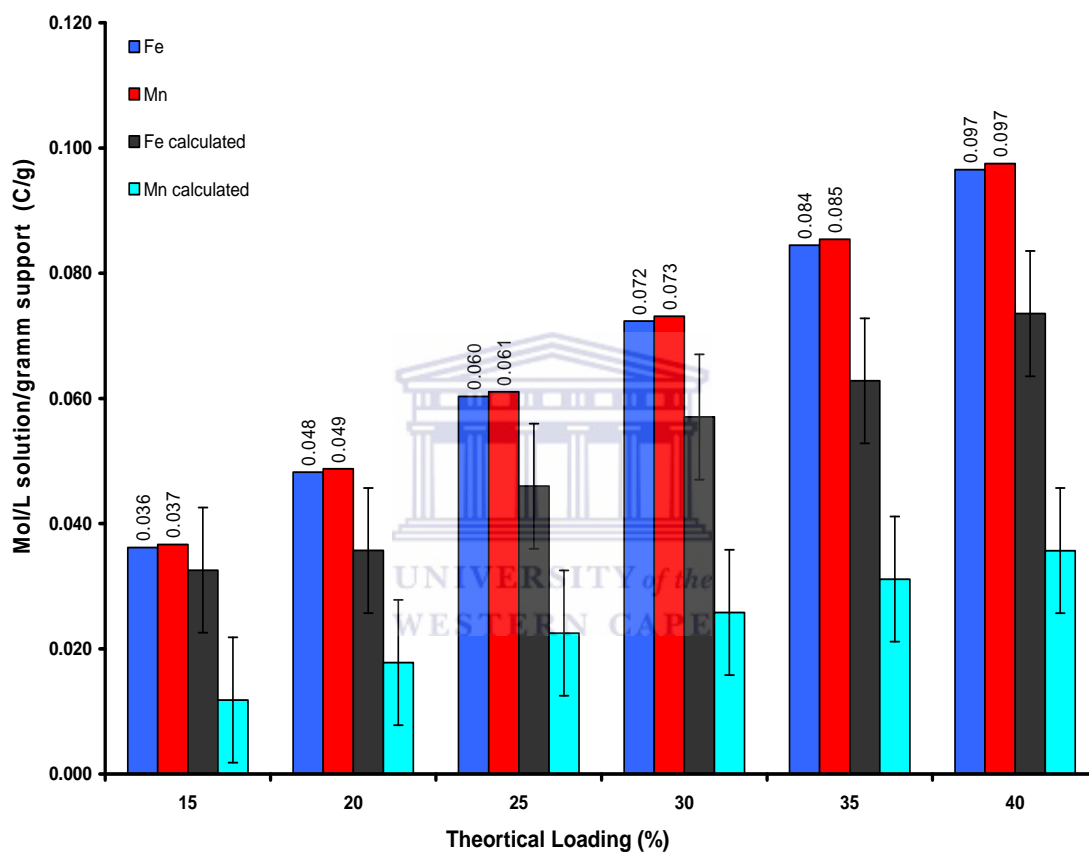


Figure 4-7: Overview of the Fe and Mn loading obtained on MCM – 41 samples using the ion exchange procedure.

The above graph (Figure 4-7) shows the concentrations of iron and manganese loaded on the support. The obtained loadings were very low in terms of the amount of metals that were loaded on the support, it is not certain at this stage if the ion exchange process between iron (Fe^{3+}), manganese (Mn^{2+}) and the support (MCM-41) occurred, this observation has also been reported by other authors (Lang et al., 2002). The actual ratio

obtained on the support was approximately of 2 iron to 1 manganese in one case (ion 15 %), and around 1.5 in iron to 1 in Mn for the remaining samples.

4.2.3 Surface structure and topology study by High resolution transmission microscopy

The HRTEM was conducted on a Technai G² F 20 X-Twin MAT microscope according to the procedure described in section 3.4.3.1. In terms of the HRTEM images obtained, the carrier was first analyzed followed by the synthesized catalysts. Figures 4.8 show two images of the support taken at two different magnifications.

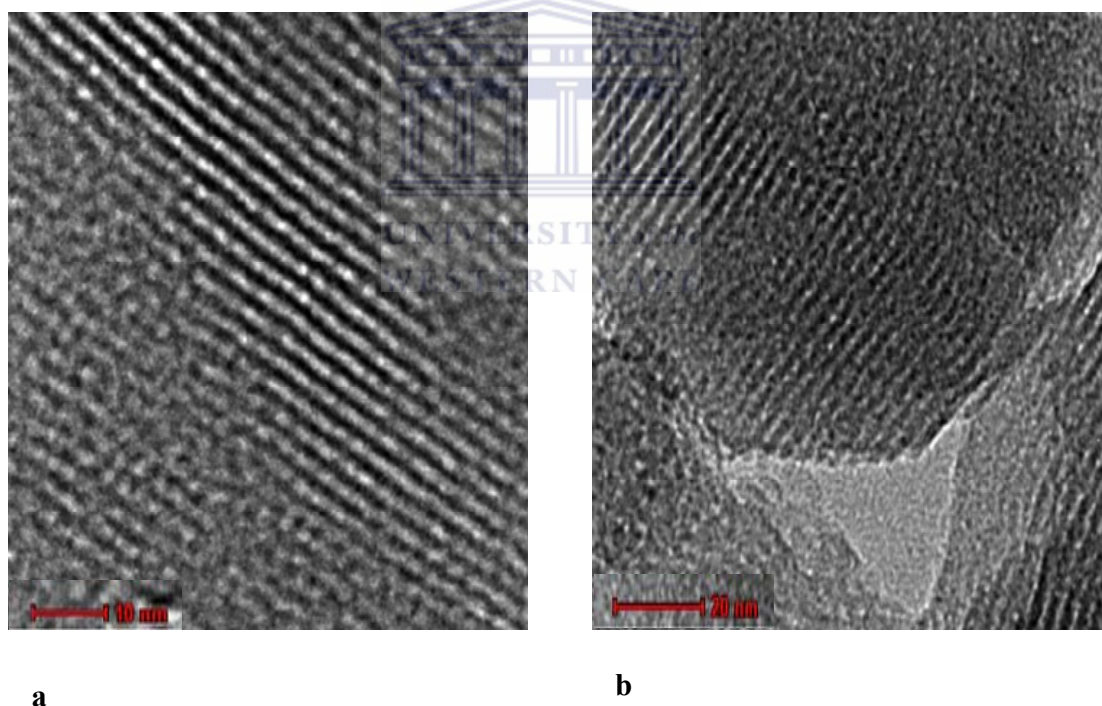


Figure 4-8: HRTEM images of the carrier (MCM – 41) at 10 nm (a) and 20 nm (b) magnification.

On the above image (Figure 4-8 a), the regular and ordered straight-channel characteristics of the MCM-41 can distinctively be seen in the middle of the image at 10 nm magnification (Velu et al., 2002); to confirm that these cylinders are empty; the SAED was conducted on different spots of the sample (Figure 4-9). The pore size of the support was determined by BET and was 2.8 nm (Table 4.9) which is close to 2.5 nm obtained by the HR-TEM technique. Image (b) taken at 20 nm magnification also confirm the nature of the support, which is composed of ordered straight-channel, once again confirming the nature of the support used in this study.

The next images (Figure 4-9) represent the wet 30 catalyst synthesized by wet impregnation and taken at 10 nm (a) and 20 nm (b) of magnification.

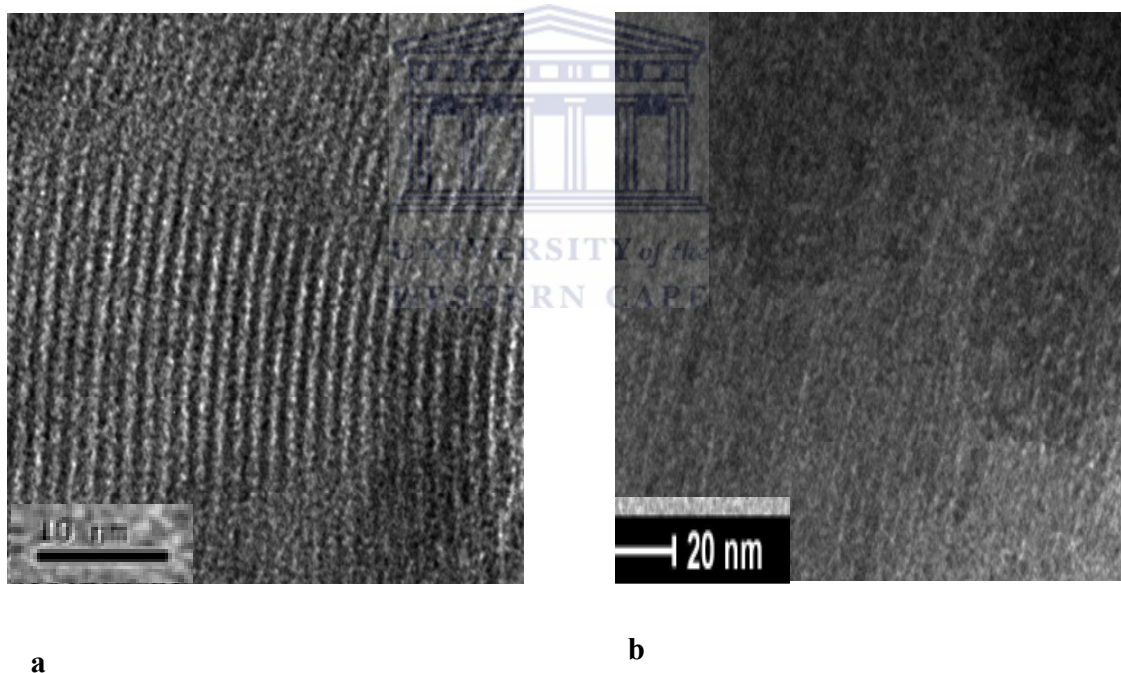


Figure 4-9: HRTEM images of a Wet 30 catalyst at two different magnifications.

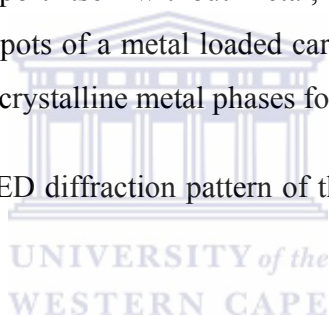
Figure 4-9 (a) shows the wet 30 catalyst image where ordered straight channel are preserved and unaffected by the presence of metals but the pores are filled with metal particles, the particles are not individually visible at this resolution but can be confirmed

with the SAED technique (Figure 4-9 a and b). Figure 4-9 (b) on the other hand shows the same catalysts image but taken at 20 nm magnification, the agglomeration of particulates cannot be observed on the support because the sample has been treated in the water bath sonicator for 5 minutes before the analysis by HRTEM, but dark spots showing decomposed compound due to the effect of sonicator can be seen in the top part of the image (b) (Xiang-Ying et al., 2006).

4.2.4 Crystalline phases study by selected area electron diffraction

The SAED was conducted on a Technai G² F 20 X-Twin MAT according to the procedure described in section 3.4.4.2. One image of the carrier (MCM-41) is shown (Figure 4-10) showing the support itself without metal, and two images (Figure 4-11 a and b) taken on two different spots of a metal loaded carrier (Wet 30) are also shown to certify the presence of the new crystalline metal phases formed on the support.

Figure 4-10 represents the SAED diffraction pattern of the MCM-41 support before the loading process.



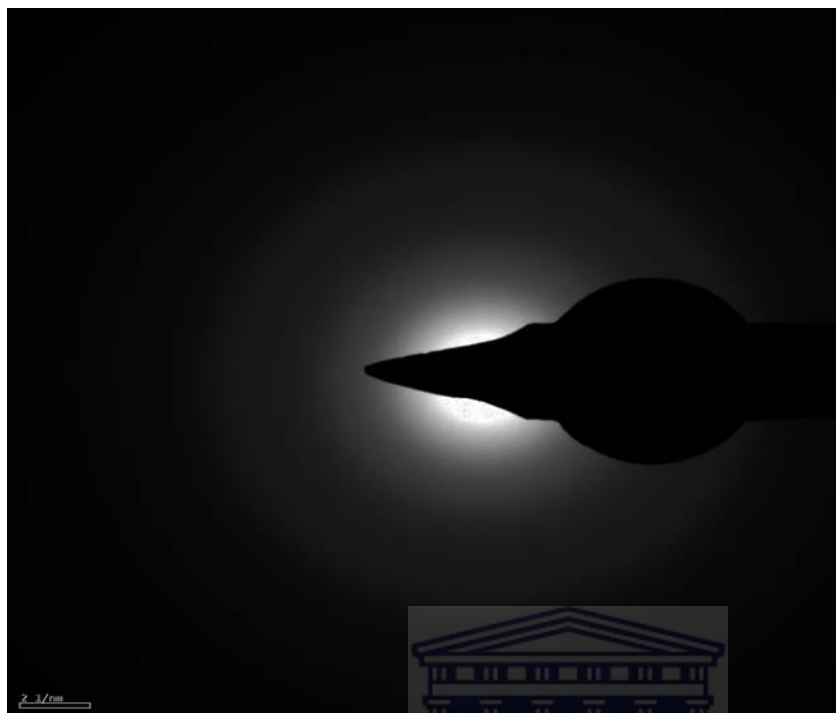


Figure 4-10: Selected area electron diffraction of the carrier (MCM – 41).

The SAED pattern of the carrier (MCM-41) shown in Figure 4-10 does not give any hint of crystallinity that can be identified apart from the diffuse rings which are characteristic of large number of randomly orientated grains representing the amorphous MCM-41 basic structure (Goodhew, 2001). This image serves as the reference when comparing to other SAED patterns of catalysts that have been loaded with metals.

Figure 4–11 (a) represents the SAED diffraction pattern of the wet 30 catalyst after the loading by wet impregnation and Figure 4–10 (b) represents the SAED diffraction pattern of the same sample (wet 30) prepared by wet impregnation as described in section 3.3.2.1 and taken on a different spot.

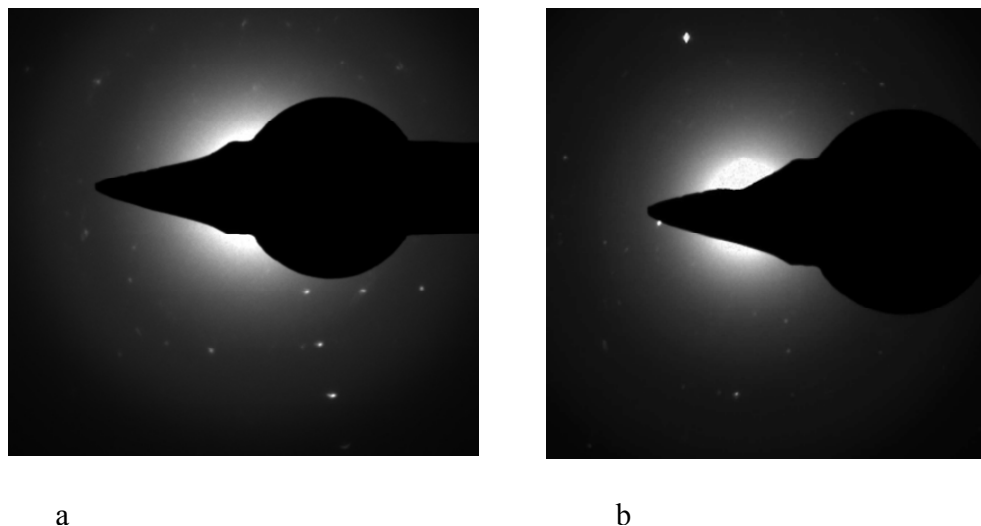


Figure 4-11: SAED images of the Wet 30 catalyst on two different spots.

The SAED diffraction patterns of the catalyst loaded at wet 30 % by wet impregnation Figure 4-11 (a and b) shows the presence of crystalline metal particles dispersed on the carrier. These small grains are attributed to the presence of metal oxide species (Fe_2O_3 and Mn_2O_3) dispersed on the support starting to show some crystalline phases (Goodhew, 2001). The crystalline phases formed on the catalysts are not of good quality to say with confidence that new structure have been formed on the substrate. The SAED results as obtained at this stage need to be confirmed by other techniques such as XRD and FTIR.

4.2.5 Crystalline phases study by X-ray diffraction spectroscopy

The XRD spectra of all the samples were obtained according to the procedure described in section 3.4.2.1, and the experiments were run on two different machines (Phillips PW 3830/40 mpd and D8 Advance from Bruker AXS) for two different purposes; first, to assess the characteristic of the mesoporous silica in the low 2θ range and secondly, at higher 2θ angles to assess whether or not there is formation of any new phase on the support after metal impregnation or ion exchange.

Figure 4-12 shows a low angle XRD of the support (MCM-41) analyzed on the D8 Advance from Bruker AXS.

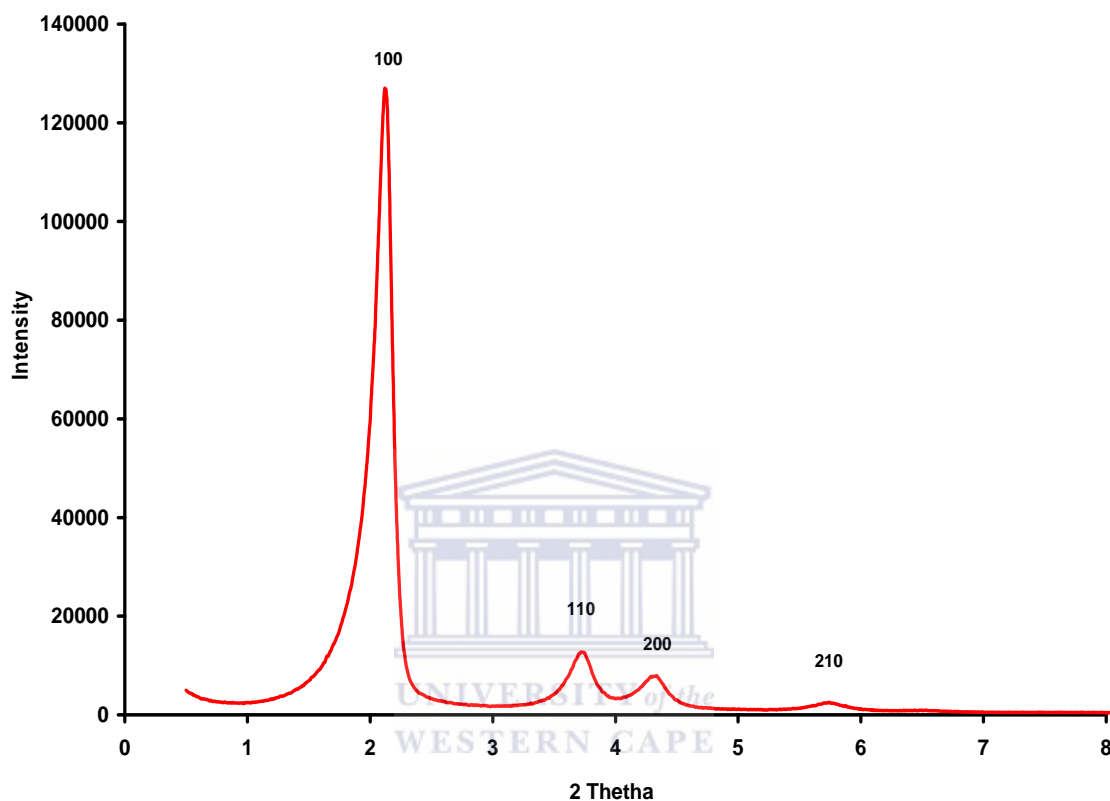


Figure 4-12: Low 2θ angle XRD of the carrier (MCM – 41).

The low angle XRD of MCM-41 as shown in Figure 4-12 shows four low-angle reflections corresponding to d_{100} , d_{110} , d_{200} and d_{210} which are characteristic of the ordered mesoporous structure of the hexagonal type (MCM-41) (Xiang-Ying et al., 2006). This XRD graph will be considered as the base line spectra of the catalyst and will be compared to the graphs of the various catalysts to see how these peaks are affected during the wet and ion exchange procedures. One will also notice how intense these four peaks are, showing high ordering of interplanar spacing (d_{100} , d_{110} , d_{200} and d_{210}) of the porous structure.

Figure 4-13 presented below, shows the wide angle XRD spectra of the carrier (MCM - 41) run on the Phillips PW 3830/40 machine between 3 – 60° 2 θ .

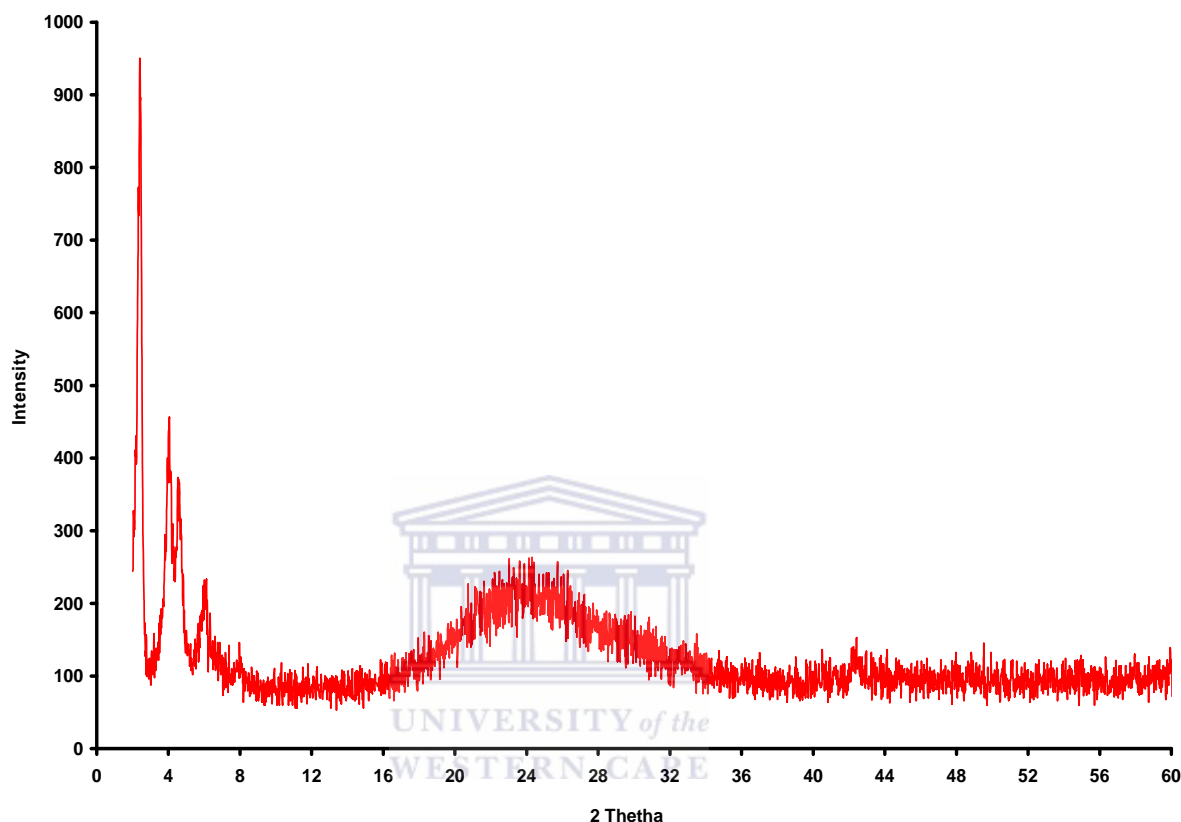


Figure 4-13: Wide 2 θ angle XRD of carrier (MCM – 41).

The XRD of MCM-41 in Figure 4-13 shows in the lower angle 2 θ range (1 – 8° 2 θ), four different peaks (d_{100} , d_{110} , d_{200} and d_{210}) which are characteristic peaks of the hexagonal symmetry of the MCM-41 (Xiang-Ying et al., 2006) and a broaden signal at around 24 ° 2 θ which shows the amorphous nature of the silica pore wall.

Figure 4-14 shows the low angle XRD spectra of the different catalysts (wet 15, 20 and 25) synthesized by wet impregnation and calcined at 400 °C and the carrier MCM-41.

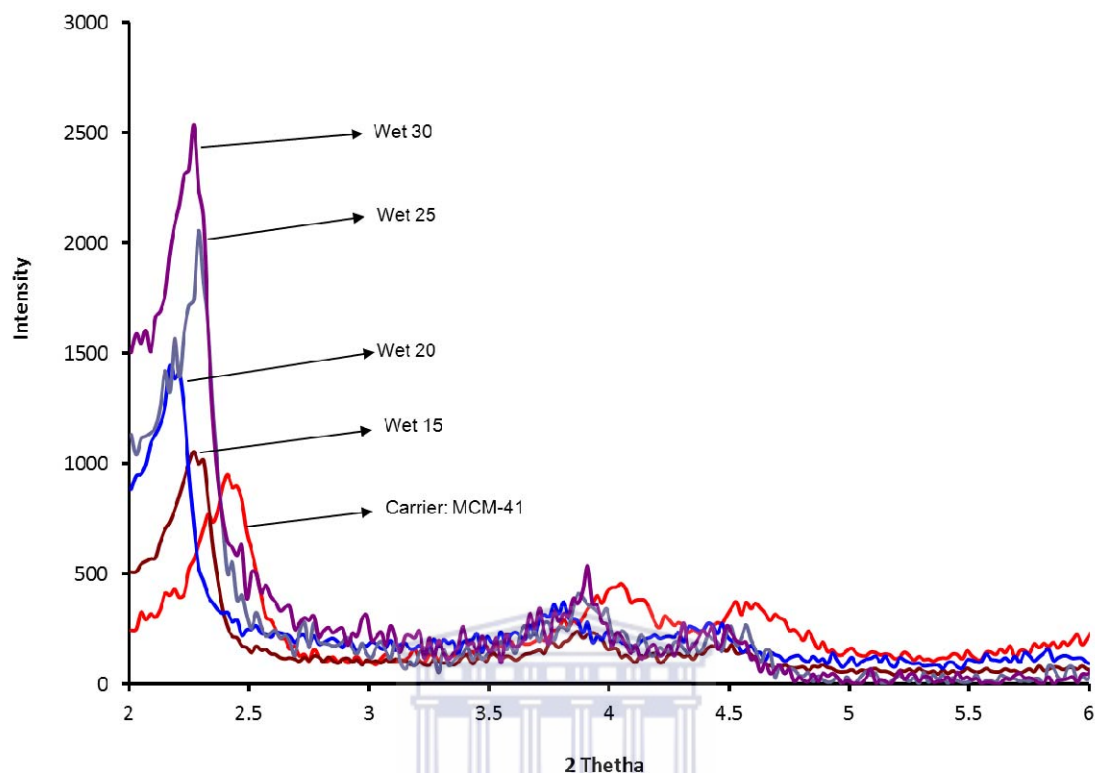


Figure 4-14: Low angle XRD of catalysts synthesized by wet impregnation and calcined at 400 °C.

Figure 4-14 shows that when the loading is done by wet impregnation, the d_{100} , d_{110} , d_{200} have broaden and shifted to the long angle, while the d_{210} peaks has completely disappeared due to the presence of metal particles disturbing the hexagonal symmetry of the support (Savidha et al., 2004); (Velu et al., 2002).

Figure 4-15 presents the low angle XRD spectra of different catalysts synthesized by ion exchange and calcined at 400 °C see preparation method in section 3.3.3.1.

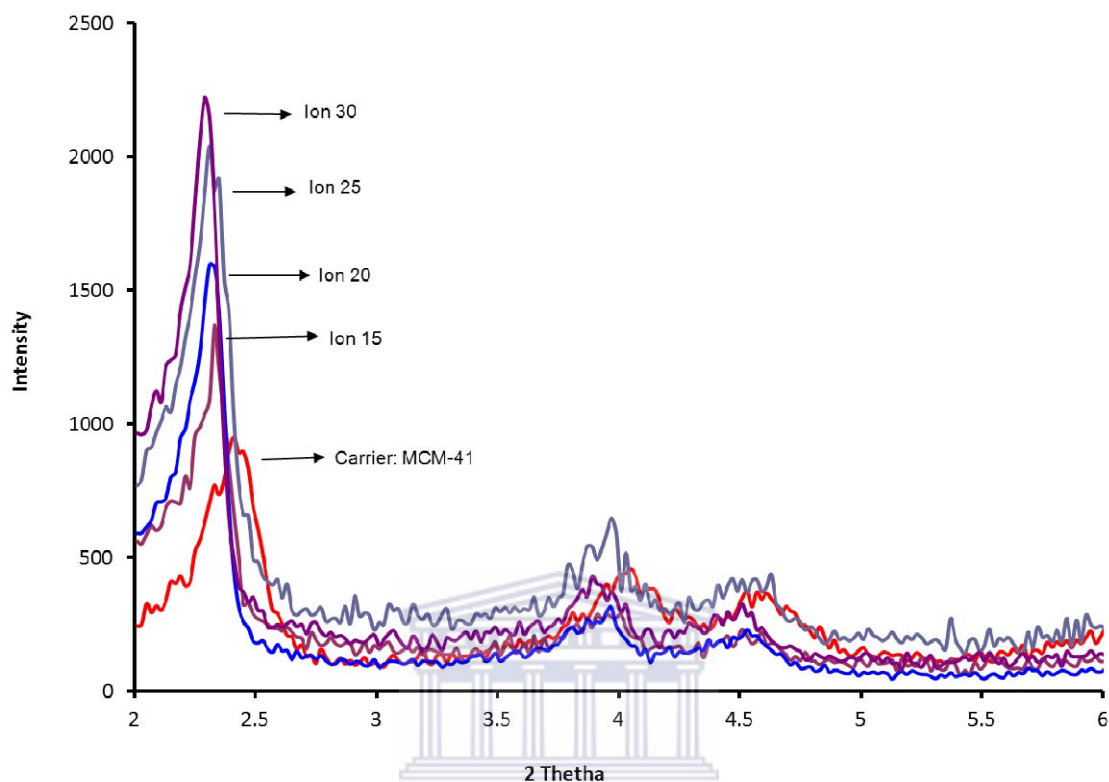


Figure 4-15: Low angle XRD of catalysts synthesized by ion exchange and calcined at 400 °C.

It can be seen from the XRD graph (Figure 4-15) that the amount of metal loaded on the support had an impact on the d_{210} peak which has completely disappeared, followed by the peaks intensity reduction indicating a slight reduction of the hexagonal symmetry of the MCM-41 (Xiang-Ying et al., 2006); (Savidha et al., 2004). When compared with the XRD graph of the wet impregnated catalysts, a strong shift to left was observed compared to the shift observed for the ion exchange catalysts. As it was observed during the elemental mapping and the EDS in terms of metal content, the wet impregnated catalysts carried a lot more of metal loaded on the substrate, that aspect can be linked to the peak intensities when the ion exchange XRD graphs are compared with the wet impregnated XRD graphs. Less intense peaks for the wet impregnated samples, and intense peaks for the ion exchange samples.

Figure 4-16 shows the wide angle XRD spectra of five different catalysts synthesized by ion exchange and calcined at 400 °C and Figure 4-17 shows the wide angle XRD spectra of five different catalysts synthesized by wet impregnation and calcined at 400 °C.

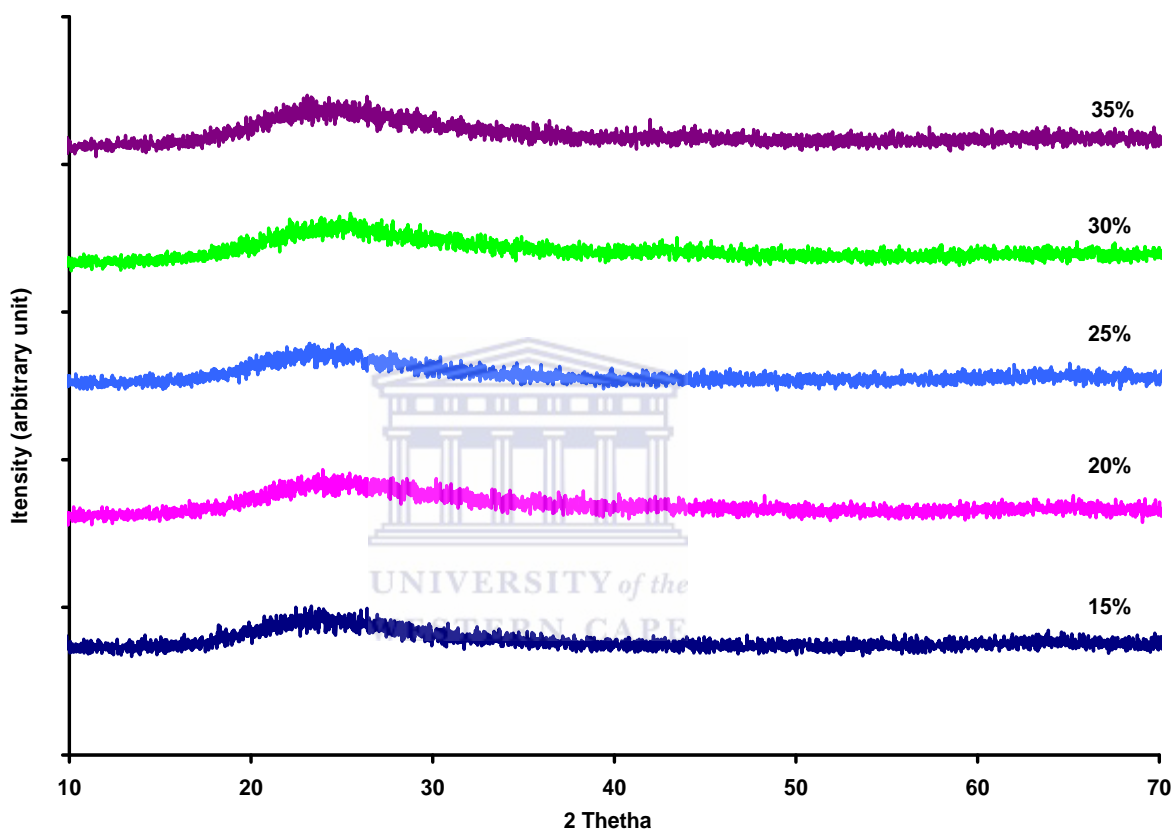


Figure 4-16: Wide angle XRD of catalysts synthesized by ions exchange and calcined at 400 °C.

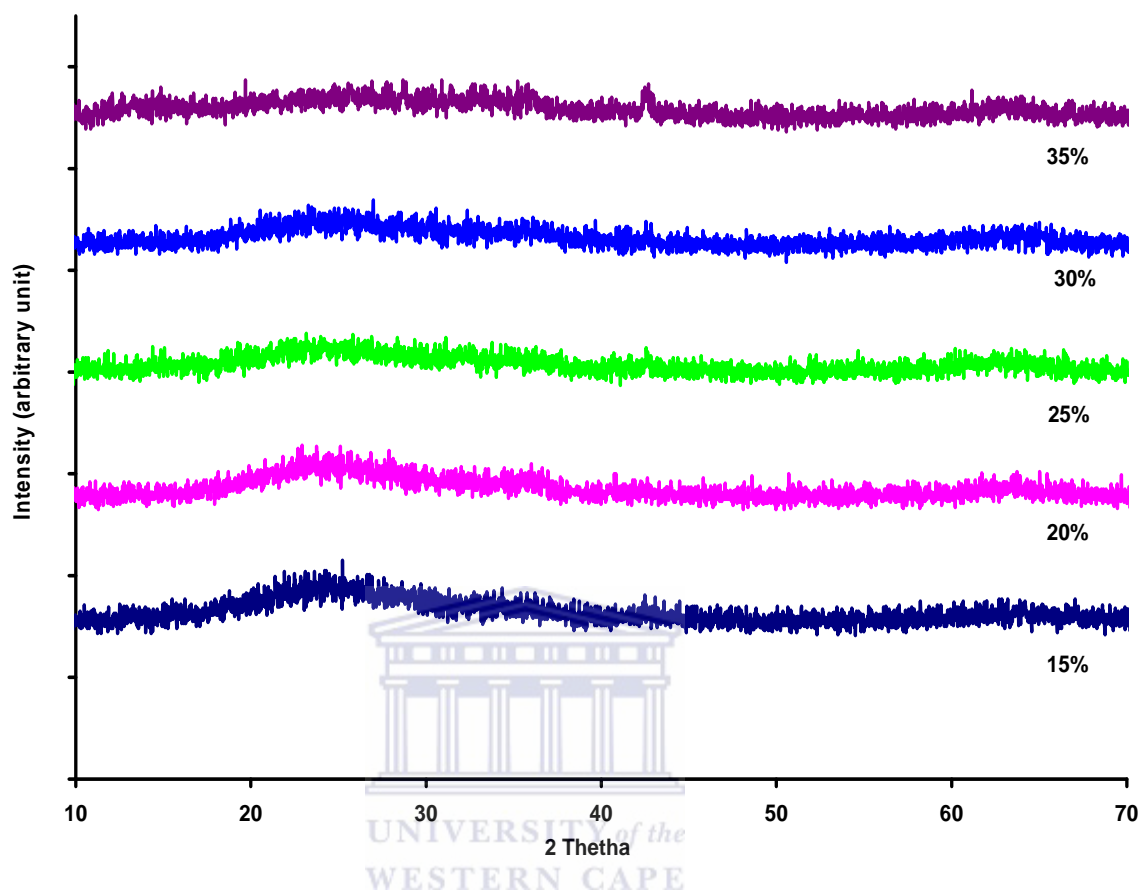


Figure 4-17: Wide angle XRD of catalysts synthesized by wet impregnation and calcined at 400 °C.

The two graphs (Figures 4-16 and 4-17) represent the XRD spectra of the series of catalysts prepared by either ion exchange or wet impregnation respectively after calcinations at 400 °C. It can be seen from these two graphs that there are no peaks indicating new crystalline metal phases on the surface of the catalyst even though ICP and AAS confirmed the metal presence in each case (Table 4.2 and 4.3), the metal phases expected (Fe_2O_3 and Mn_2O_3) are still below the resolution capacity of the XRD technique and need to be confirmed by other advanced characterization techniques.

4.2.6 Surface area and pore size distribution study by N₂-B.E.T (BRUNAUER – EMMET –TELLER)

Table 4.9 shows the BET surface area and pore size of wet and ion exchanged catalysts including the carrier; the analysis was carried out on a Micrometrics Tri Star 3000 as is described in section 3.4.5.2.

Table 4.9: Nitrogen BET surface areas and pore size of catalysts synthesized from MCM – 41 as support

Samples	Catalysts synthesized by wet impregnation		Catalysts synthesized by ion exchange	
	Pore diameter (nm)	BET Surface area (m ² /g)	Pore diameter (nm)	BET Surface area (m ² /g)
Carrier (MCM-41)	2.8	1080	2.8	1080
Wet α Ion 20	2.60	774	2.59	856
Wet α Ion 25	2.59	697	2.60	888
Wet α Ion 30	2.58	677	2.59	883
Wet α Ion 35	2.73	595	2.62	852
Wet α Ion 40	2.73	622	2.61	905

The surface areas (column 3, Table 4.9) of the catalysts synthesized by wet impregnation show a decreasing trend from 1080 to 774 m²/g after the metal loading at 20 Wt % by wet impregnation and the surface area decreases below 700 m²/g to 622 m²/g. When the support was loaded at 40 wt % the minimum surface area was obtained in the case of wet impregnated sample wet 35. This trend can be observed in Figure 4-18. A different trend can be seen for the ion exchanged samples where the surface areas of different catalysts decreased from 1080 to 858 m²/g after the first loading and remained constant in the range of 800 m²/g, this trend can be observed in Figure 4-19.

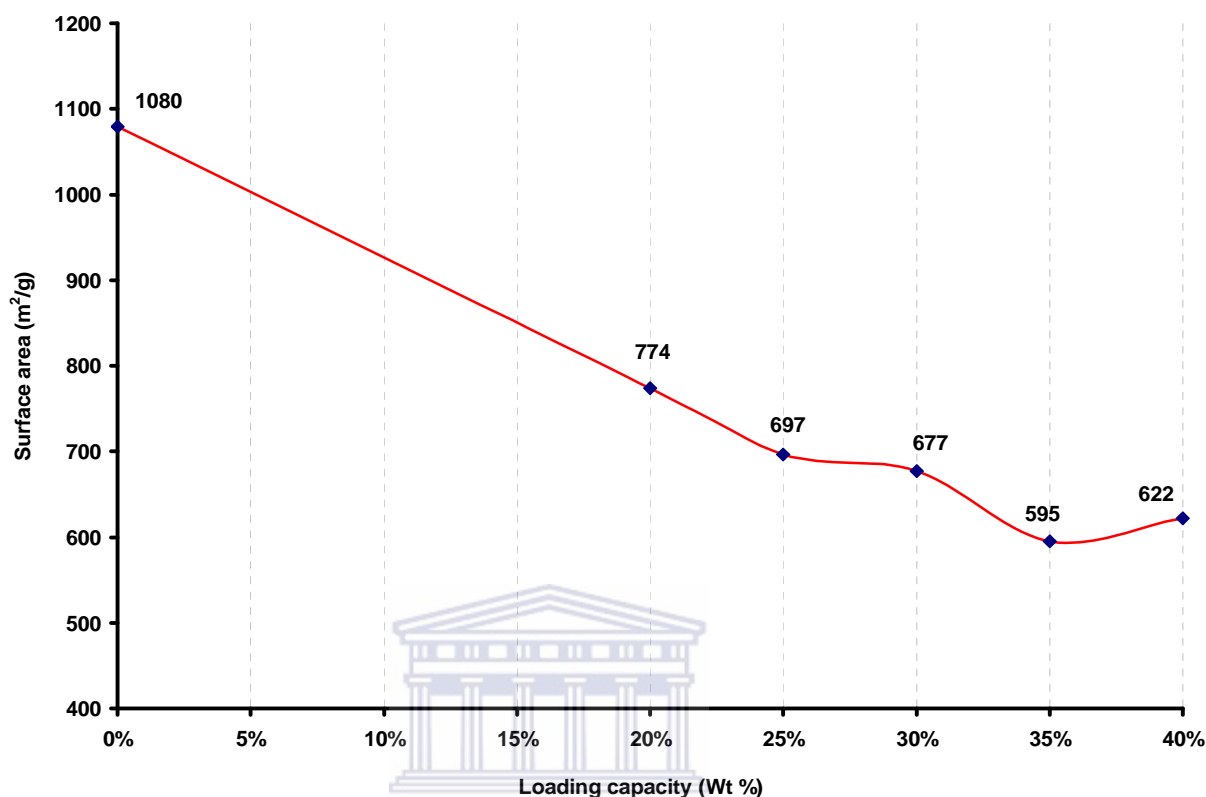


Figure 4-18: Surface area after loading of MCM-41 support by wet impregnation.

After analysis of the wet impregnated BET data, the above graph (Figure 4-18) shows a decrease in the surface area of the catalysts, this is mainly due to the deposition of the loaded material on the substrate. The surface area decreases due to the fact that the loaded metal oxide narrows the pore size of the support at different loadings capacities. Every time when the concentration of the loaded salt increases, the pores narrowed further, with an optimum reached at wet 35 corresponding to 0.810 mol of Fe and Mn per gram support. One should take into consideration the fact that, during the wet impregnation process a portion of the metal loaded is mechanically (stirring process) forced to go inside the pore of the hexagonal structure and the remaining portion is physically adsorbed on the support.

The ion exchange surface area study shows a different trend that can be observed on the following graph (Figure 4-19).

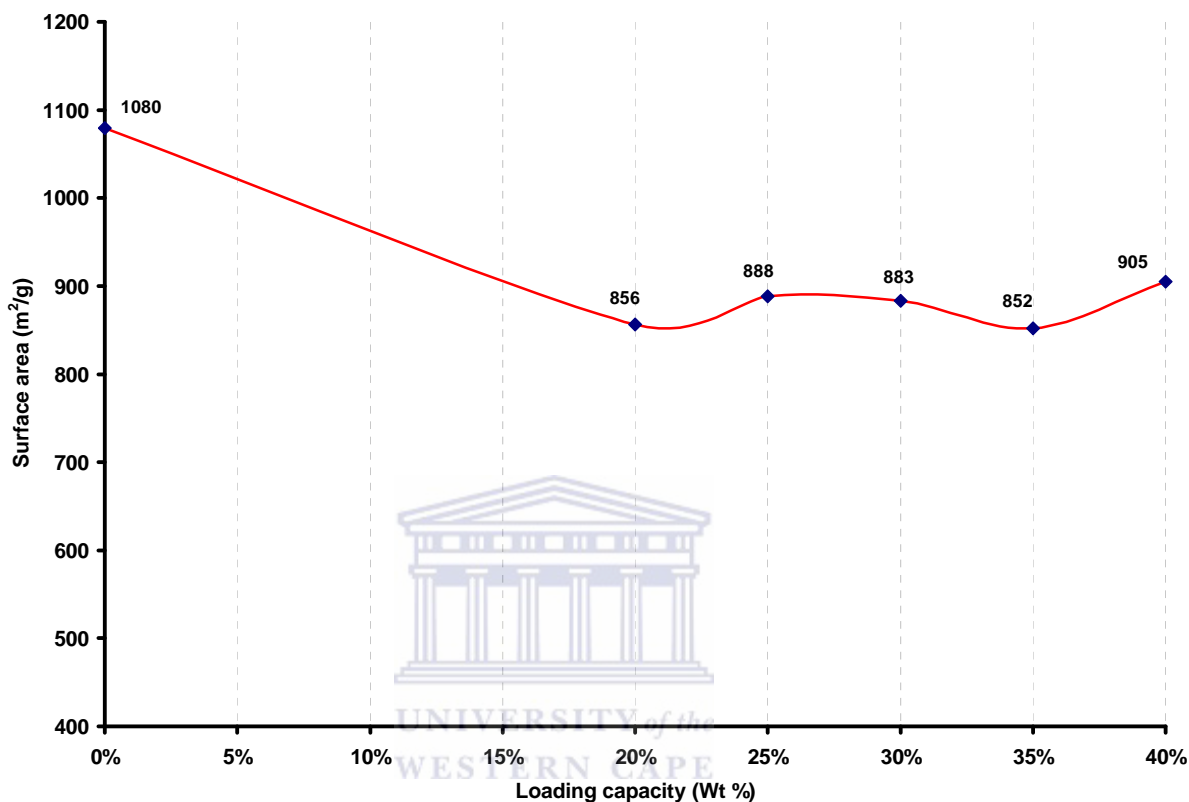


Figure 4-19: Surface areas after loading of MCM-41 support by ion exchange.

The surface area study of the ion exchanged samples shows a decreasing trend too, but the optimum loading in this case was reached at 20%, contrary to the wet impregnated samples during which the optimum was reached at 35%. This particular graph shows a low exchange capability that the MCM-41 has compare to a normal zeolite such H-Beta-25 studied further down. Once the first layer of metal has covered the exchange sites, in this particular case the metal oxide of choice being Fe than Mn during the ion exchange with reference to the ICP results, the remaining amount of metal was washed during the washing step of the catalyst synthesis.

The graph below (Figure 4-20) compares the average pore size distribution of the carrier with the pore size distribution of a wet 30 catalyst synthesized by wet impregnation.

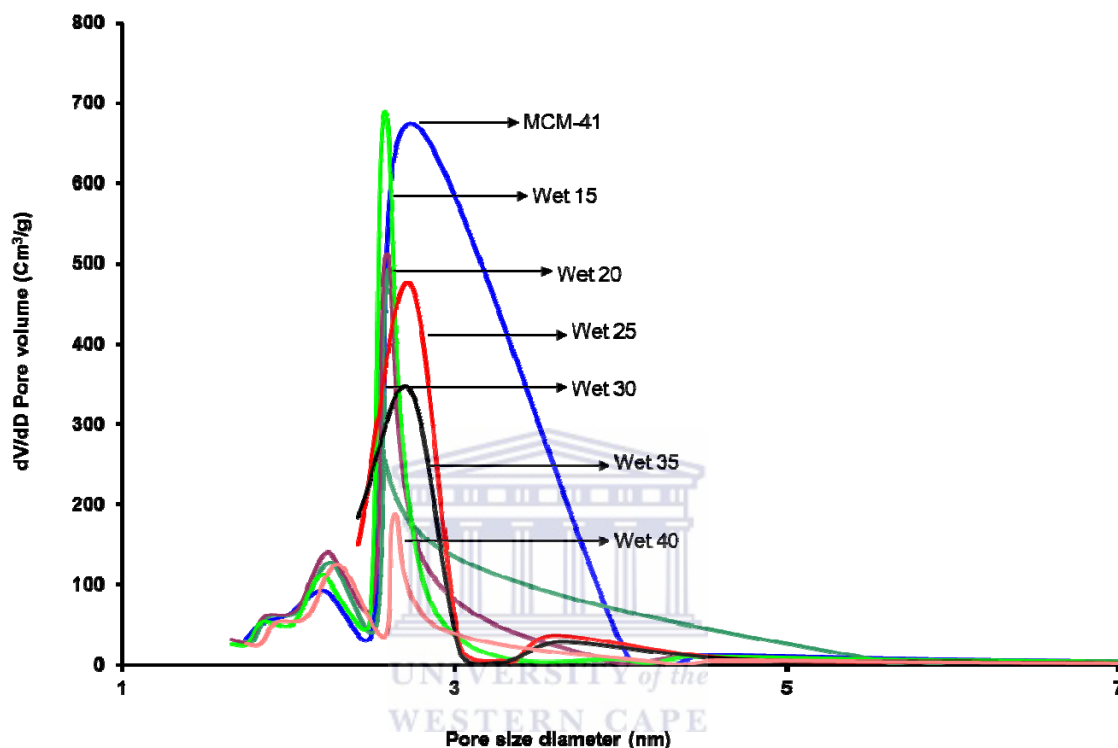


Figure 4-20: Pore size distribution of calcined carrier and wet 30 catalyst (BJH adsorption curves).

The pore size distribution of the carrier (MCM-41) shows clearly that the support is definitely a mesoporous type with a pore distribution size in the range of 2.5 nm to 4 nm. It also shows the average pore diameter is 2.8 nm and uniform in size apart from a small amount of pores at around 2.3 nm. On the other hand, the average pore size distribution of the wet 30 catalyst is narrowed, and in the range of 2.6 with a small bimodal distribution in the range of 2.3nm. The only difference that can be observed at this stage when the two graphs overlaid over each other is the width of the peak. The loaded support seems to have a small pore width while the parent material has a wide width.

This trend has been observed for all the remaining catalysts synthesized by wet impregnation.

The graph below (Figure 4-21) compares different isotherms of catalysts synthesized by wet impregnation (wet 20, 25 and 30) with the isotherm of the calcined carrier (MCMC-41).

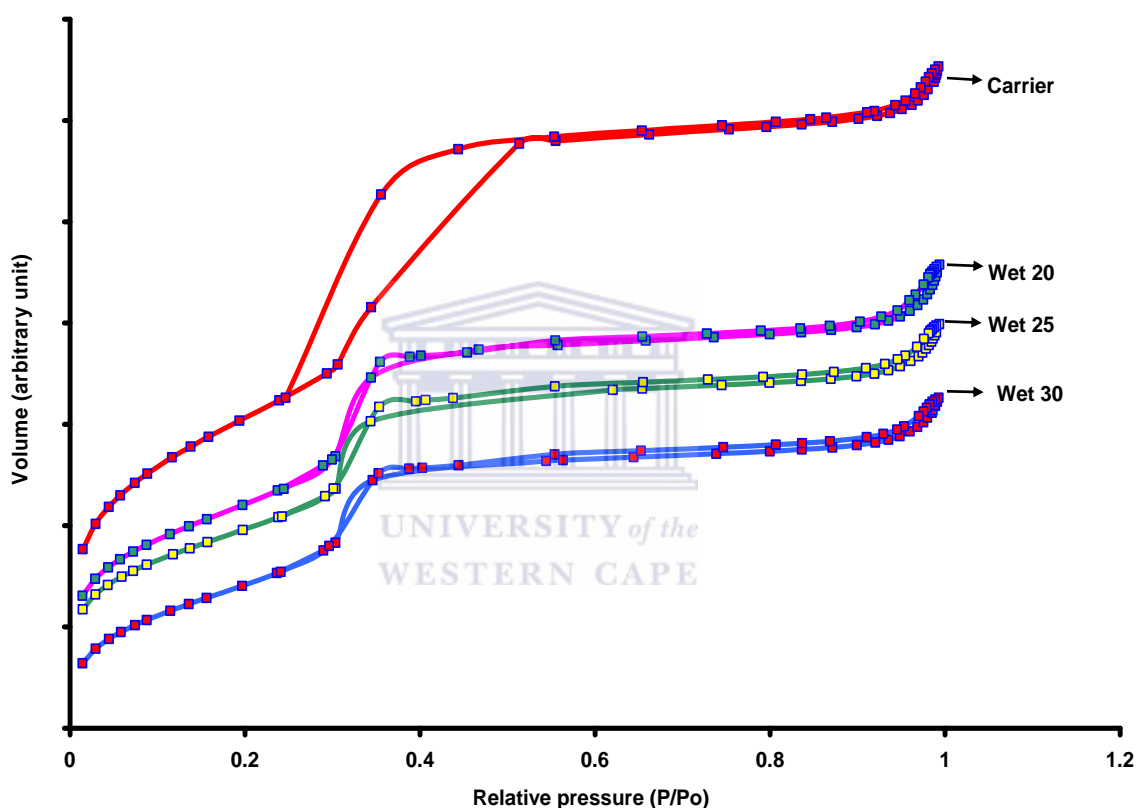


Figure 4-21: Nitrogen adsorption/desorption isotherms at 77 K of different catalysts synthesized by wet impregnation in comparison with the of the carrier's isotherm.

With an increase in the amount of metal loaded on the support by wet impregnation, the isotherms obtained are still in the same category (type A and D); the only changing aspects are the inflections points (P/P_o) which have shifted toward the higher values, 0.3 mmHg instead of 0.25 mmHg as observed on the carrier. The hysteresis loops on the metal loaded samples are very small compared to those on the parent material, this

confirms the presence of metal oxide particles inside the pores of the support contributing to the loss of mesoporosity of the substrate since the adsorption as well as the desorption are taking place in narrower cylinders compared to the cylinders of the parent material (Hartmann et al., 1999). The large loop observed on the isotherm of the parent material is attributed to the amount of gas adsorbed by the support due to the presence of large empty pore of the mesoporous support (Xiang-Ying et al., 2006).

The graph below (Figure 4-22) shows the pore size distribution of the calcined carrier and the catalyst (Ion 20) synthesized by ion exchange.

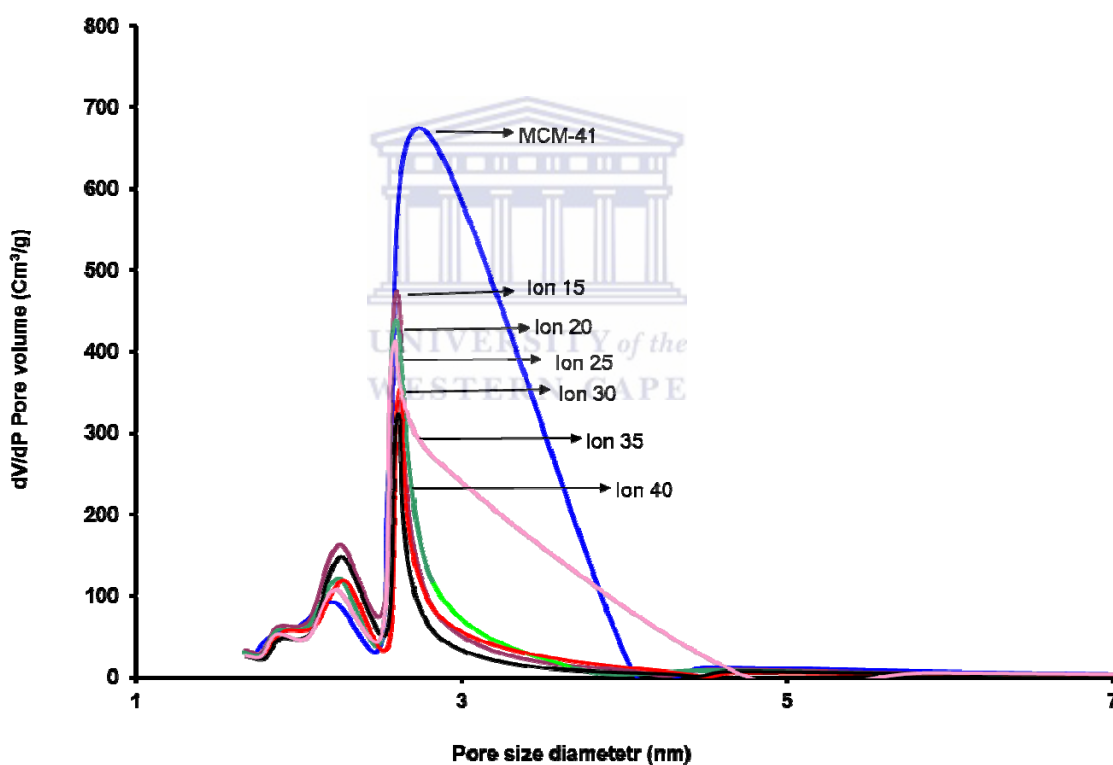


Figure 4-22: Pore size distribution of the ion 30 catalyst in comparison with the calcined carrier (BJH adsorption curves).

The above graph (Figure 4-22) shows the average pore diameter of the support which falls at 2.8 nm with uniformity in size apart from a small bimodal distribution of pores at around 2.3 nm. On the other hand, the average pore size distribution of the remaining

catalysts (ion 15 to ion 30) falls in the range of 2.6 with small bimodal distribution in the range of 2.3 nm as well. The only difference that can be observed at this stage when these different graphs are put close to each other is the width of the peak defining the pore. The loaded support appears to have a narrower pore width while the parent material has a wide pore width. This trend has been observed for all the remaining catalysts synthesized by ion exchange.

The graph below (Figure 4-23) shows the comparison between different catalyst's isotherms (Ion 20, 25 and 30) synthesized by ion exchange in comparison with the isotherm of the carrier (MCM-41).

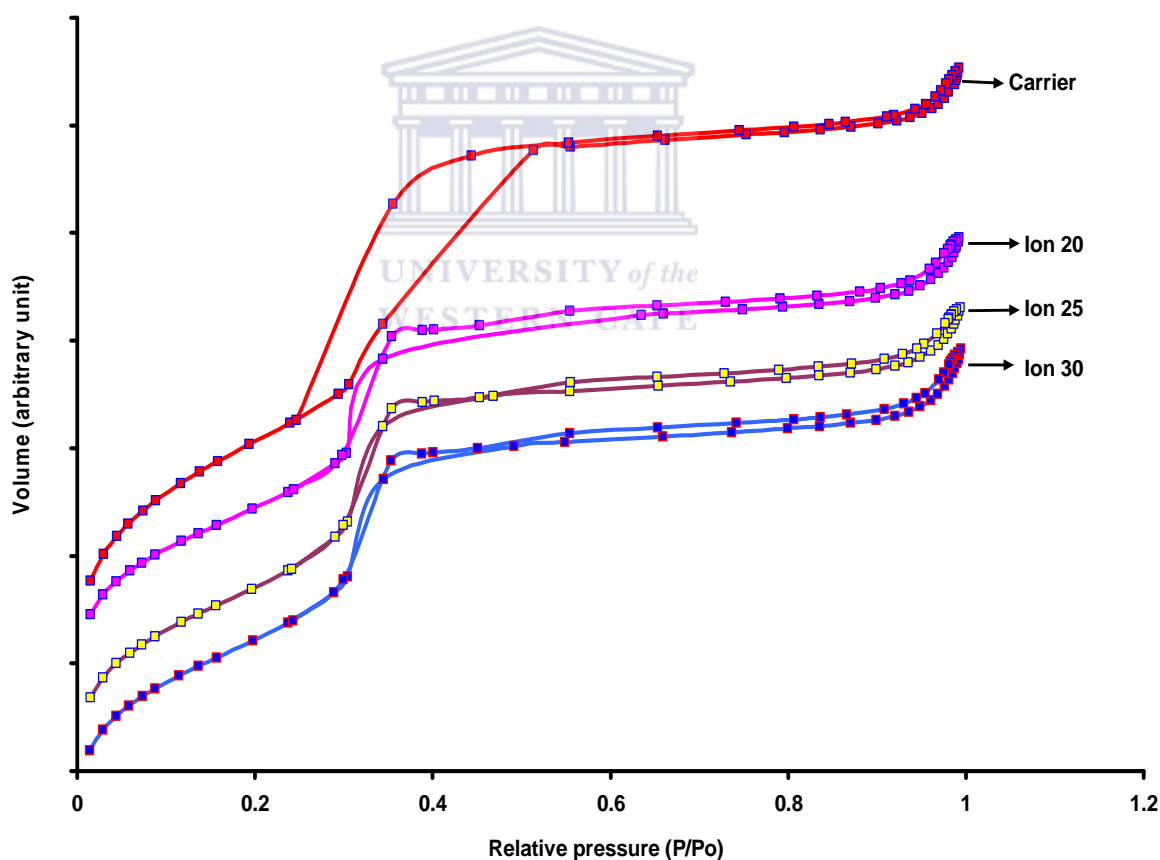


Figure 4-23: Nitrogen adsorption/desorption isotherm at 77 K of different catalysts synthesized by ion exchange in comparison with the carrier's isotherm.

The loading done by ion exchange at calculated loadings of 20, 25 and 30 % seems to have perturbed the isotherms of the catalysts when a comparison is made with the isotherm of the carrier (sharpness and height of the capillary condensation step). This anomaly is attributed to the fact that pores are no longer cylindrical but filled with small particles inside. The second inflection point P/P_0 0.25 mmHg observed on the carrier has shifted from 0.25 to 0.35 mmHg on the catalyst's isotherms due to the filling of pores with particles (Hartmann et al., 1999). The large hysteresis loop observed on the isotherm of the support is attributed to the large pore diameters of the mesoporous support (Xiang-Ying et al., 2006).

4.2.7 Chemical bonding study of the catalysts by Fourier transformed infrared spectroscopy

The FT-IR experiments were conducted on a Perkin Elmer® (Universal ATR) according to the procedure described in section 3.4.6 in the range of 500 to 4000 cm^{-1} . The catalysts synthesized by wet impregnation are analysed first, followed by the analysis of the ion exchange catalysts, all these catalysts are compared to the carrier (MCM-41) with no metal.

Figure 4-24 shows the FT-IR spectra in the scan range of 500 to 1900 cm^{-1} of the carrier (MCM-41) and the six catalysts synthesized by wet impregnation.

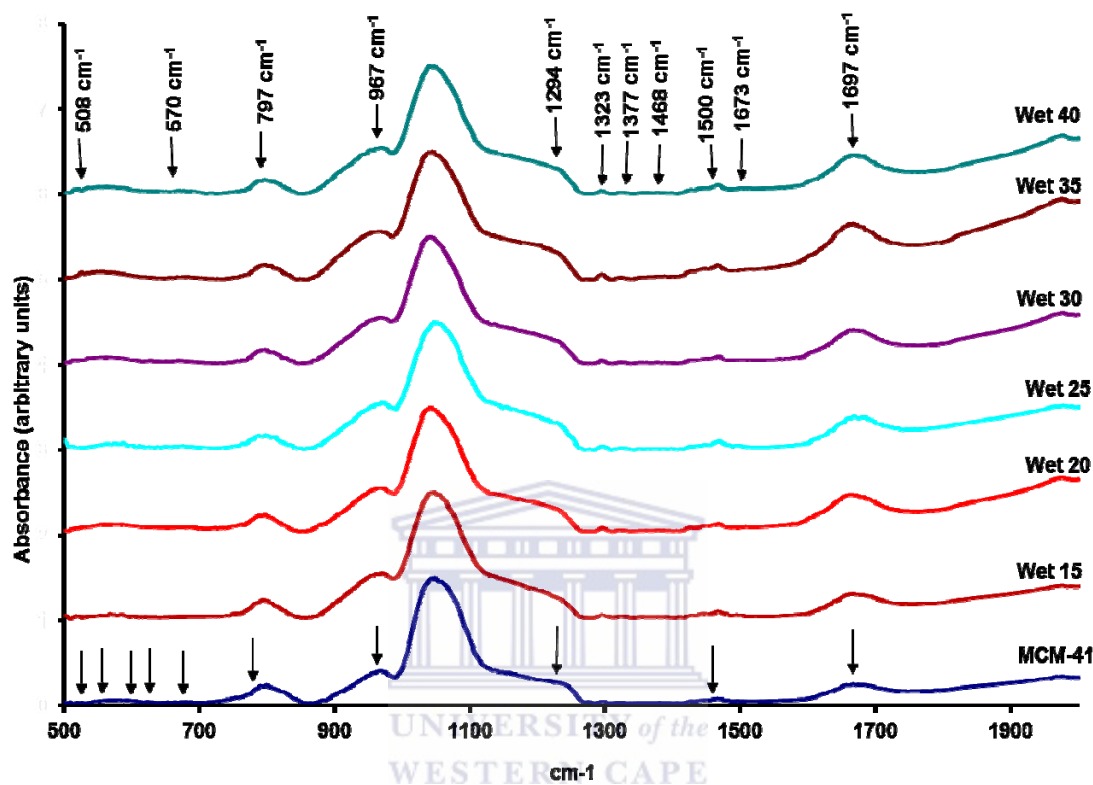


Figure 4-24: FT-IR spectra of the carrier (MCM-41) in comparison with six catalysts synthesized by wet impregnation.

The IR spectrum of the carrier shows specific bands at 509, 518, 582, 623, 677, 798, 967, 1298 and 1467 cm^{-1} assigned to the amorphous SiO_2 characteristic of the vibrations Si-O-Si bridges crosslinking the silica network (Xiang-Ying et al., 2006). These adsorption peaks characterizing the MCM-41 framework are maintained after the dispersion of Fe and Mn oxides. The broad bands around 3414 and 3378 cm^{-1} (not shown) are attributed to the adsorbed H_2O molecules while deformational vibrations of adsorbed molecules have the absorption bands at 1667 cm^{-1} (Selvaraj et al., 2003).

Figure 4-25 shows the FT-IR spectra of the carrier in comparison with the six catalysts synthesized by wet impregnation in the scan range of 500 to 1000 cm^{-1} .

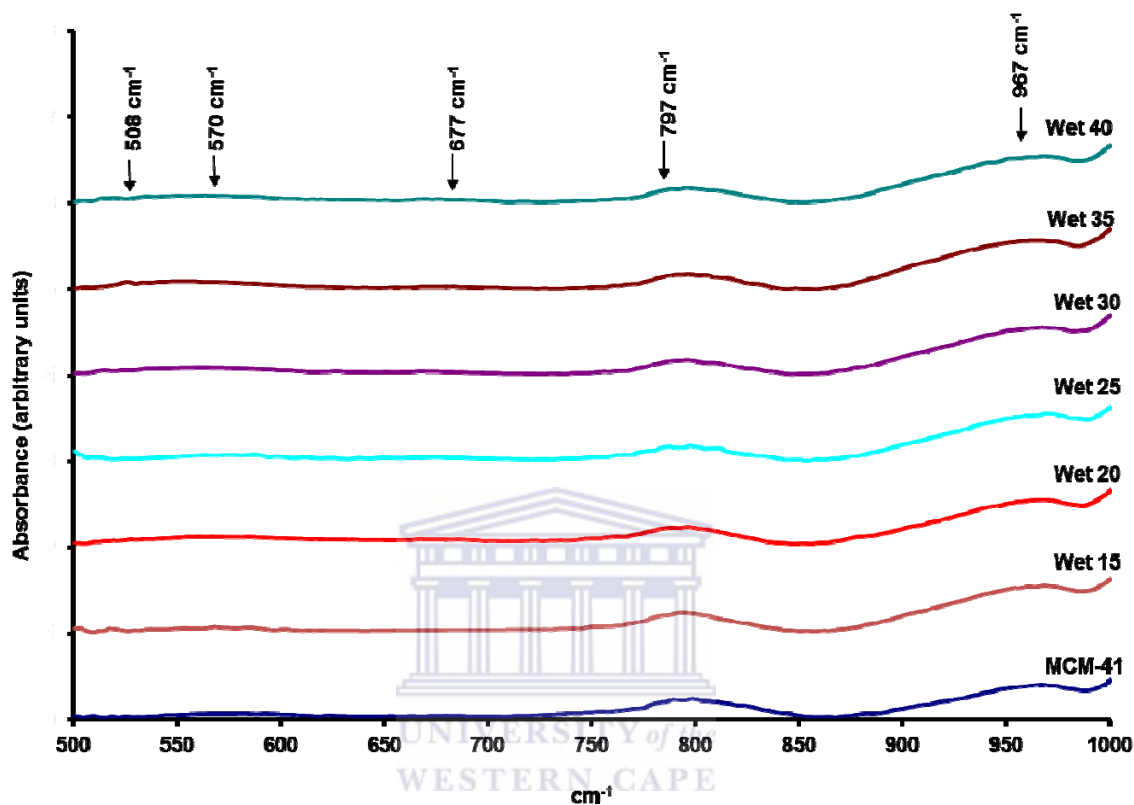


Figure 4-25: FT-IR spectra of the carrier (MCM-41) in comparison with six catalysts synthesized by wet impregnation in the scan range from 500 to 1000 cm^{-1} .

Analysis of Figure 4-25 gives the following information; the peaks observed on the support (509, 518, 582, 623, 677, 798 and 967, cm^{-1}) remain the same after the loading. However, there is a new set of peaks that have emerged on the support, these peaks were observed at 525 and 568 cm^{-1} , when compared to the data base of inorganic compound such as Fe_2O_3 and Mn_2O_3 , no similarity with the bands of the two compounds has been observed. In the lower ranges, bands of Fe_2O_3 are expected at 547, 721 while the bands of Mn_2O_3 are expected at 525, 578, 664, 721 cm^{-1} .

Figure 4.26 shows the FT-IR spectra of the carrier in comparison with the six catalysts synthesized by wet impregnation in the scan range of 1000 to 1800 cm^{-1} .

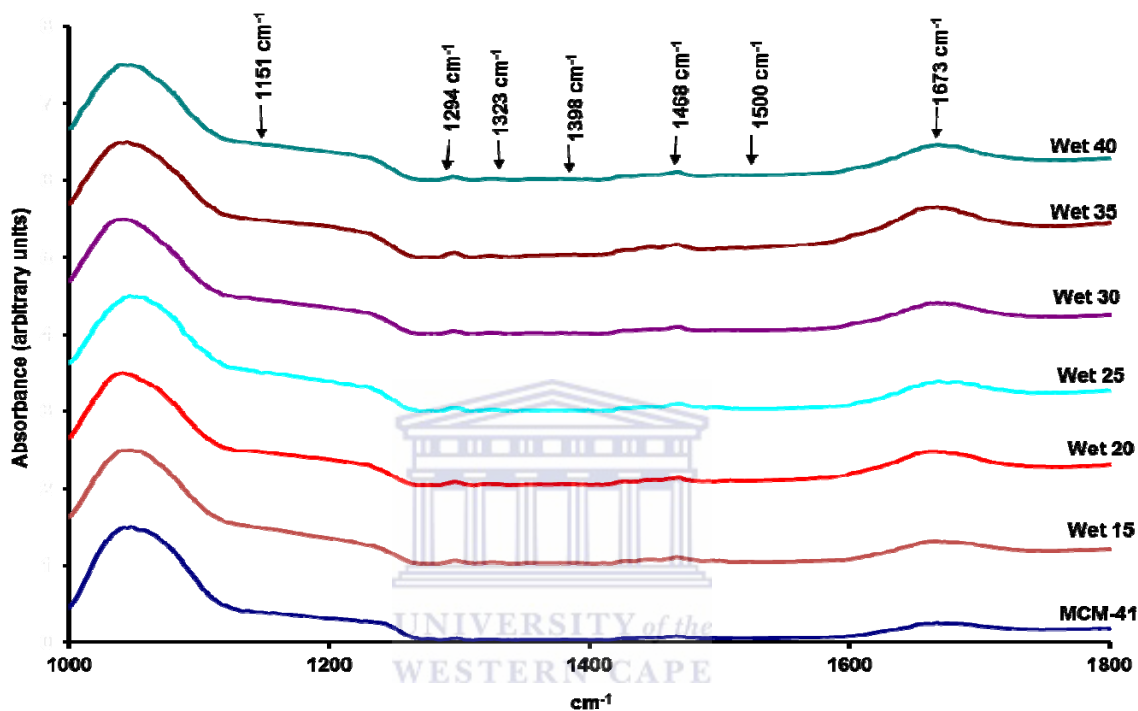


Figure 4-26: FT-IR spectra of the carrier (MCM-41) in comparison with six catalysts synthesized by wet impregnation in the scan range of 1000 to 1800 cm^{-1} .

Figure 4-26 shows the formation of three new bands that have been formed on the support at the following wave lengths: 1322, 1379 and 1500 cm^{-1} . These three peaks have been compared to the data base of Fe_2O_3 and Mn_2O_3 bands; there is only one corresponding peak at around 1378 cm^{-1} which is attributed to the two compounds at the same time. The alteration of existing peaks usually means breaking of existing bonds, and the formation of new peaks usually means new bonds with the support have been created or new compounds have been formed on the support. In this case, the support keeps its existing structure but few un-identified peaks have been formed with only one peak being identified.

Figure 4-27 shows the FT-IR spectra in the scan range of 500 to 1900 cm^{-1} for the carrier (MCM-41) and the six catalysts synthesized by ion exchange procedure.

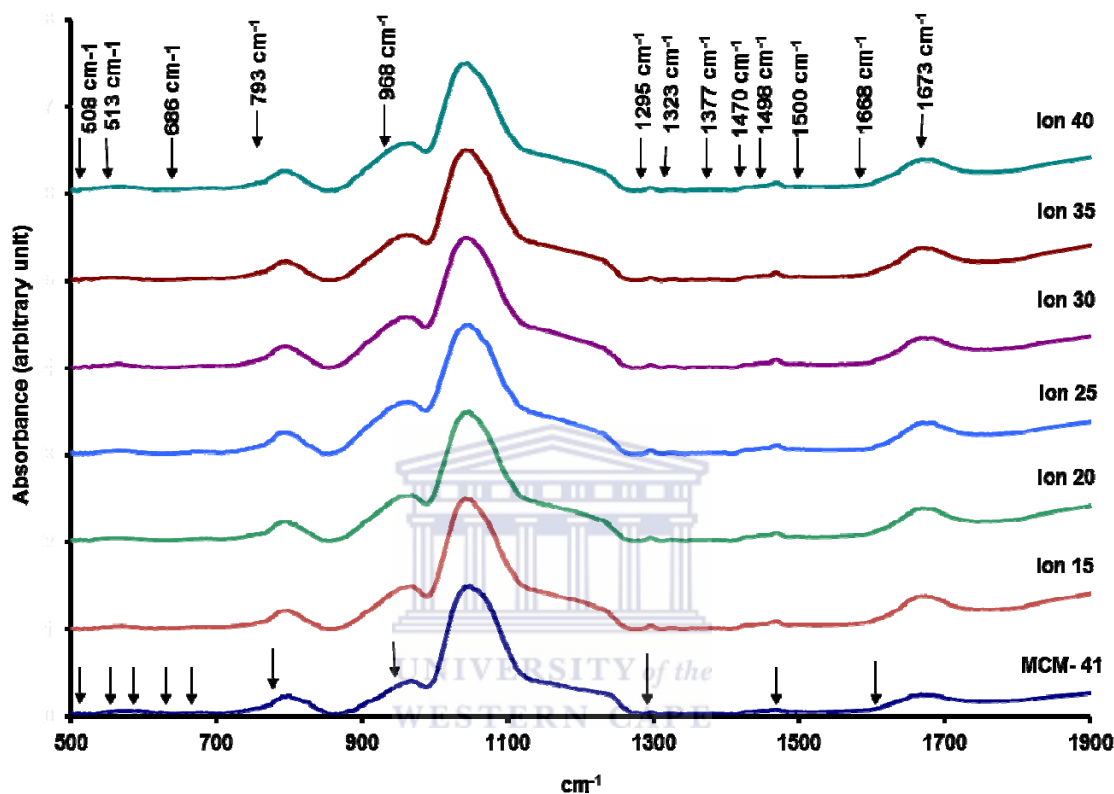


Figure 4-27: FT-IR spectra of the carrier (MCM-41) in comparison with six catalysts synthesized by ion exchange in the scan range of 1000 to 1900 cm^{-1}

The FT-IR spectra of the ion exchange catalysts (Figure 4-27) does not reveal anything new when compared to the spectra of the wet impregnated catalysts in the same range (Figure 4-27); peaks at 509, 518, 582, 623, 677, 798, 967, 1298 and 1677 cm^{-1} characteristic of the MCM-41 (Xiang-Ying et al., 2006) are still present on the catalysts.

Figure 4-28 shows the FT-IR spectra in the scan range of 500 to 1900 cm^{-1} for the carrier (MCM-41) and the six catalysts synthesized by ion exchange procedure.

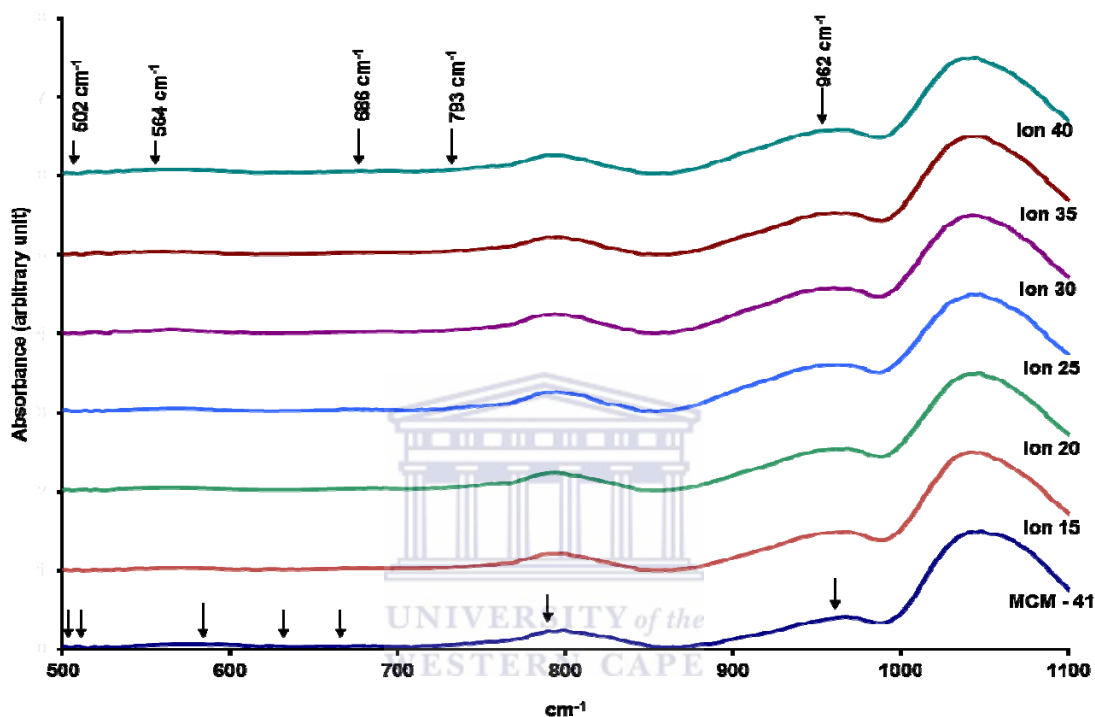


Figure 4-28: FT-IR spectra of the carrier (MCM-41) in comparison with six catalysts synthesized by ion exchange in the scan range of 1100 to 1900 cm^{-1}

The spectrum (Figure 4-28) revealed the formation of two new peaks in the lower range at 559 and 693 cm^{-1} on all the six catalysts, the peaks characteristic of the support remained unchanged despite the loading of metal oxides on the support.

Figure 4.29 shows the FT-IR spectra in the scan range of 1100 to 1900 cm^{-1} for the carrier (MCM-41) and the six catalysts synthesized by ion exchange procedure.

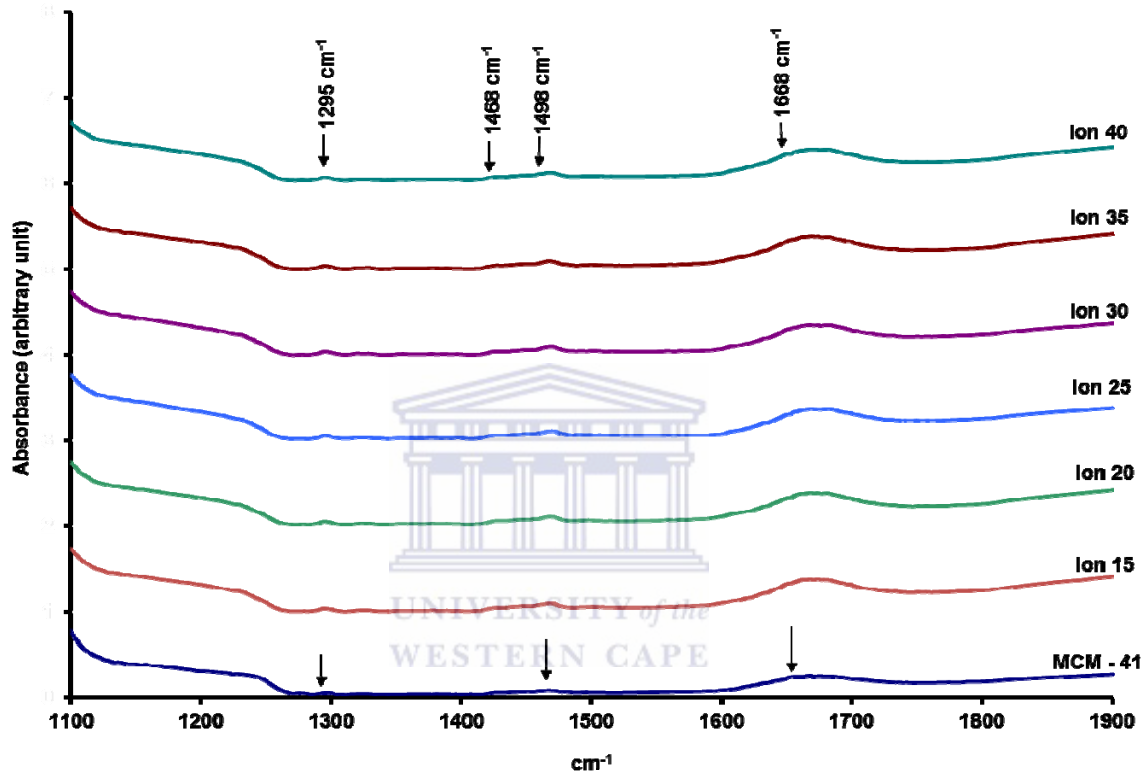


Figure 4-29: FT-IR spectra of the carrier (MCM-41) in comparison with six catalysts synthesized by ion exchange in the scan range of 1100 to 1900 cm^{-1} .

In the range of 1100 to 1900 cm^{-1} , Figure 4-29 shows two new peaks at 1323 and 1397 cm^{-1} with the peak at 1397 cm^{-1} been also identified for the two crystalline phases (Fe_2O_3 and Mn_2O_3). Once more, the FT-IR as a tool of analysis needs to be supported by other techniques in order to make sure that the results reveal here can be complemented and confirmed by other analysis techniques.

4.2.8 Structural study of the catalysts by thermo-gravimetric analysis

The TGA was conducted on a Q500 thermo gravimetric analyzer according to the procedure described in section 3.4.7.2. The purpose of the analysis was to understand the stability behaviour of the catalysts once submitted to a high temperature environment and to study the mass lost as a function of time and temperature.

Figure 4-30 shows a study of the carrier TGA signal analyzed section by section to understand its mass loss over time.

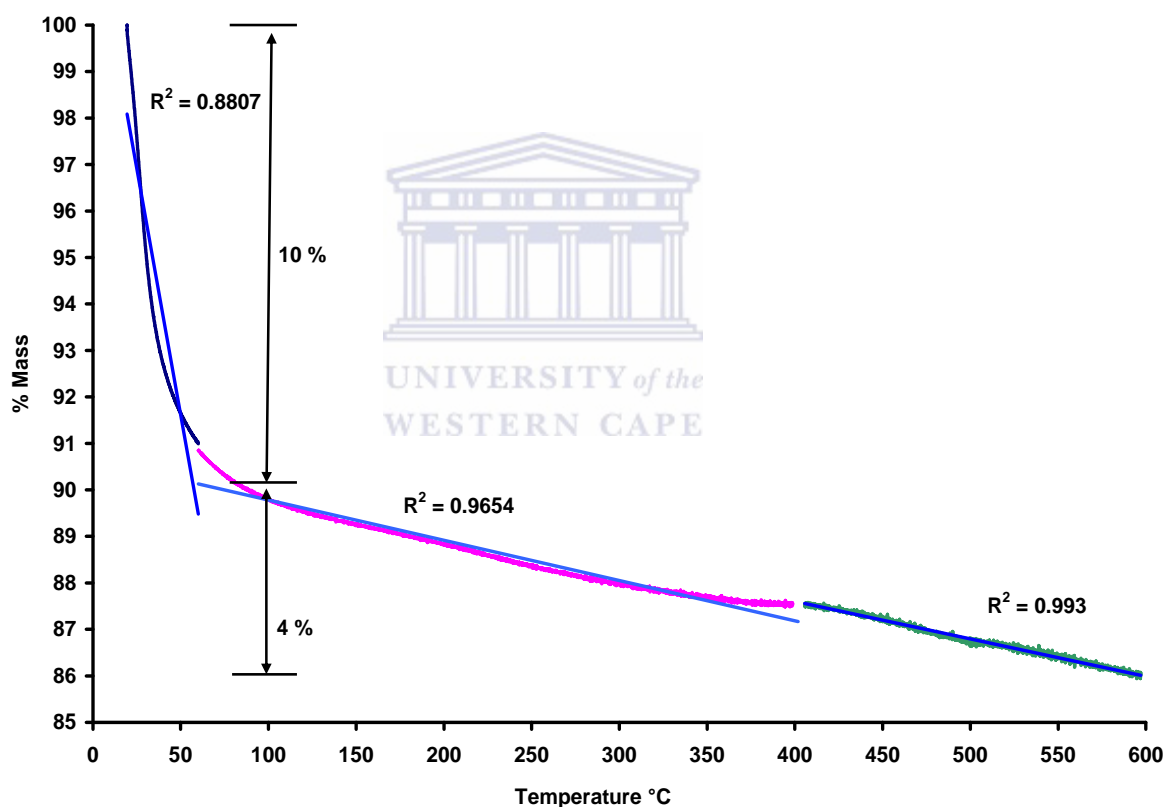


Figure 4-30: TGA graph of a carrier (MCM-41)

The weight loss by TGA (Figure 4-30) of the carrier (MCM-41) shows three regions that can be identified on the graph, the first region occurs between 50–100 °C and is explained by rapid loss of moisture (10 %) from the pores of the catalyst at low temperatures followed by a second region which shows the thermal stability of the catalyst up to 400 °C (mass loss 3-4 %). The region above 400 °C displays a slightly increased rate of mass loss which may indicate slow structural decomposition, however no de-hydroxylation is observed up to 600 °C (Widmann et al., 2001).

Figure 4-31 shows the trend of two randomly chosen catalysts (wet 25 and wet 30) in comparison with the carrier and analyzed under the same conditions.

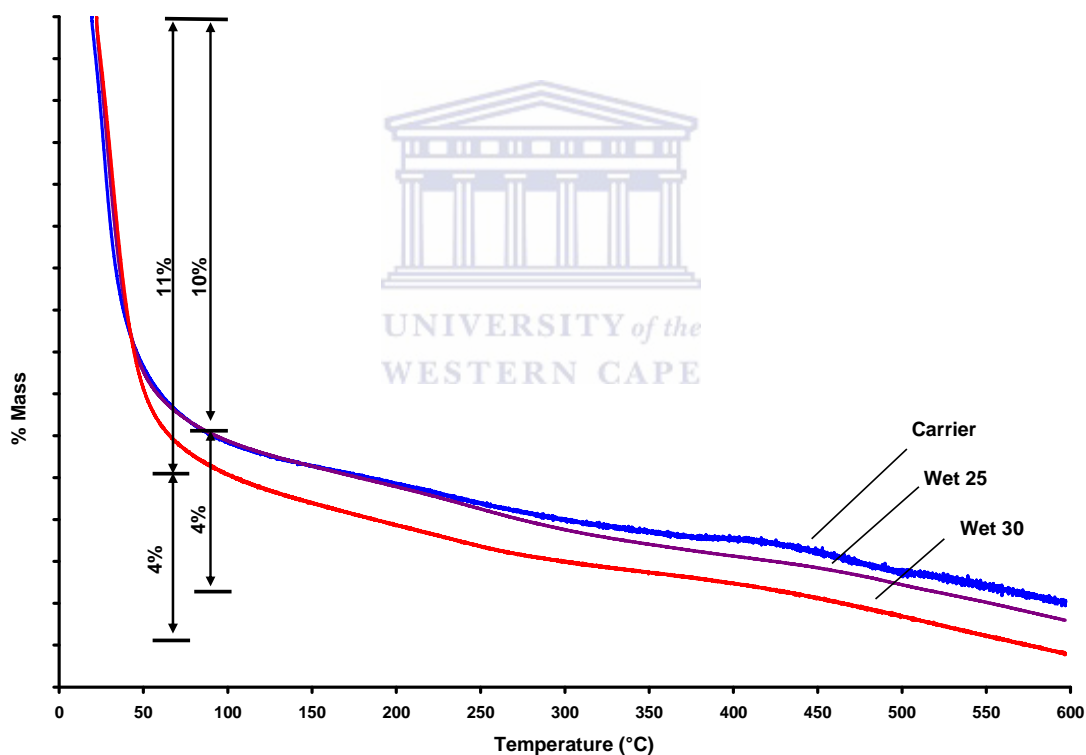


Figure 4-31: TGA graphs of two different catalysts (wet 20 and wet 30) in comparison with the TGA graph of the carrier.

The loaded catalysts graphs (wet 20 and wet 30) show a similar trend as the MCM-41 carrier apart from a high moisture content observed on the wet 30 catalyst (11 %). Most

TGA curves display weight losses due to chemical reactions (decomposition and loss of water of crystallization, reduction of metal oxides), physical transitions (vaporization, evaporation, sublimation desorption, drying) (Marbán et al., 2001). In the present case, only the loss of water by vaporization has been observed, no reduction of metal oxides was observed, which is in accordance with the XRD results obtained (Figure 4-16 and 4-17) where no new crystalline phase was observed on the support after thermal treatment of the catalysts. The experiment could not reach 900 °C due to the delimitation of the instrument used.

4.2.9 Reducibility study of the catalysts by temperature programmed reduction

The TPR was conducted on a Micrometrics Autochem. Analyzer, a mixture of H₂/Ar was used during the experiment at a flow rate of 50 mL/min. Details of the experimental conditions and methodology can be found in section 3.4.8.1 and 2.6.5.12 respectively.

It is often difficult to compare TPR results obtained in different laboratories or reported literature data since there is no general agreement on optimum experimental parameters for conducting TPR experiments such as the heating rate, the composition of the reducing gas mixture, and their flow rate. These factors can, apart from the particle size, greatly affect the rate of reduction (Xiang-Ying et al., 2006). Since TPR is a bulk process, not all particles are exposed to the reducing gas at the same time and thus a dependence of the temperature maximum on the particle size is expected (Velu et al., 2002). However, metal oxides supported on inert carriers may exhibit different reduction behaviour compared with the unsupported counterparts (Xiang-Ying et al., 2006).

Figure 4-32 shows the TPR profiles of the different catalysts synthesized by wet impregnation at different loadings of iron and manganese. The base line (MCM-41) represents the carrier MCM-41 without any metal being loaded onto it as the reference material. For the purpose of this TPR analysis a batch of catalysts were synthesized specifically with either Fe or Mn separately to make two different baseline monometallic

catalysts with a single metal loaded on the carrier MCM-41. Details of the synthesis can be found in section 3.3.2 for the wet impregnated samples and section 3.3.3 for the ion exchange samples. The samples were named wet Fe 20 %, wet Mn 20 %, ion Fe 20% and ion Mn 20 % to differentiate them from the previous batch of catalysts where the two metals were loaded at the same time on the same support (MCM-41).



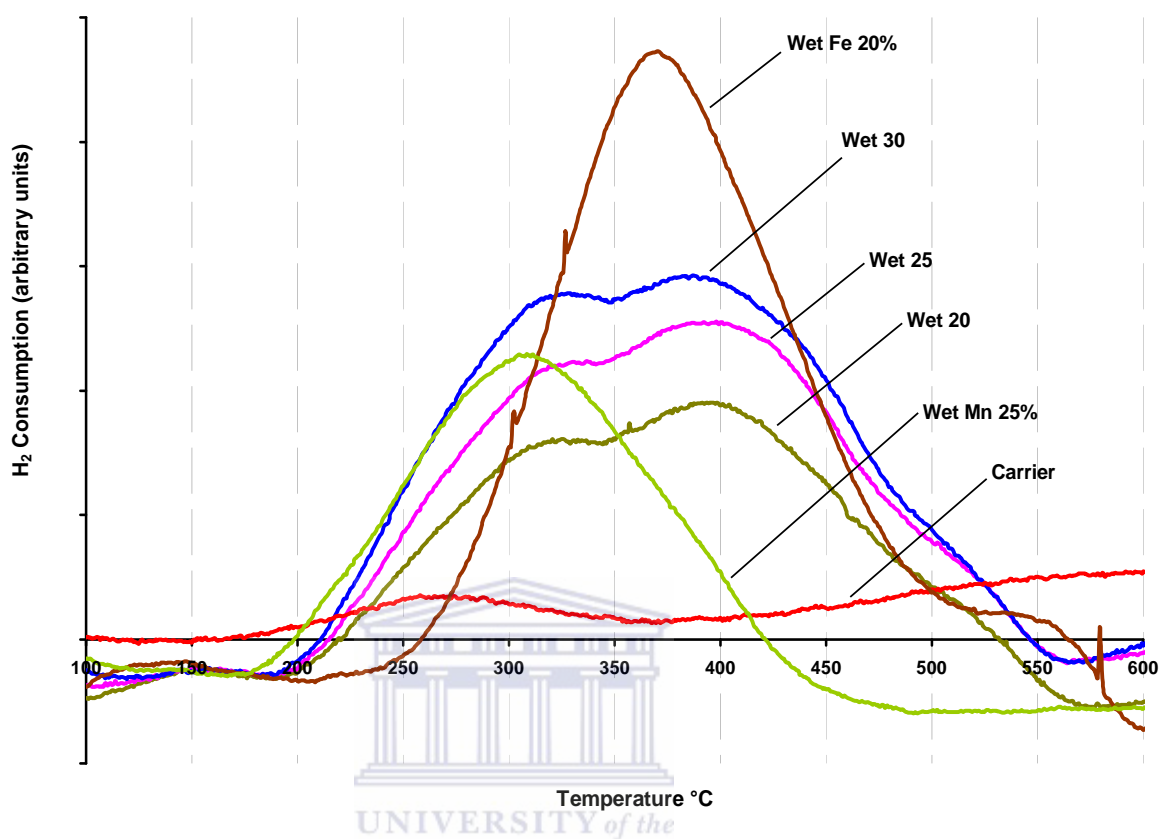


Figure 4-32: H_2 - TRP profiles of wet impregnated samples of Fe and Mn at different loadings.

Figure 4-32 shows the comparison of five different catalysts synthesized by wet impregnation in comparison to a zero % carrier calcined under the same conditions as the catalysts (see section 3.3.2). For the catalyst loaded with iron only at 20 % (wet Fe 20 %), the iron oxide reduction peak appears at 375 °C with a strong signal meaning high H_2 consumption with less effect of the support while in the case of the catalyst synthesized using only manganese (wet Mn 20 %) the metal reduction appears at 310 °C with a weaker signal maybe due to loading, meaning less H_2 consumption and thus less manganese on the support (Velu et al., 2002). The two catalysts used here, wet Mn 20 % and wet Fe 20% have been synthesis just for the TPR characterization technique, that the reason why they cannot be found anywhere else in the thesis. A second weak signal can also be observed on the wet Fe 20 % at around 550 °C meaning a second reduction of the

metal oxide. The two peaks confirm the transformation of two single metal oxides on both catalysts to their reduced metallic form, one is attributed to iron (Fe^{x+}) and the second is attributed to manganese (Mn^{x+}) as confirmed by EDS. It is difficult at this stage to say which oxidation state the metal oxides were in on the support since the broad signal observed due to the effect of the support, can easily cover multiple reduction steps (Xiang-Ying et al., 2006). On the other hand, when the carrier is loaded with both iron and manganese, two distinct different peaks appear in each case for each of the three differently prepared catalysts synthesized at three different theoretical loadings by wet impregnation (30, 25 and 20 %); the first peak on both catalysts appears at 315 °C and seems to be closer to 310 °C, in comparison with the single metal loaded on the carrier which in this case is manganese (Mn^{x+}), this peak is thus attributed to the reduction of manganese oxide, while the second peak observed for all these catalysts synthesized by the combination of metals appears at around 380 °C which in this case seems to be closer to the iron (Fe^{x+}) peak that appeared at 370 °C when iron was the only metal loaded on the carrier, this second peak has thus been attributed to the reduction of iron oxide. The appearance of the two peaks confirms the presence of two different metal oxides in the synthesized catalysts that were formed using the carrier MCM-41 when wet impregnation is used as the metal loading synthesis method. The TPR profiles of these different catalysts has in the present case confirmed one reduction peak with a single loaded metal and two different reduction peaks when the catalysts were loaded with iron and manganese. It is also evident that the Fe peak is higher than Mn peak, indicating that the metal to metal ratio was not 1: 1 as it was confirmed by the ICP results. An interesting comment can also be made on the increase of the metal loading observed on the three peaks (wet 20, wet 25 and wet 30); the amount of hydrogen consumed during the process is directly proportional to the amount of metal oxides present on the catalysts. Each peak corresponds to a certain amount of salt loaded during the synthesis of the catalysts. Figure 4-33 shows different TPR profiles of catalysts synthesized by ion exchange, one when iron was used as a single metal and three when iron and manganese were ion exchanged with the carrier.

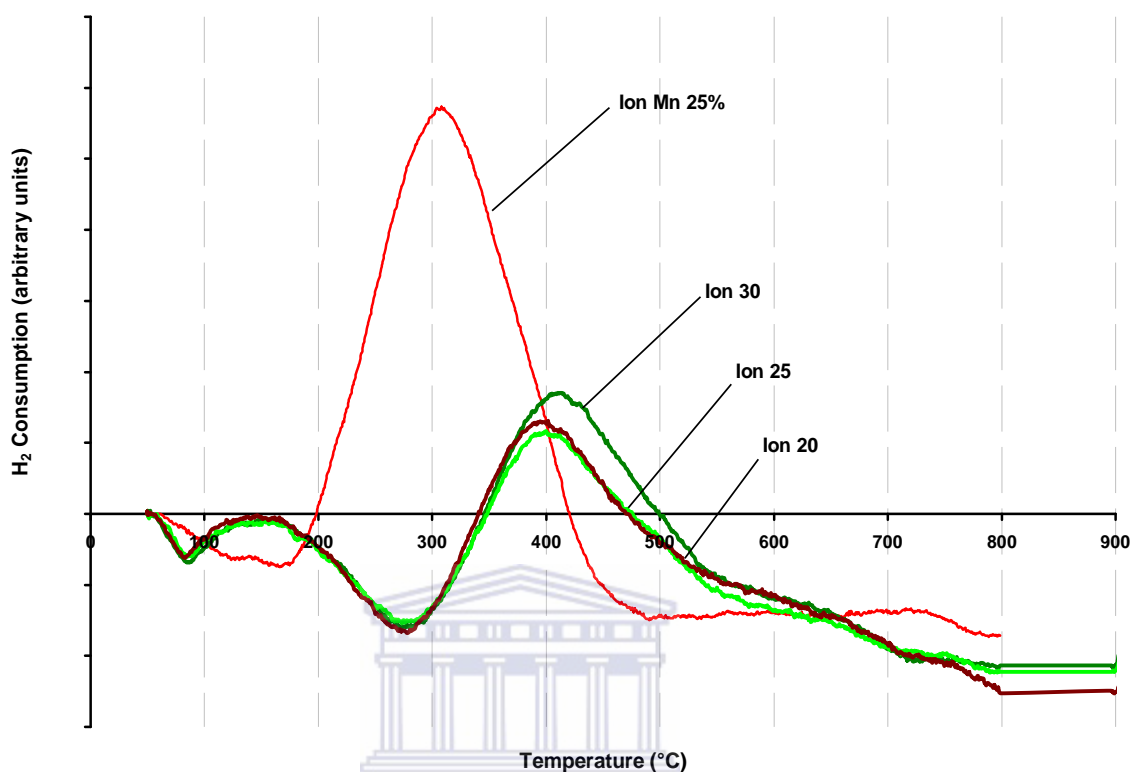


Figure 4-33: TRP profiles of ion exchanged samples of Fe/Mn in comparison with an ion exchanged sample of Mn.

From Figure 4-33, it can be observed that with a single metal, in this case manganese ion exchanged onto the carrier, the reduction peak appears at 310 °C and the peak appearance corresponds with the information in Figure 4-32. The three other catalysts where iron and manganese were ion exchanged onto the support do not come with two different reduction peaks as we expected but on the contrary with only one reduction peak, which appears for all metal loaded catalysts at around 400 °C and corresponds to the iron reduction ($\text{Fe}^{\text{x}+}$) similar to the wet impregnated samples in Figure 4-32. The absence of manganese on the support is attributed to the competition between the two ions during the ion exchange process during which trivalent ions such as Fe^{3+} can more easily be exchanged onto the support than divalent ions such as Mn^{2+} (Velu et al., 2002).

The TPR of the ion exchanged samples also show that there was very little difference in the metal loading achieved for each of the different ion exchanged samples, this shows a maximum loading is achieved already with ion 20 % and increasing the concentration of the ion exchange solution did not correlate with an increase in metal loading. Hence this ion exchange method showed the maximum capacity of the ion exchange sites was around 20 %; one should also notice the baseline offset drift due to the Thermal conductivity detector bridge, normally attributed to poor calibration of the machine. (Samples ion 20, ion 25 and ion 30)

The TPR study of the catalysts synthesized by wet impregnation as well ion exchange provides some important information of the reducible nature of the metal oxides loaded onto the catalysts; it is clear at this stage that the wet impregnated catalysts displayed two different reduction temperatures that are attributed to the two different metal oxides present on the support while the ion exchanges catalysts displayed only one reduction temperature attributed to only iron. Further investigations will be needed in order to be able to interpret say with confidence the oxidation state metal oxides loaded on to the support, what are the implication of using MCM-41 as support and to what extent the loading process can be improved.

Summary of the synthesis and characterization

Fe-Mn/MCM – 41 catalysts

The scanning electron microscopy (SEM) compared to the HR-TEM and SAED was a bit poor in terms of information obtained, the images obtained in the present work confirm the porous nature of the silica host and the images showed fine dispersion of small submicron agglomerated particles of the silica host as well as metal oxides crystallites on the support.

The EDS extended to elemental mapping on different elements composing the catalysts showed some well dispersed catalysts in terms of the loaded elements. Mn and Fe were

found to be well dispersed on the wet impregnated samples while the elemental mapping of the ion exchange catalysts did not reveal the presence of Mn. The present work has demonstrated that using two simple loading techniques such as wet impregnation and post-ion exchange, well balanced catalysts in term of elemental dispersion can be obtained, creating more active sites where the reduction is supposedly to take place.

The present work has also shown that the synthesis of the catalysts by both wet impregnation and post ion exchange with the MCM-41 as support resulted in some meaningful results in the case of the wet impregnation compared to the post ion exchange, reaching the targeted molar ratio of 1 to 1 in terms of Fe and Mn. The optimum ratio is achieved at around 35 wet % (see Table 4.3) which gives a total surface area of 595 m²/g. With regards to the post ion exchange process, the targeted ratio of one to one could not be achieved due to the competition between the two ions (Fe³⁺ and Mn²⁺) on the few existing active sites available on the support; Fe³⁺ was the favorable ion than Mn²⁺, (see Table 4.5). After the mass balance of the post ion exchange samples, we have discovered that, the unattached manganese ions have been washed during the washing step of the catalysts preparation. In conclusion, two graphs summarizing the loading process (Figures 4-6 and 4-7) have been displayed; both graphs show two similar histograms which represent the targeted loading of 1 to 1 molar ratio and the two different histograms below showing what in practice can be obtained compared to the targeted loading. The accuracy of the method was conducted by analyzing standard solutions and the results obtained had a standard deviation of 0.001.

The HR-TEM was conducted on different catalysts starting with the calcined carrier. The image of the calcined carrier (Figure 4-8) showed the regular cylindrical pores of the support with a pore diameter of 2.5 nm which is closed to the 2.8 nm pore diameter obtained from the BET. The pictures of the catalyst displayed in the thesis (Figure 4-9) where dark spots assigned to the oxides were able to be seen on the support. It is difficult to tell at this stage where these oxides can be found on the support; inside the pores or

outside the pores. The SAED on the other hand confirms the presence of these new amorphous phases present on the support.

The X-ray spectroscopy was conducted with the purpose to identify any new particular phase formed on the support. From the obtained results (Figures 4-14, 4-15, 4-16 and 4-17). On both wet impregnated and ion exchanged catalysts, no particular new structures were identified on the support. The results obtained imply that these new structures were present on the support but they are still in their amorphous state. The SAED diffraction pattern confirms our findings at this point when few spots have been seen on the support and not crystalline structures (Figure 4-11). Few changes of the X-ray spectroscopy were observed on the low range on the majority of the spectrums obtained, where the intensities of different peaks decreased due to the presence of particles inside the structure of the support.

The BET results obtained after both wet impregnation and post ion exchange showed approximately similar trends; sharp loss of surface area at the beginning of the loading followed by a slow decrease of surface after the first loading. The optimum for the wet impregnated catalysts was obtained at 525 m²/g corresponding to 35 wet % while the optimum for the ion exchange catalyst was achieved at around 35 wet % too, corresponding to 852 m²/g of surface area. The isotherm and the pore size distribution behave the same way for both samples (Figure 4-5, 4-6, 4-7 and 4-8).

FT-IR spectrum of the catalysts synthesized by both wet impregnation as well as post ion exchange did not reveal too much in term of new bands identified on the support a part from the existing characteristic bands belonging to the support, which in most cases were present before and after the synthesis of the catalysts.

The TGA as a complimentary analysis was conducted to assess what has already been said in term of new phases formed on the support. It is clear that after running the TGA that the catalysts only lost moisture in the first region below 100° C, followed by a long stable region where a slow structural decomposition was observed. However, no de-

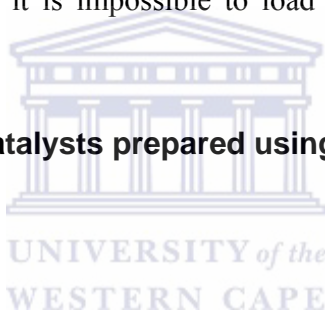
hydroxylation could be observed up to 600 °C. The TGA reveals stable catalysts since they all showed the same patterns with minor differences in their moisture contents.

The TPR has been the most revealing technique in terms of results obtained. The single loaded catalysts with Mn and Fe have in each case reveal one reductive site on the catalyst meaning one oxide type formed in each case. On the other hand, when the metal were simultaneously loaded, the wet impregnated catalysts reveal two reductive sites, one assigned to the presence of Mn and another assigned to the presence of Fe; these results were in agreement with the elemental mapping of the ion exchange catalyst. In conclusion, the present work has demonstrated that it is possible to load two metals on the support by wet impregnation and create two different types of active sites, while with the post ion exchange process it is impossible to load two ions at different oxidation stages.

4.3 Characterization of catalysts prepared using H – Beta - 25 zeolites as support

4.3.1 Introduction

The following section summarizes the characterization of the catalysts obtained when H - Beta - 25 zeolite from SÜD Chemie was used as support. The characterization techniques used for these catalysts are limited to a few techniques compared to those done on the catalysts obtained when MCM - 41 was used as support. The preparation methods used for the synthesis of the catalysts can be found in section 3.3.4.1 and 3.3.4.2 for both wet impregnated samples and ion exchange samples supported on H-Beta-25 respectively. The reason for performing the experiments shown in this section is to compare using a microporous support ($< 7.5 \text{ \AA}$ pore size) to synthesize a new set of catalysts and compare the results of the synthesis procedure obtained with these catalysts (Fe-Beta-25) against the results obtained with the catalysts synthesized when MCM-41 with much larger pore size (2-3 nm) was used as the supporting material. The set of catalysts synthesized with H-Beta-25 zeolites are named according to the synthesis method used. The catalysts



synthesized by wet impregnation are called 5 %/Fe-Beta-25 and 10 %/Fe-Beta-25 depending on the loading percentage of salt used, and the catalysts synthesized by ion exchange are named according to the concentration of the salt solution used, i.e: 0.01/Fe-Beta-25, 0.05/Fe-Beta-25, 0.1/Fe-Beta-25 and 0.2/Fe-Beta-25. It has been reported by companies such as SÜD Chemie and Zeolist Ltd that it was possible to prepare a DeNO_x catalysts using H-Beta-25 as a substrate, and the catalyst has been proven to be successful at large scale. It was impossible to get a commercial sample, that why we have decided to synthesized our own catalyst; a Fe-Beta-25 catalyst has been prepared in the laboratory and will be used as a commercial product for comparison purpose. The catalysts as prepared will be characterized by ICP for metal content, HRTEM for surface structure and topological study, XRD for crystalline phase's study and N₂-BET for surface area and pore size distribution.

4.3.2 Surface structure and topology study by High resolution transmission microscopy

The following image (Figure 4-34) show the Fe-beta-25 zeolite synthesized by ion exchange

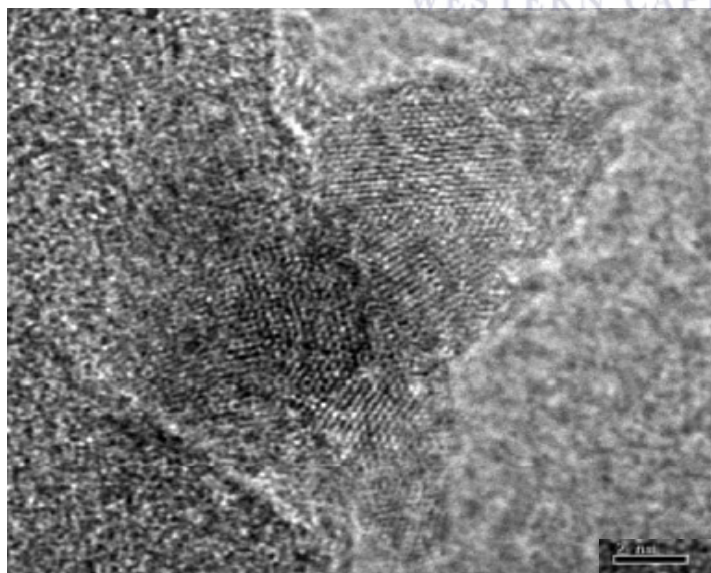


Figure 4-34: HRTEM of the Fe-Beta-25 catalyst loaded by ion exchange

The nature of micro-porous zeolite can be seen in the center of the image where small parallel lines are visible. These pores are very small (below 2 nm) when a comparison is made with the pore of the MCM-4 1 with large pore size diameter.

4.3.3 Crystalline phases study by X-ray diffraction spectroscopy

The XRD spectra of all the samples were obtained according to the procedure described in section 3.4.2.1, and the experiments were conducted on the D8 Advance from Bruker AXS from $2\theta = 5$ to 60° to assess the characteristic of the H-Beta-25 zeolites alone first and secondly, to assess whether or not there is formation of any new phase on the support after metal impregnation and ion exchange with the support.

Figure 4-35 shows the XRD pattern of the pure H-Beta-25 zeolites run from $2\theta = 5$ to 60°

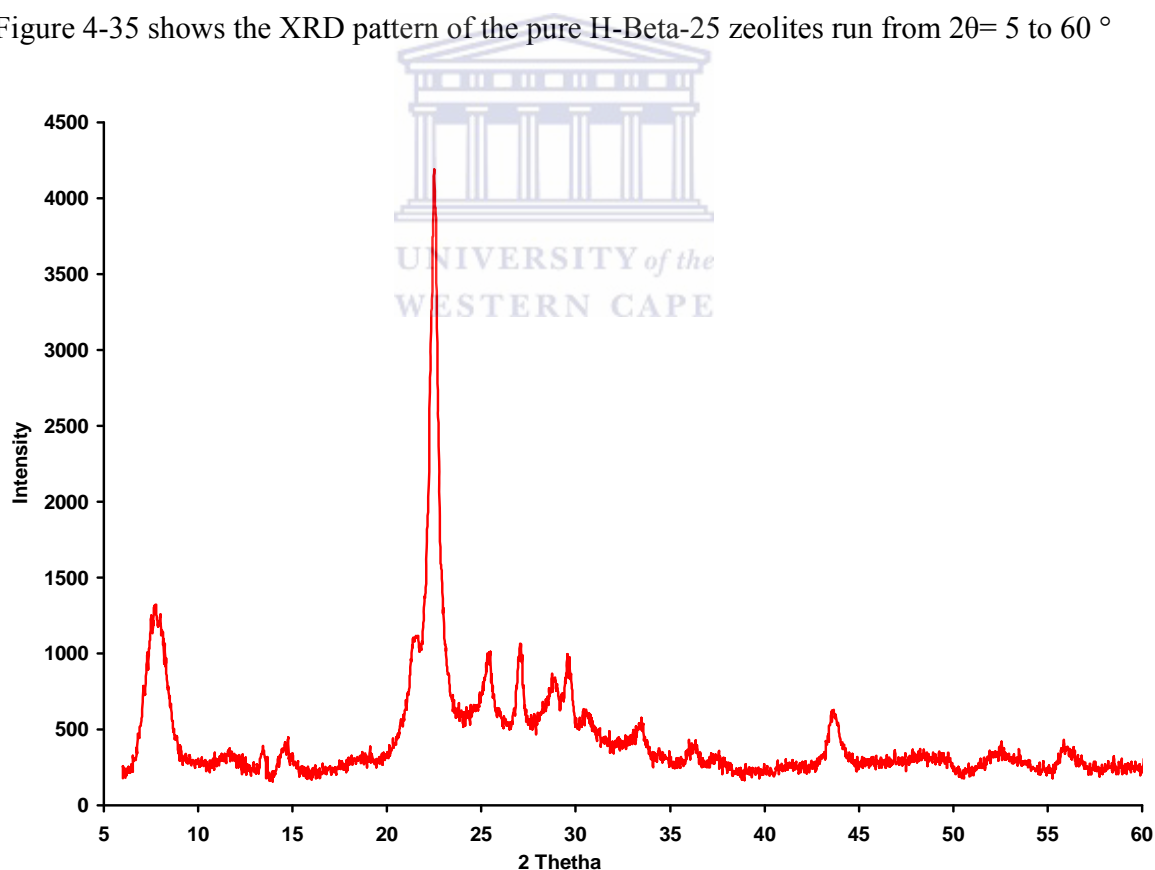


Figure 4-35: XRD profile of a pure H-Beta zeolite

The XRD pattern of the H-Beta zeolite from SÜD Chemie confirms the pattern obtained by Treacy and Higgins (Treacy, 2007). This spectra as obtained will serve as reference and will be compared to the XRD graphs of the H-Beta metal loaded catalysts synthesized by both ion exchange and wet impregnation.

Figure 4-36 shows the XRD pattern of the support (H-Beta-25) in comparison with the two catalysts synthesized by wet impregnation.

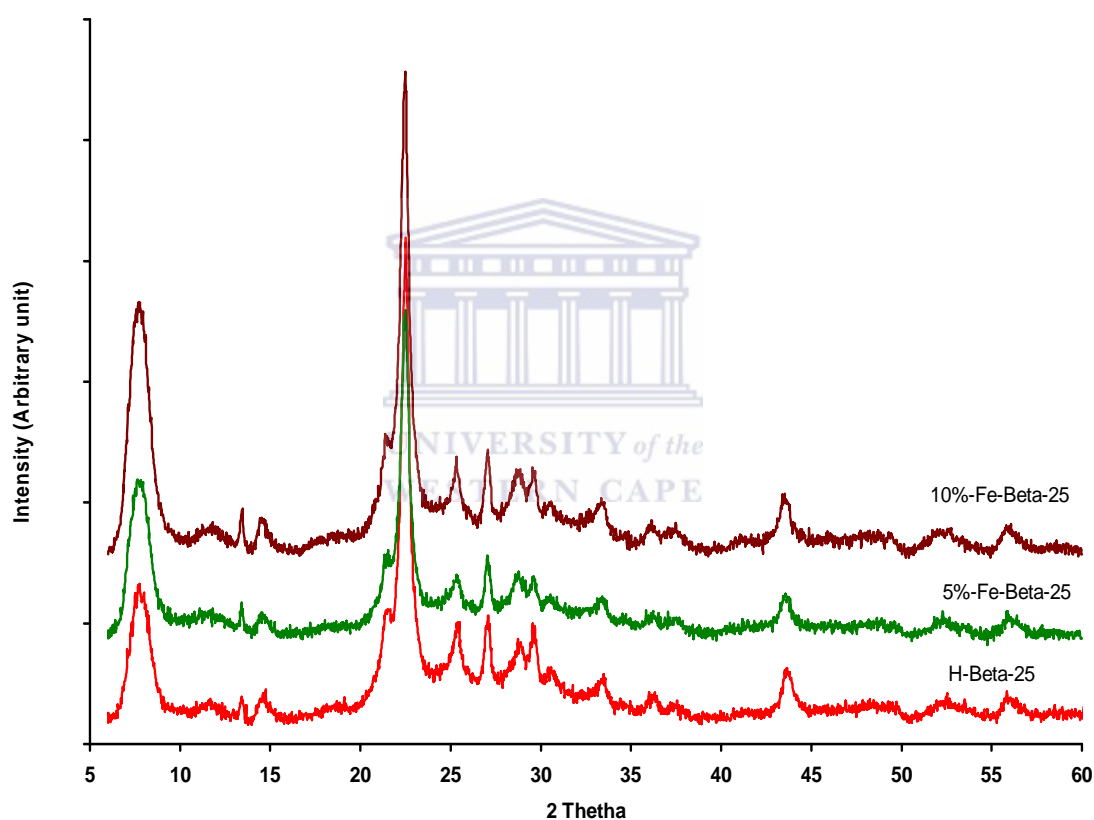


Figure 4-36: XRD profile of a pure H-Beta zeolite in comparison with two Fe-Beta catalysts synthesized by wet impregnation.

From the above graph (Figure 4-36), the peak observed at $2\theta = 13.5^\circ$ has seen an increase in intensity when the peak observed on the catalyst synthesized at 10% is compared to the intensity of the peak observed on the support. This increase of intensity is attributed to the presence of a metal oxide at that particular intensity (Velu et al., 2002). The

remaining peaks are still constant in term of their intensities compared to those observed on the support, except for the two peaks observed at $2\theta = 29$ and $2\theta = 29.6^\circ$ with the first increasing its intensity while the second peak loses its intensity. The increase in intensity is attributed to the presence of a metal oxide, while the decrease in terms of intensity is attributed to the presence of particulates inside the structure of the zeolite (Velu et al., 2002).

Figure 4-37 shows the XRD pattern of the catalysts synthesized by ion exchange in comparison with the XRD pattern of the H-Beta-25 zeolites.

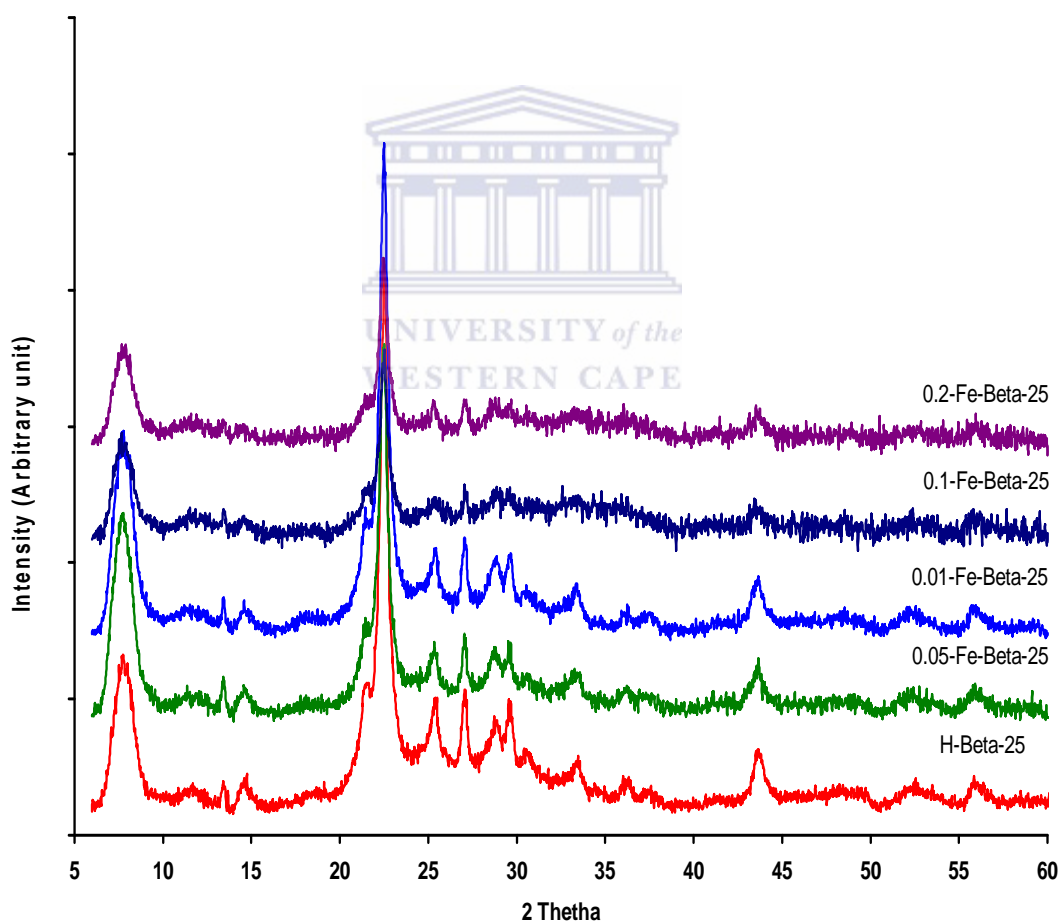


Figure 4-37: XRD profile of a pure H-Beta zeolite in comparison with four Fe-Beta catalysts synthesized by ion exchange.

From the above graph (Figure 4-37), different peaks observed on the support are still present on the catalysts with the majority of the peaks having lost their intensity as the metal loading increased while some have completely disappeared on the catalysts. The loss of intensity was attributed to the presence of metal particulates inside the structure of the zeolite occluding the pores; while the decrease of intensity is attributed to the loss of porosity or crystallinity at that particular angle (Velu et al., 2002). This was further confirmed with N₂-BET analysis.

4.3.4 Surface area and pore size distribution study by N₂-B.E.T (BRUNAUER – EMMET –TELLER)

The BET surface area and pore size distribution of the wet impregnated and ion exchanged catalysts including the carrier were carried out on a Micrometrics Tri Star 3000 as it is described in section 3.4.5.1

Table 4.10 presents different surface areas and average pore diameter size of the support (H-Beta-25) zeolites and six other catalysts; two synthesized by wet impregnation and four by ion exchange.

Table 4.10: Nitrogen BET areas and mesopore diameter of catalysts synthesized from H-Beta-25 zeolites

Catalysts Name	Calculated Loading	Total surface area (m²/g)	BJH Micro-pore surface are (m²/g)
H-Beta zeolite (Support)	0 (zero)	616	232
Wet impregnation catalysts			
5 %- Fe-Beta-25	5 %	591	217
10 % Fe-Beta-25	10 %	427	198
Ion exchange catalysts			
0.01/Fe-Beta-25	0.01 M	577	222
0.05/Fe-Beta-25	0.05 M	550	220
0.1/Fe-Beta-25	0.1 M	499	206
0.2/Fe-Beta-25	0.2 M	439	203

From Table 4.10, it can be seen that the zeolite H-Beta-25 used as support already had a lower total surface area compared to the MCM-41 surface used as support (616 m²/g compared to 1076 m²/g). With the first loading taking place at 5 % wet impregnation, the catalysts lost 25 m²/g surface area representing 4 % of the initial specific surface area that the support had. The second loading taking place at 10 % wet impregnation caused the support to lose 31 % of its initial specific surface area; it is difficult at this stage to say with confidence whether or not only the internal microporous surface area (SA) of the support has been affected as the N₂-BET cannot measure micropores surface area directly. The wet impregnation method itself is used because it was found that the metal deposition will affect both the internal and external surface area (Lawrence, 2005). For the ion exchanged catalysts, the specific surface areas of these different catalysts 0.01/Fe-Beta-25, 0.05/Fe-Beta-25, 0.1/Fe-beta-25 and 0.2/Fe-Beta-25 have decreased to 94, 89, 1

and 71 % respectively of the original value showing that of Fe incrementally exchanged with the support. Comparing the ion exchange and the wet impregnation procedures, it can once again be confirmed by the result obtained at this stage that wet impregnation still has a high possibility of giving more iron as the loading achieved was higher compared to the ion exchange method.

Figure 4-38 show the hysteresis of the support (H-Beta-25) in comparison with the hysteresis of the two catalysts synthesized by wet impregnation at 5 and 10 % respectively.

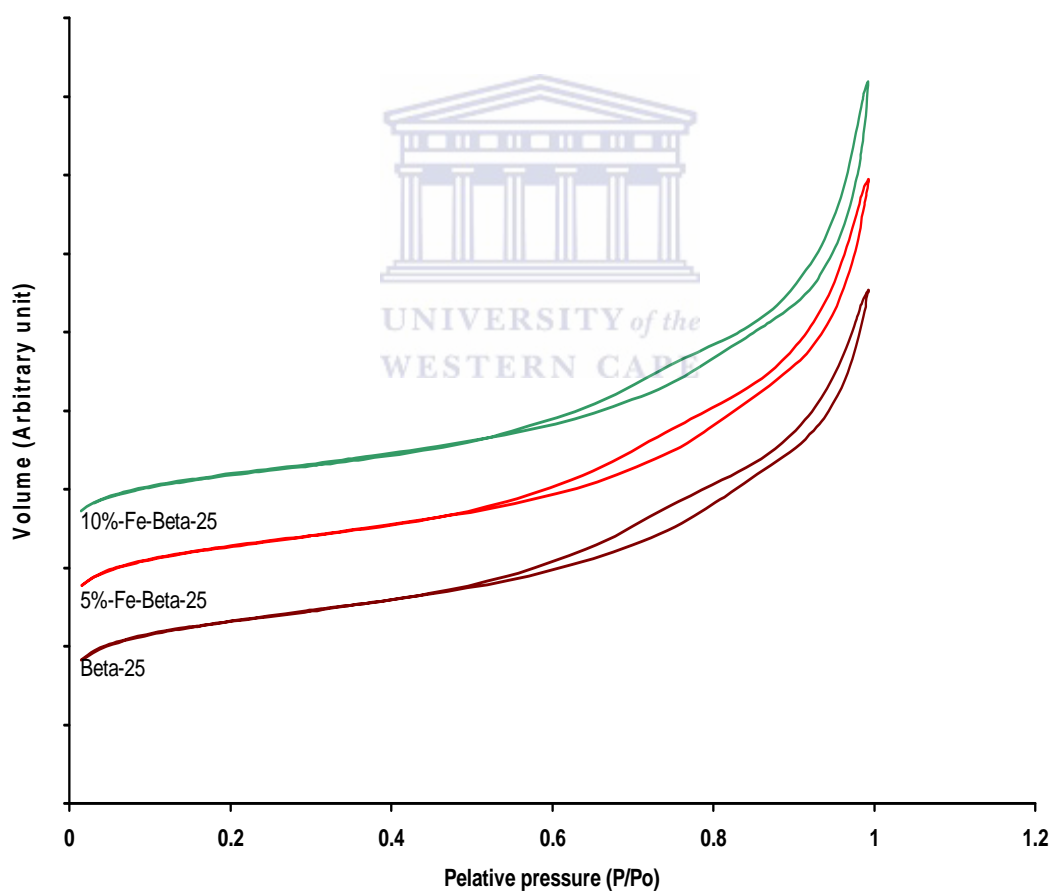


Figure 4-38: Nitrogen adsorption/desorption isotherm at 77 K of the calcined support (H-Beta) in comparison with two catalysts synthesized by wet impregnation (5 %-Fe-Beta-25 and 10 % Fe-Beta-25).

The hysteresis of the three materials (Figure 4-38) are all characteristic of microporous materials of type B (see Figure 2-11) according to the IUPAC classification of powder with the inflection point found above the relative pressure of 0.4 mmHg compared to the mesoporous materials where the inflection point can be found between 0.2 and 0.4 mmHg (Savidha et al., 2004). The hysteresis as obtained do not show any particular difference (inflection point, sharpness of the loop) between the hysteresis of the parent material and the hysteresis of the two catalysts.

Figure 4-39 shows the mesopore size distribution of the support (H-Beta-25) and the two catalysts synthesized by wet impregnation.



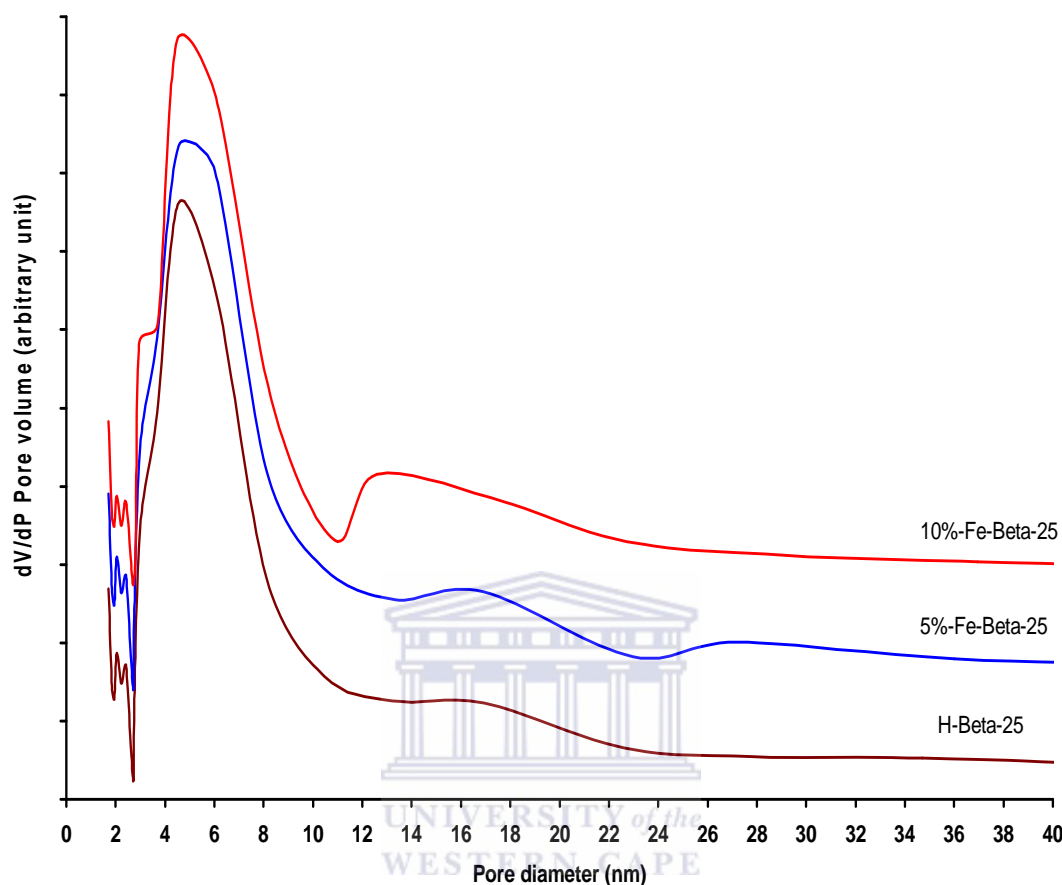


Figure 4-39: Pore size distribution of support (H-beta-25) in comparison with the pore size distribution of two catalysts (5 %Fe-Beta-25 and 10 %Fe-Beta-25).

The pore size distribution of the three materials shows bi model pore distribution size, with a large amount of pores in the mesoporous range and the rest of the powder in the micro region indicating intergranular voids being in the mesoporous region, with the rest of pores in the microporous region.

Figure 4-40 shows the hysteresis of the support in comparison with the hysteresis of three catalysts synthesized by wet impregnation.

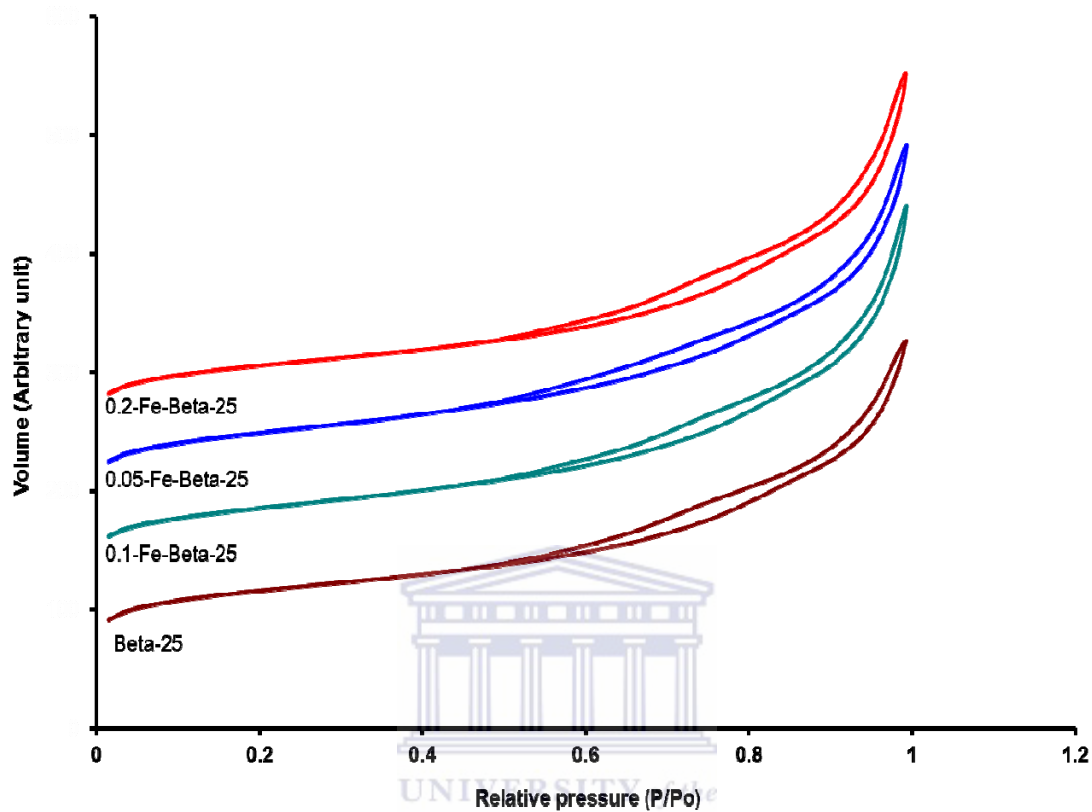


Figure 4-40: Hysteresis of the support (H-Beta-25) in comparison with the hysteresis of three catalysts synthesized by wet impregnation.

The hysteresis of the three catalysts as obtained after synthesis by ion exchange are still similar to the hysteresis of the parent material (H-Beta-25), this implies that, despite the ion exchange of metal onto the zeolite support, the metals inside the pores have no impact on the porosity of the support, but the reduction of the pore size can only be observed upon inspection of Table 4.10 where a systematic decrease in the pore size diameter can be observed.

Figure 4-41 shows the mesopore size distribution of the support (H-Beta-25) and three different catalysts synthesized by ion exchange.

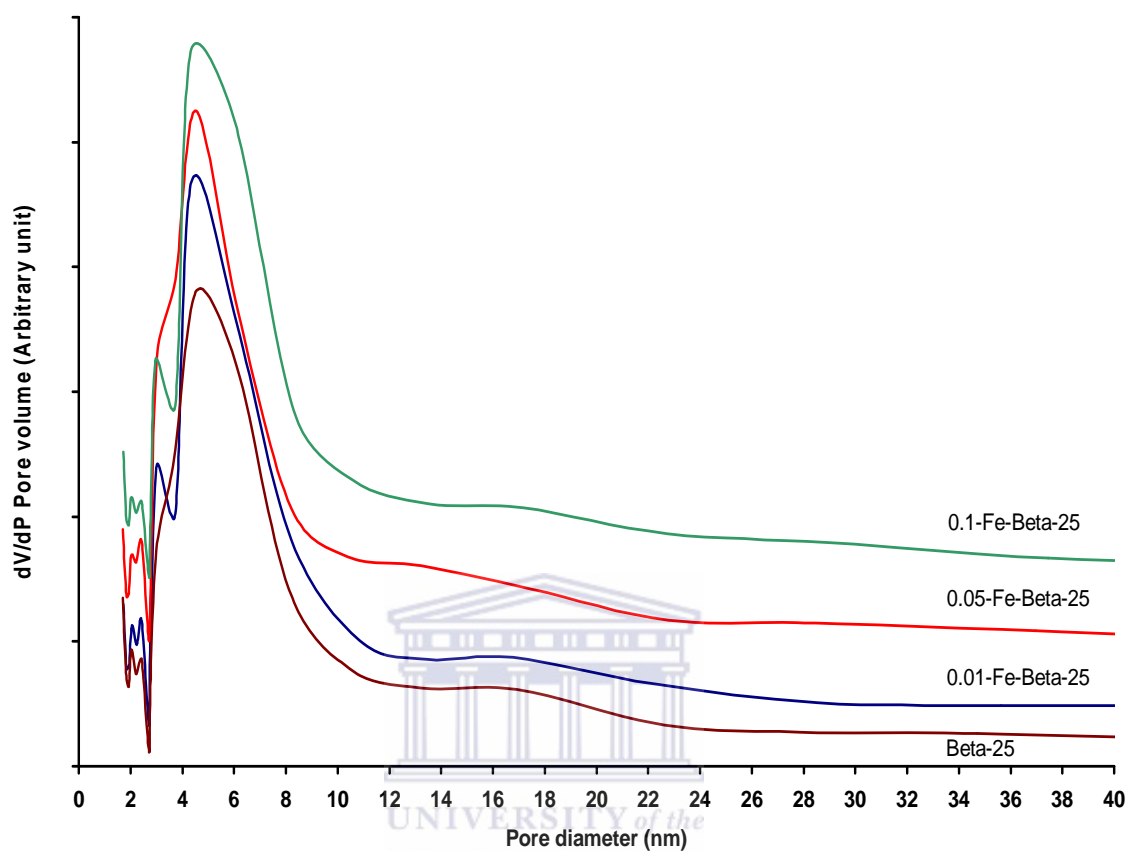


Figure 4-41: Pore size distribution of support (H-beta-25) in comparison with the pore size distribution of three catalysts (0.1Fe-Beta-25, 0.05Fe-Beta-25, 0.01-Fe-Beta-25).

The pore size distribution of the four catalysts (Figure 4-41) as shown incremental filling of the inter-particle voids with the metal; The N_2 gas used for analysis did not allow direct measurement of the micropore region. The BET total surface area is given in Table 4.10. Figure 4-41 was obtained from BJH incremental adsorption data.

4.3.5 Chemical bonding study of the catalysts by Fourier transformed infrared spectroscopy

The FT-IR experiments were conducted on a Perkin Elmer® (Universal ATR) according to the procedure described in section 3.4.5.1 in the range of 500 to 2000 cm^{-1} . The catalysts synthesized by wet impregnation are analysed first, followed by the analysis of

the ion exchange catalysts, all these catalysts were compared to the carrier (H-Beta-25) with no metal loading.

Figure 4-42 shows the FT-IR spectra of the support (H-Beta-25) in comparison with the spectrum of the two catalysts synthesized by wet impregnation taken in the range of 500 to 2100 cm^{-1} .

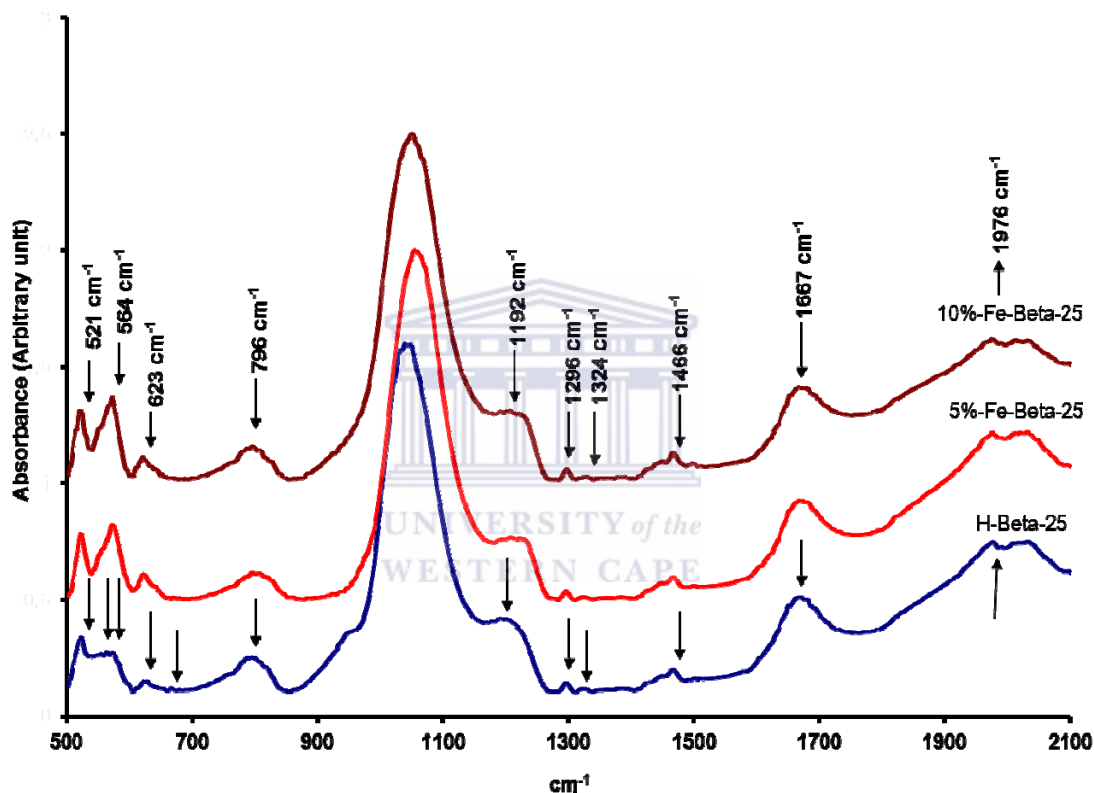


Figure 4-42: FT-IR spectra of the support (H-Beta-25) and two catalysts taken in the range of 500 to 2100 cm^{-1} .

The FT-IR spectrum of the support H-Beta-25 (Figure 4-42) shows specific bands at 524, 564, 574, 623, 667, 796, 1192, 1296, 1324, 1466, 1667, and 1976 cm^{-1} . These different bands are assigned to the internal tetrahedra (asymmetrical stretch, symmetrical stretch and T-O bend) and external tetrahedra (Double rings, pore opening, symmetrical stretch and asymmetrical stretch) of the H-Beta-25 zeolite (Breck et al., 1974; Weitkamp and Puppe et al., 1999). After the wet impregnation process, these specific bands of the

zeolite are still present on the spectrum, apart from the appearance of three new bands at 1208, 1388 and 1497 cm^{-1} assigned to the presence of iron on the support. The new metallic phase as obtained was also confirmed by the XRD pattern conducted on the same catalysts. An important aspect to be remembered at this stage was the reduction of the catalysts under nitrogen atmosphere to reduce the oxide into its metallic form.

Figure 4-43 shows the FT-IR spectra of the support (H-Beta-25) in comparison with the spectra of the four catalysts synthesized by ion exchange taken in the range of 500 to 2100 cm^{-1} .

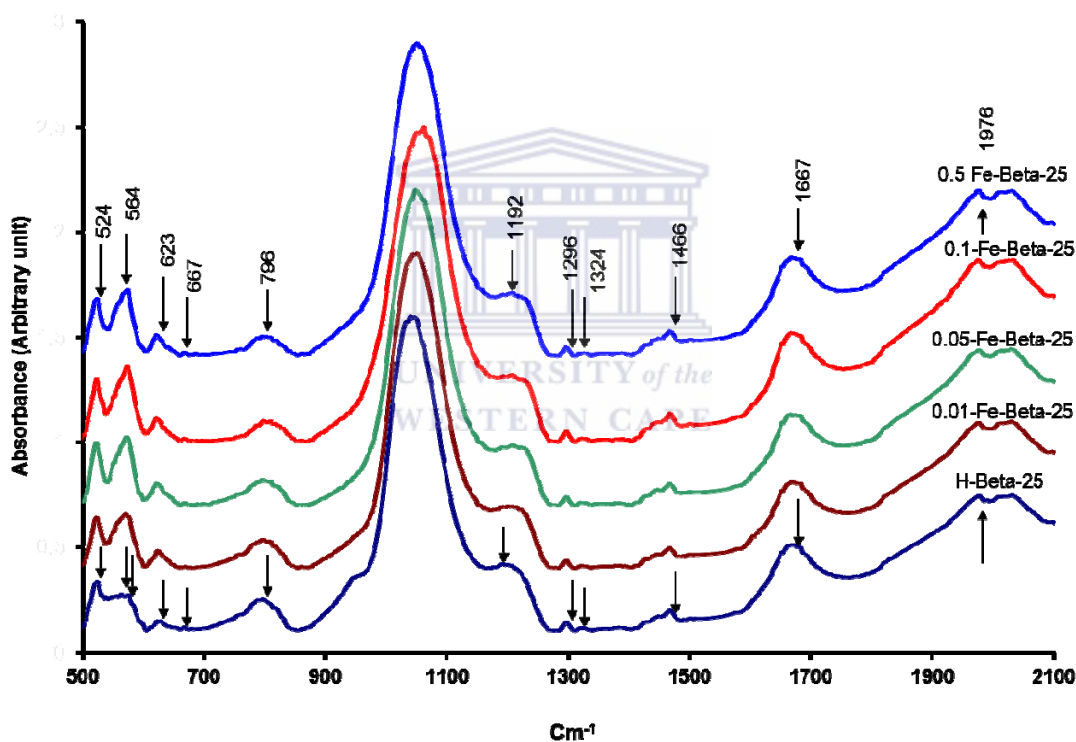


Figure 4-43: FT-IR spectra of the support (H-Beta-25) and four catalysts taken in the range of 500 to 2100 cm^{-1} .

The FT-IR spectrum of the ion exchanged catalysts showed once again the characteristic bands of the Zeolite support at 524, 564, 574, 623, 667, 796, 1192, 1296, 1324, 1466, 1667, and 1976 cm^{-1} . These different bands have been assigned to the internal tetrahedra (asymmetrical stretch, symmetrical stretch and T-O bend) and external tetrahedra

(Double rings, pore opening, symmetrical stretch and asymmetrical stretch) of the H-Beta-25 zeolite (Breck et al., 1974; Weitkamp and Puppe et al., 1999). After the ion exchange process two new specific bands have emerged on the catalysts, 1207 and 1387 cm^{-1} and the two new bands were once again assigned to the presence of the ion in its metallic form.

Summary of the synthesis and characterization

Fe - Beta – 25 catalysts

The surface area as well as the pore size distribution obtained from the catalysts synthesized using the H-Beta-25 zeolite as support confirmed the microporous nature of the support with pore size below 20 Å, and a loop on the isotherm starting at high relative pressure (0.45) compared to mesoporous counterpart where the loop starts a bit earlier between (0.3 and 0.4). The ion exchange and the wet impregnation conducted on the zeolites had a minor impact on the surface area in both cases, but that impact was insignificant compared to the same procedure conducted on the MCM-41. It is clear to us at this stage to say that the catalysts from zeolites and MCM-41 as support will have different catalytic effect since they present a huge gap in their surface areas. Low surface area implies low activity while high surface area implies high catalytic activity.

The XRD patterns of the catalysts synthesized by both wet impregnation and ion exchange show a decrease in peak's intensities in the two cases, with less new peaks formed. The decrease in intensity confirmed the presence of particulates inside the structure of the support, while new peaks formed confirmed the presence of iron on the support.

The FT-IR was conducted as complementary analysis since it did not provide many details in terms of the nature of the new bands identified on the catalysts. At least, the work has shown that the synthesis of catalysts by both ion exchange and wet

impregnation with the H-Beta-25 was an easy process since the support was in its H form making the ion exchange process easy.



CHAPTER 5

5 CONCLUSIONS AND RECOMMENDATIONS

This chapter underlines and summarizes the major issues addressed in the thesis. These first points are followed by considering possible directions for future work and recommendations in the choice of substrate and characterization techniques when it comes to bimetallic loading process.

5.1 Conclusions

Fe-Mn/MCM – 41 catalysts

This study has shown that the synthesized catalysts could be used as DeNO_x catalysts such as Fe-Mn/MCM-41 and Fe-Beta-25 can be synthesized using two different substrates such as MCM-41 and H-Beta-25 zeolite that can be incorporated with two different metal oxides; Fe and Mn in the case of MCM-41 and a single metal such as Fe in the case of H-Beta-25, using either wet impregnation or ion exchange.

The results obtained in this study highlight the fact that MCM-41 used as a substrate presents less exchangeable sites compared to H-Beta-25 which presents high density of exchangeable sites for metal incorporation onto its structure. These two particular characteristics have made H-Beta-25 the substrate of choice for ion exchange and MCM-41 the substrate of choice for wet impregnation.

Contrary to what has been claimed by other authors, the molar ratio of one to one in terms of Fe and Mn is not achievable when loading the mesoporous substrate with metal; but a ratio closer to 1:1 of Fe:Mn (0.167 Mol/g Fe and 0.164 Mol/g Mn) can be achieved when wet impregnation is used as the metal loading method. The highest ratio achieved during this study with the ion exchange method (ion 20 %) 0.054 Mol/g was around 2:1 of Fe:Mn, showing preferential adsorption of Fe during metal loading in this binary metal system.

Different methods were used to characterize the catalysts. EDS as a qualitative analysis has shown that the two metals of interest in this case Fe and Mn were present on the support but at different atomic ratio, depending on the % loading and upon the loading method used. ICP and AAS as quantitative analysis methods showed that Mn and Fe were present on the MCM-41 support and an optimum molar were achievable at a calculated loading of 30 % (0.303 Mol/g Fe and 0.297 Mol/g Mn) of wet impregnated samples and 30 % loading when ion exchange was used as the metal loading method of choice (0.057 Mol/g Fe and 0.026 Mol/g Mn). The difference between the ICP and AAS results has led this present work to consider ICP as the method of choice for analysis despite the matrix effect that can affect the final result.

The morphological study of the catalysts (Fe-Mn/MCM-41) showed some sub-micron spherical particles attributed to the presence of metal oxides particles; this first method was followed by the elemental mapping of the catalysts using mapping technique. The mapping showed well distributed metal was obtained in both cases (wet impregnation as well ion exchange) but revealing the near absence of Mn on the ion exchange catalysts.

The ICP which was retained as the analysis method of choice revealed some deviation of results between the theoretical loading and the calculated loading in the case of the Fe-Mn/MCM-41. These deviations were mainly due to the weakness of the ICP as a method of analysis, and secondly due to inconsistent metal loading during the synthesis of the catalysts as a result of the preparation method during which the dilution factor and other procedures used could have introduced errors that may have also impacted on the final results obtained.

The thermogravimetric study as well as the Fourier transformed infrared were not very revealing in terms of new structures or new type of bonds formed on the support. The high resolution microscopy coupled with the SAED analysis revealed the hexagonal structure of the Si support as well as the pore size of the support prior to metal loading

which was around 2.5 nm close to the value obtained from the BET analysis, which was 2.8 nm.

The SAED revealed the amorphous nature of the mesoporous Si support matrix showing typical diffuse rings, while the analysis of the metal loaded catalysts confirmed the formation of new crystalline structures on the MCM-41 support. The low XRD as well as the wide angle XRD were not able to resolve the new crystalline metal structures formed on the support that the SAED was able to reveal, due to the very small particle size of the loaded metals, which was below the nanometer range. The BET surface of different catalyst obtained was found to correlate with the loading capacity. An increase in the loading capacity resulted in a decrease in surface area with the optimum loading obtained at a theoretical loading of 35 weight % for the wet impregnated samples and 30 weight % for the ion exchange samples.

The most revealing characterization method was the TPR; with this method, wet impregnated samples showed that two types of metal oxides were loaded on the support, which amounts were dependent upon the loading capacity. The ion exchange samples showed one peak attributed to reduction of the loaded Fe oxide on the support, confirming that Mn could not be exchanged onto the mesoporous support in the presence of the competing Fe species during ion exchange.

Fe - Beta – 25 catalysts

The study of the ion exchange process on the Fe-Beta-25 catalyst has shown interesting results contrary to results obtained using ion exchange to incorporate metals onto the MCM-41 when the (Fe and Mn) bimetallic system was used. It was clear that the micro porous zeolite used in this study presented more exchangeable sites than the MCM-41 as there was no maximum metal loading capacity shown during ion exchange of Fe onto the support, unlike the case of MCM-41. This aspect was shown by the steady decrease in the BET surface area at increasing metal loadings on H-Beta-25 (0.01 % Fe-Beta-25: 222

m²/g; 0.05 % Fe-Beta-25: 220 m²/g; 0.1 % Fe-Beta-25: 206 m²/g; 0.2 % Fe-Beta-25: 203 m²/g).

The XRD pattern of the metal loaded H-Beta-25 showed a decrease in peak intensity which was attributed to the presence of metallic particles inside the structure of the H-Beta-25 zeolite after the wet impregnation as well as ion exchange process.

The HRTEM images resolved pores in the microporous region characteristic of the Beta zeolite which were in the Angstrom region compared to the nanometer sized pores of the MCM-41 that are in the mesoporous region.

This study demonstrated that:

- It is possible to incorporate two different metals oxides within the structure of the mesoporous silica (MCM-41) by wet impregnation and not by ion exchange.
- Wet impregnation and ion exchange do not lead to the same results when MCM-41 is used as a substrate.
- High metal loading capacities were achievable at different applied loadings: in the case of wet impregnation the highest loading achieved was 35 % (0.810 Mol/g support) and in the case of ion exchange the maximum loading was achieved at 20 % (0.054 Mol/g support) where after no more metal could be incorporated.
- The study of the bimetallic system such as Fe-Mn/MCM-41 was previously conducted, but no proof of the existence of the two metals on the support has been presented in literature; in this study, a methodical approach of attaining the bimetallic system was conducted and enough proof to confirm the state of the two metal oxides on the support has been given.
- It was shown that substrates such as mesoporous silica (MCM-41) can accommodate two metals or one metal oxide mainly due to its large pore diameter, but that competitive adsorption plays a role in the metal ratio achievable depending on the preparation method chosen.

- It is clear that MCM-41 contrary to H-Beta-25 does not have exchangeable hydrogen limiting its possibility of incorporating more metal onto its structure during ion exchange compared to the zeolite substrate, the only mode of attachment of metal oxides in mesoporous silica is believed to be by grafting.
- H-Beta-25 used as support does not present a limit to the tested loading capacity, unlike the MCM-41 substrate.
- HRTEM images of the two catalysts (Fe-Mn/MCM-41 and Fe-Beta-25) support the argument of well dispersed catalysts in both cases that should lead to good catalytic activities.

5.2 Recommendations for future work

The DeNO_x project as mentioned in the introduction is still an ongoing project, this first stage of the project has laid down a foundation and future catalytic studies will take it from here for comparative purpose.

This work has shown the schematic for the design of a rig for DeNO_x tests which has been built, and improvement of the rig for advanced studies such kinetics and mechanism of NO_x will be necessary.

Other methods of incorporating metals oxides onto the MCM-41 substrate needs to be investigated and results obtained need to be compared to the two methods studied here.

Limitations in terms of characterization facilities have also been an important factor that needs to be addressed so that scientific conclusion can be drawn after study of the synthesized catalysts.

6 REFERENCES

Ajaikumar S. & Pandurangan, A. 2009, "Efficient synthesis of quinoxaline derivatives over ZrO_2/MxO_y (M = Al, Ga, In and La) mixed metal oxides supported on MCM-41 mesoporous molecular sieves", *Applied Catalysis A: General*, vol. 357, no. 2, pp. 184-192.

Amiridis M., Zhang T. & Farrauto, R.J. 1996, "Selective catalytic reduction of nitric oxide by hydrocarbons", *Applied Catalysis B: Environmental*, vol. 10, no. 1-3, pp. 203-227.

Anderson J. & Pratt K. 1988, *Introduction to characterization and testing of catalysts*, Academic Press edn, Harcourt Brace Jovanovich, London.

Arous W., 2007, "Selective catalytic reduction of NO by NH_3 on Cu (II) ion-exchanged offretite prepared by different methods", *Topics in Catalysis*, vol. Volume 42-43, Numbers 1-4, pp. 51-54.

Baiker A., 1987, "Introduction to the characterization and testing of catalysts", *Applied Catalysis*, vol. 29, no. 2, pp. 390-390.

Blanco J., Avila, P., Suárez, S., Martín, J.A. & Knapp, C. 2000, "Alumina- and titania-based monolithic catalysts for low temperature selective catalytic reduction of nitrogen oxides", *Applied Catalysis B: Environmental*, vol. 28, no. 3-4, pp. 235-244.

Chang T. & Fang C. 1999, "Reactivity of titanosilicates-supported catalysts for the selective catalytic reduction of NO with NH_3 ", *Applied Catalysis A: General*, vol. 180, no. 1-2, pp. 123-131.

Chuan S., Cheng, M., Zhenping, Q., Xuefeng, Y. & Bao, X. 2002, "On the selectively catalytic reduction of NO_x with methane over Ag-ZSM-5 catalysts", *Applied Catalysis B: Environmental*, vol. 36, no. 3, pp. 173-182.

Dumesic J., Topsøe, H. & Boudart, M. 1975, "Surface, catalytic and magnetic properties of small iron particles : III. Nitrogen induced surface reconstruction", *Journal of Catalysis*, vol. 37, no. 3, pp. 513-522.

References

- Dumesic, J.A., Topsøe, N.-., Topsøe, H., Chen, Y. & Slabiak, T. 1996, "Kinetics of Selective Catalytic Reduction of Nitric Oxide by Ammonia over Vanadia/Titania", *Journal of Catalysis*, vol. 163, no. 2, pp. 409-417.
- Economidis N., Peña, D.A. & Smirniotis, P.G. 1999, "Comparison of TiO₂-based oxide catalysts for the selective catalytic reduction of NO: effect of aging the vanadium precursor solution", *Applied Catalysis B: Environmental*, vol. 23, no. 2-3, pp. 123-134.
- Forzatti P., 2000, "Environmental catalysis for stationary applications", *Catalysis Today*, vol. 62, no. 1, pp. 51-65.
- Frache A., Palella, B., Cadoni, M., Pirone, R., Ciambelli, P., Pastore, H.O. & Marchese, L. 2002, "Catalytic DeNO_x activity of cobalt and copper ions in microporous MeALPO-34 and MeAPSO-34", *Catalysis Today*, vol. 75, no. 1-4, pp. 359-365.
- García-Bordejé E., Pinilla, J.L., Lázaro, M.J. & Moliner, R. 2006, "NH₃-SCR of NO at low temperatures over sulphated vanadia on carbon-coated monoliths: Effect of H₂O and SO₂ traces in the gas feed", *Applied Catalysis B: Environmental*, vol. 66, no. 3-4, pp. 281-287.
- Garin F., 2001, "Mechanism of NO_x decomposition", *Applied Catalysis A: General*, vol. 222, no. 1-2, pp. 183-219.
- Gongshin Q., Ralph T. Y. & Ramsay C. 2002, "Low-temperature SCR of NO with NH₃ USY-supported manganese oxide-based catalysts", *Catalysis Letters*, vol. 87, No. 1 - 2, pp. 67-71.
- Gongshin Q., & Ralph Y. T. 2005, "Ultra-active Fe/ZSM-5 catalyst for selective catalytic reduction of nitric oxide with ammonia", *Applied Catalysis B: Environmental*, vol. 60, no. 1-2, pp. 13-22.
- Gongshin Q. & Yang, R.T. 2003, "Low-temperature selective catalytic reduction of NO with NH₃ over iron and manganese oxides supported on titania", *Applied Catalysis B: Environmental*, vol. 44, no. 3, pp. 217-225.
- Gongshin Q., Yang, R.T. & Chang, R. 2004, "MnO_x-CeO₂ mixed oxides prepared by co-precipitation for selective catalytic reduction of NO with NH₃ at low temperatures", *Applied Catalysis B: Environmental*, vol. 51, no. 2, pp. 93-106.

References

Goodhew J., Humphreys, j. & Beanland, R. 2001, "Electron Microscopy and Analysis" in *Electron Microscopy and Analysis*, ed. Taylor and Francis, Taylor and Francis, London, pp. 47-48.

Grzybek T., 2007, "Layered clays as SCR DeNOx catalysts", *Catalysis Today*, vol. 119, no. 1-4, pp. 125-132.

Haber J., Block, H. & Delmon, B. 1995, "Manual of methods and procedures for catalyst characterization (Technical report)", *Pure and Applied Chemistry*, vol. 67, NOS 8/9, no. 1995, pp. 1257-1306.

Hamada H., Kintaichi, Y., Sasaki, M., Ito, T. & Tabata, M. 1990, "Highly selective reduction of nitrogen oxides with hydrocarbons over H-form zeolite catalysts in oxygen-rich atmosphere", *Applied Catalysis*, vol. 64, pp. L1-L4.

Sjövall H. & Blint R. and L. Olsson. 2007, "Identification of absorbed species on Cu-ZSM-5 under NH₃ SCR conditions Normal 0 false false false", *Topics in Catalysis*, vol. Volume 42-43, Numbers 1-4, pp. 113-117.

Hao X., Zhang, Y., Wang, J., Zhou, W., Zhang, C. & Liu, S. 2006, "A novel approach to prepare MCM-41 supported CuO catalyst with high metal loading and dispersion", *Microporous and Mesoporous Materials*, vol. 88, no. 1-3, pp. 38-47.

Hartmann M., Racouchot, S. & Bischof, C. 1999, "Characterization of copper and zinc containing MCM-41 and MCM-48 mesoporous molecular sieves by temperature programmed reduction and carbon monoxide adsorption", *Microporous and Mesoporous Materials*, vol. 27, no. 2-3, pp. 309-320.

Hevia M. & Pérez-Ramírez, J. 2008, "Assessment of the low-temperature EnviNOx® variant for catalytic N₂O abatement over steam-activated FeZSM-5", *Applied Catalysis B: Environmental*, vol. 77, no. 3-4, pp. 248-254.

Huang B., Huang, R., Jin, D. & Ye, D. 2007, "Low temperature SCR of NO with NH₃ over carbon nanotubes supported vanadium oxides", *Catalysis Today*, vol. 126, no. 3-4, pp. 279-283.

References

- Huang J., Tong, Z., Huang, Y. & Zhang, J. 2008, "Selective catalytic reduction of NO with NH₃ at low temperatures over iron and manganese oxides supported on mesoporous silica", *Applied Catalysis B: Environmental*, vol. 78, no. 3-4, pp. 309-314.
- Huang B., Huang, R., Jin, D. & Ye, D. 2007, "Low temperature SCR of NO with NH₃ over carbon nanotubes supported vanadium oxides", *Catalysis Today*, vol. 126, no. 3-4, pp. 279-283.
- Hums, E. 2008, Tailored NO_x emission control for stationary sources considering a cost effective concept. *Personnel communication*
- Hums E. 1998, "Is advanced SCR technology at a standstill? A provocation for the academic community and catalyst manufacturers", *Catalysis Today*, vol. 42, no. 1-2, pp. 25-35.
- Huuhtanen M., Rahkamaa-Tolonen, K., Maunula, T. & Keiski, R.L. 2005, "Pt-loaded zeolites for reducing exhaust gas emissions at low temperatures and in lean conditions", *Catalysis Today*, vol. 100, no. 3-4, pp. 321-325.
- Iwamoto M., Sato, S., Yu-u, Y., Yahiro, H. & Mizuno, N. 1991, "Cu-ZSM-5 zeolite as highly active catalyst for removal of nitrogen monoxide from emission of diesel engines", *Applied Catalysis*, vol. 70, no. 1, pp. L1-L5.
- Jarvis K. & Gray, A. (eds) 1992, *Handbook of Inductively Coupled Plasma Mass Spectroscopy*, Capman and Hall, New York.
- Koebel M., Madia, G. & Elsener, M. 2002, "Selective catalytic reduction of NO and NO₂ at low temperatures", *Catalysis Today*, vol. 73, no. 3-4, pp. 239-247.
- Krishna K. & Makkee, M. 2006, "Preparation of Fe-ZSM-5 with enhanced activity and stability for SCR of NO_x", *Catalysis Today*, vol. 114, no. 1, pp. 23-30.
- Krishna K., Seijger, G., B., Van den Bleek B., Makkee, M. & and Calis H. P. A. July 2004, "Preparation of Ceria-zeolite catalysts by different techniques and its effect on selective catalytic reduction of NO with NH₃ at high space velocities", *Topics in Catalysis*, vol. 30/31, pp. 115-121.
- Landong L., Jixin, C., Zhang, S., Guan, N., Richter, M., Eckelt, R. & Fricke, R. 2004, "Study on metal-MFI/cordierite as promising catalysts for selective catalytic reduction of nitric oxide by propane in excess oxygen", *Journal of Catalysis*, vol. 228, no. 1, pp. 12-22.

References

- Lang N., Delichere, P. & Tuel, A. 2002, "Post-synthesis introduction of transition metals in surfactant-containing MCM-41 materials", *Microporous and Mesoporous Materials*, vol. 56, no. 2, pp. 203-217.
- Lawrence P., 2005, *Leading Edge Catalysis Research*, 20th edn, Nova Science Publishers, Inc, New York.
- Li Y. & Armor, J.N. 1993, "Selective catalytic reduction of NO_x with methane over metal exchange zeolites", *Applied Catalysis B: Environmental*, vol. 2, no. 2-3, pp. 239-256.
- Long R. & Yang, R.T. 2002, "Low temperature selective catalytic reduction (SCR) of NO with NH₃ over Fe-Mn based catalysts", *Chemical Communication*.
- Lyon R., Cole, J.A., Kramlich, J.C. & Chen, S.L. 1990, "The selective reduction of SO₃ to SO₂ and the oxidation of NO to NO₂ by methanol", *Combustion and Flame*, vol. 81, n^o. 1, pp. 30-39.
- Marbán G. & Fuertes, A.B. 2001, "Low-temperature SCR of NO_x with NH₃ over NomexTM rejects-based activated carbon fibre composite-supported manganese oxides: Part I. Effect of pre-conditioning of the carbonaceous support", *Applied Catalysis B: Environmental*, vol. 34, n^o. 1, pp. 43-53.
- Meinhard S., Rolf, S. & Groves, M. 2005, *Uhde EnviNOx process for the combined reduction of N₂O and NO_x emissions from nitric acid plants*, ThyssenKrupp tech forum, Dortmund. <http://www.uhde.eu>
- Metcalf E., 1987, *Atomic Absorption and Emission Spectroscopy*, New York: Willey.
- Muñiz J., Marbán, G. & Fuertes, A., B. 2000, "Low temperature selective catalytic reduction of NO over modified activated carbon fibres", *Applied Catalysis B: Environmental*, vol. 27, no. 1, pp. 27-36.
- Orton E., 2003. "Thermal Gravimetric Analysis". www.ortonceramic.com
- Pantazis C. & Pominos, P. 2006, "Synthesis of highly loaded Cu/Ce mesoporous silica. Active catalyst for the simultaneous reduction of SO₂ and NO with Co", *Chemical Communication*. 1268-1270
- Pârvolescu V.I., Grange, P. & Delmon, B. 1998, "Catalytic removal of NO", *Catalysis Today*, vol. 46, no. 4, pp. 233-316.

References

- Pieterse, J.A.Z. & Booneveld, S. 2007, "Catalytic reduction of NO_x with H₂/CO/CH₄ over PdMOR catalysts", *Applied Catalysis B: Environmental*, vol. 73, no. 3-4, pp. 327-335.
- Qi G. & Yang, R.T. 2005, "Ultra-active Fe/ZSM-5 catalyst for selective catalytic reduction of nitric oxide with ammonia", *Applied Catalysis B: Environmental*, vol. 60, no. 1-2, pp. 13-22.
- Qi G. & Yang, R.T. 2003, "Low-temperature selective catalytic reduction of NO with NH₃ over iron and manganese oxides supported on titania", *Applied Catalysis B: Environmental*, vol. 44, no. 3, pp. 217-225.
- Rahkamaa-Tolonen K., Maunula, T., Lomma, M., Huuhtanen, M. & Keiski, R.L. 2005, "The effect of NO₂ on the activity of fresh and aged zeolite catalysts in the NH₃-SCR reaction", *Catalysis Today*, vol. 100, no. 3-4, pp. 217-222.
- Ramachandran B., Herman, R.G., Choi, S., Stenger, H.G., Lyman, C.E. & Sale, J.W. 2000, "Testing zeolite SCR catalysts under protocol conditions for NO_x abatement from stationary emission sources", *Catalysis Today*, vol. 55, no. 3, pp. 281-290.
- Richter M., Trunschke, A., Bentrup, U., Brzezinka, K.W., Schreier, E., Schneider, M., Pohl, M.M. & Fricke, R. 2002, "Selective Catalytic Reduction of Nitric Oxide by Ammonia over Egg-Shell MnO_x/NaY Composite Catalysts", *Journal of Catalysis*, vol. 206, no. 1, pp. 98-113.
- Savidha R. & Pandurangan, A. 2004, "Vapour phase isopropylation of phenol over zinc- and iron-containing Al-MCM-41 molecular sieves", *Applied Catalysis A: General*, vol. 262, no. 1, pp. 1-11.
- Selvaraj M., Pandurangan, A., Seshadri, K.S., Sinha, P.K. & Lal, K.B. 2003, "Synthesis, characterization and catalytic application of MCM-41 mesoporous molecular sieves containing Zn and Al", *Applied Catalysis A: General*, vol. 242, no. 2, pp. 347-364.
- Shimura F., 1989, *Semiconductor silican crystal technology*, Academic Press Inc, San Diego.
- Singoredjo L., Slagt, M., Van Wees, J., Kapteijn, F. & Moulijn, J.A. 1990, "Selective catalytic reduction of NO with NH₃ over carbon supported copper catalysts.", *Catalysis Today*, vol. 7, no. 2, pp. 157-165.
- Sjövall H., Fridell, E., Erik, F. & Richard, J. 2007, "Identification of adsorbed species on Cu-ZSM-5 under NH₃ SCR", *Topics in Catalysis*, vol. 42-43, no. 2007, pp. 113-113.

References

Szostak R. 1989, "Molecular Sieves, principles of synthesis and identification" Van Nostrand Reinhold, New York.

Tang X., Hao, J., Honghong Y. & Junhua, L. 2007, "Low-temperature SCR of NO with NH₃ over AC/C supported manganese-based monolithic catalysts", *Catalysis Today*, vol. 126, no. 3-4, pp. 406-411.

Thomas S.A. 2005, *Selective Catalytic Reduction (SCR) Technology for the Control of Nitrogen Oxide Emissions from Coal-Fired Boilers*, U.S. Department of energy, Washington, DC.

Treacy M. & Higgins, J. 2007, "Powder pattern identification table" in *Collection of Simulated XRD Powder Patterns for Zeolites (fifth)* Elsevier Science B.V., Amsterdam, pp. 10-16.

Meinhard N., Siefert R., Groves M., Uhde wins contract for EnviNOx tail gas treatment unit", 2006, *Focus on Catalysts*, vol. 2006, no. 7, pp. 7-7.

Valdés-Solís T., Marbán, G. & Fuertes, A.B. 2001, "Low-temperature SCR of NO_x with NH₃ over carbon-ceramic cellular monolith-supported manganese oxides", *Catalysis Today*, vol. 69, no. 1-4, pp. 259-264.

Valdés-Solís T., Marbán, G. & Fuertes, A.B. 2003, "Low-temperature SCR of NO_x with NH₃ over carbon-ceramic supported catalysts", *Applied Catalysis B: Environmental*, vol. 46, no. 2, pp. 261-271.

Velu S., Wang, L., Okazaki, M., Suzuki, K. & Tomura, S. 2002, "Characterization of MCM-41 mesoporous molecular sieves containing copper and zinc and their catalytic performance in the selective oxidation of alcohols to aldehydes", *Microporous and Mesoporous Materials*, vol. 54, no. 1-2, pp. 113-126.

Weitkamp J., Puppe L., 2000, "Zeolites and catalysis", *Solid State Ionics*, vol. 131, no. 1-2, pp. 175-188.

Widmann G., 2001, *Interpreting TGA curves*, Mettler Toledo, Giessen, Germany. <http://us.mt.com>

Xiang-Ying H., Yin-Qing, Z., Jun-Wei, W., Zhou, W., Zhang, C. & Liu, S. 2006, "A novel approach to prepare MCM-41 supported CuO catalyst with high metal loading and dispersion", *Microporous and Mesoporous Materials*, vol. 88, no. 1-3, pp. 38-47.

References

Yogo K., Ihara, M., Teresaki, I. & Kikuchi, E. 1993, "Carrier-mediated transport of H1-antagonist at the blood barrier: A common transport system of H1-antagonists and lipophilic basic drugs", *Catalysis letter*, vol. 17, no. 303.

Yoshikawa M., Yasutake, A. & Mochida, I. 1998, "Low-temperature selective catalytic reduction of NO_x by metal oxides supported on active carbon fibers", *Applied Catalysis A: General*, vol. 173, no. 2, pp. 239-245.

Zhenping Z., Zhenyu, L., Shoujun, L. & Niu, H. 1999, "A novel carbon-supported vanadium oxide catalyst for NO reduction with NH₃ at low temperatures", *Applied Catalysis B: Environmental*, vol. 23, no. 4, pp. L229-L233.

Zhuang S., Magara, H., Yamazaki, M., Takahashi, Y. & Yamada, M. 2000, "Catalytic conversion of CO, NO and SO₂ on the supported sulfide catalyst: I. Catalytic reduction of SO₂ by CO", *Applied Catalysis B: Environmental*, vol. 24, no. 2, pp. 89-96.



7 APPENDICES

7.1 Loading calculations

The atomic percentage of the two ions Fe and Mn is based on the support

In order to achieve 30 % loading capacity, the following calculations were done:

1 atom of Fe has the atomic mass of 55.85

1 atomic of Mn has the atomic mass of 54.94

The total atomic mass of the two ions is equal to 110.79



If the following loading (30 %) of metals needs to be achieved on a 100g support, the following calculation needs to be done:

For 30 % ----- 100g

$$\text{For 1 \% ----- } \frac{100}{30} = 3.33 \text{ g}$$

Once again, we know that within the total atomic mass of 110.79g, we have 55.85g of Fe

For 1g ----- $\frac{55.85}{110.79}$ or the support used has the following mass 30g

For 30g ----- $\frac{55.85}{110.79} \times 30 = 7.39$

Once again we now that within the total mass of 110.79, we only have 54.94g of Mn

For 1g ----- $\frac{54.94}{110.79}$

For 30g ----- $\frac{54.94}{110.79} \times 30$



In order to achieve the ratio of on to one in terms of Fe and Mn

Iron will give us the following ratio

For 55g -----403.866g

For 7.39g ----- $\frac{403.866}{55.85} \times 7.39 = 54.26\text{g of Fe(NO}_3)_3 \cdot 9\text{H}_2\text{O}$

And for **Manganese**

For 54.94 ----- 204.982

$$\text{For 14.88 ----- } \frac{204.982}{54.94} \times 14.88 = 55.5\text{g of } (\text{CH}_3\text{COO})_2\text{.Mn.4H}_2\text{O}$$

These calculations are based on the fact that 100g of MCM-41 is considered as 100 % of the supporting material, thus for any mass of MCM-41 that one would like to use, the 30 % of the support can be work out this way.

Practical case

Mass of support: 2g

100 % ----- 2g

$$1\% \text{ ----- } \frac{2\text{g}}{100\%}$$

In case 15 % and 20 % are the amount to be loaded

For Iron

$$15\% \text{ ----- } \frac{15\% \times 2\text{g}}{100\%} = \frac{30\text{g}}{100} = 0.3\text{g} \quad (1)$$



Appendices

$$20\% \text{ ----- } \frac{20\% \times 2\text{g}}{100\%} = \frac{4\text{g}}{10} = 0.4\text{ g} \quad (2)$$

$$110.79\text{g} \text{ ----- } 55.85\text{g of Fe}$$

$$1\text{g} \text{ ----- } \frac{55.85}{110.79} \quad (3)$$

(1) in (3)

$$0.3\text{g} \text{ ----- } \frac{55.85 \times 0.3}{110.79} = 0.151\text{ g} \quad (4)$$

(2) in (3)

$$0.4\text{g} \text{ ----- } \frac{55.85 \times 0.4}{110.79} = 0.201\text{g} \quad (5)$$



$$55.85\text{g Fe} \text{ ----- } 403.866$$

$$1\text{g} \text{ ----- } \frac{403.866}{55.85} \quad (6)$$

(4) in (6)

$$0.151 \text{ ----- } \frac{0.151 \times 403.866}{55.85} = 1.092\text{g of Fe} \cdot (\text{NO}_3)_3 \cdot 9\text{H}_2\text{O}$$

(5) in (6)

Appendices

$$0.201\text{g} \text{-----} \frac{0.201 \times 403.866}{55.85} = 1.454\text{g of Fe}(\text{NO}_3)_3 \cdot 9\text{H}_2\text{O}$$

Loading (%)	Mass of salt (Fe(NO ₃) ₃ ·9H ₂ O)	Mass of Fe
15	1.092	0.151
20	1.454	0.201
25	1.822	0.251
30	2.184	0.302
35	2.553	0.353
40	2.914	0.403

For manganese

$$15\% \text{-----} \frac{15\% \times 2\text{g}}{100\%} = \frac{30\text{g}}{100} = 0.3\text{g} \quad (1)$$

$$20\% \text{-----} \frac{20\% \times 2\text{g}}{100\%} = \frac{4\text{g}}{10} = 0.4\text{g} \quad (2)$$

$$110\text{g} \text{-----} 54.94 \text{ Fe}$$

$$1\text{g} \text{-----} \frac{54.94}{110.79} \quad (3)$$

(1) in (3)

Appendices

$$0.3\text{g} \text{-----} \frac{54.94 \times 0.3}{110.79} = 0.149 \text{ g} \quad (4)$$

(2) in (3)

$$0.4\text{g} \text{-----} \frac{54.94 \times 0.4}{110.79} = 0.198 \text{ g} \quad (5)$$

$$55.85\text{g Fe} \text{-----} 204.982$$

$$1\text{g} \text{-----} \frac{204.982}{54.94} \quad (6)$$

(4) in (6)

$$0.151 \text{-----} \frac{0.149 \times 204.982}{54.94} = 0.555\text{g of } (\text{CH}_3\text{COO})_2\text{Mn} \cdot 4\text{H}_2\text{O}$$

(5) in (6)

$$0.201\text{g} \text{-----} \frac{0.198 \times 204.982}{54.94} = 0.739\text{g of } (\text{CH}_3\text{COO})_2\text{Mn} \cdot 4\text{H}_2\text{O}$$



UNIVERSITY of the
PHILIPPINES

Appendices

Loading (%)	Mass of salt (Mn(CH₃COO)₂·4H₂O) (g)	Mass of Mn
15	0.555	0.149
20	0.739	0.198
25	0.925	0.248
30	1.112	0.298
35	1.295	0.347
40	1.481	0.397



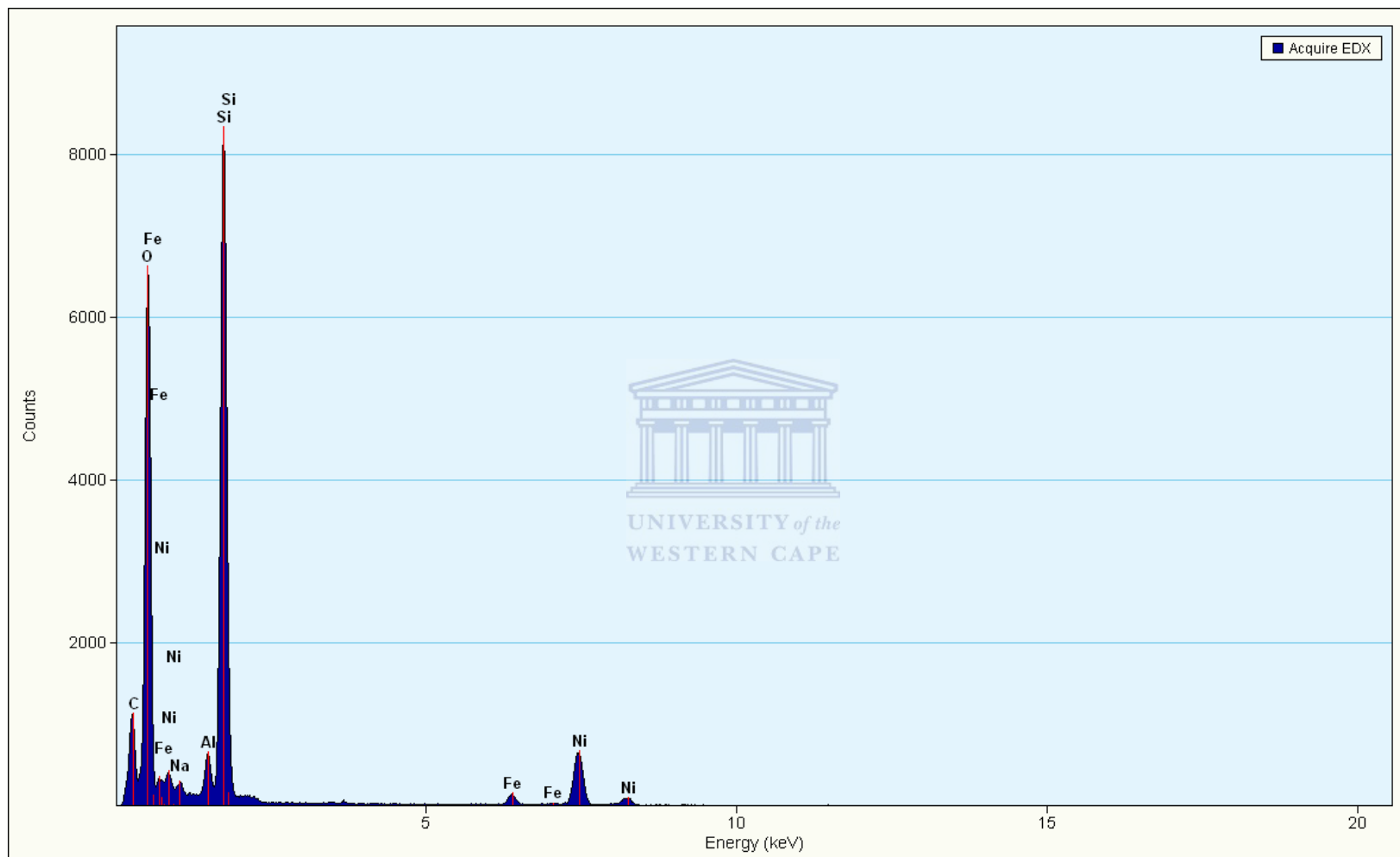
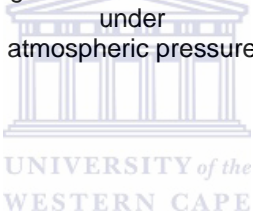


Figure 7-1: EDS images of the 10 % Fe-Beta-25 catalyst synthesized by wet impregnation.

7.2 ANNEX I: Overview of techniques and analysis mode used for NOx analysis

Title of publication	Author	Year of publication	Reactor type	Analyzer model
SCR of NO by NH ₃ on Cu (2) ion -exchanged offretite prepared by different methods	Arous W.	2007	Micro-flow reactor	NO, NH ₃ , N ₂ O, N ₂ , O ₂ and H ₂ O were analyzed by a quadrupole mass spectrometer (Balzers QMS 421)
Testing zeolite SCR catalysts under protocol conditions for Nox abatement from stationary emission sources	Bala R.	2000	Vertical quartz tube reactor on a porous glass fritted	NO was monitored by a chemiluminescence detector and NH ₃ periodically monitored by an ion selective electrode
SCR of NO by Ammonia over Egg-shell MnOx/NaY composite catalysts	Richter M.	2002	Flow system equipped with an integral flow reactor	Analysis of the product flow was conducted using gas chromatography (HP 6890 series) on two parallel capillary columns linked to thermal conductivity detectors. A HP-Plot Molesieve column served for separation of N ₂ , O ₂ , and Co, and Poraplot Q column for separation of NO, N ₂ O, H ₂ O, NH ₃ and CO ₂
Identification of absorbed species on Cu-ZSM-5 under NH ₃ SCR conditions	Sjovall H.	2007	In situ flow reactor (Harrick Praying Mantis Drift cell)	The in situ FTIR spectroscopy measurements were performed using a BioRad FTS 6000 spectrometer in diffuse reflectance model
Pt-loaded zeolites for reducing exhaust has emissions at low temperatures and in lean conditions	Huuhtanen M.	2005	Tubular quartz reactor	The outlet concentrations of propene, NO, N ₂ O, NO ₂ , CO, and CO ₂ were measured by Gasmet TM FT-IR analyzer
MnOx-CeO ₂ mixed oxides prepared by co-	Qi G.	2004	Fixed bed reactor quartz reactor	Chemiluminescent NO/NOX analyzer (Thermo Environmental instrument Inc. model 42C)

Appendices

precipitation for SCR of NO with NH ₃ at low temperature				
Low-temperature SCR of NO _x with NH ₃ over carbon-ceramic cellular monolith-supported manganese oxides	Valdes T.	2001	Quartz reactor	Chemiluminescent analyzer (Rasemount Analytical, Model 951A)
SCR of NO with NH ₃ at low temperatures over iron and manganese oxides supported on mesoporous silica	Huang J.	2008	Quartz tubular down-flow reactor	Chemiluminescent NO/NO_x analyzer (Thermo Environmental instrument Inc. model 42C)
Comparison of TiO ₂ -based oxide catalysts for the SCR of NO: effect of aging the vanadium precursor solution	Nicolaos V.	1999	Plug flow differential reactor under atmospheric pressure 	The reactor effluent was analyzed with a thermal conductivity detector . N ₂ and O ₂ are separated with a Porapak-Q column (Supelco, stainless steel 1/8in., 15 ft long). In order to determine the concentration of unreacted ammonia, the effluent of the reactor passed through a solution of boric acid (0.016) for certain amount of time
Low temperature SCR of NO _x with NH ₃ over Nomex TM rejects-based activated carbon fibre composite-supported manganese oxides	Marban G.	2001	Vertical quartz reactor	The NO/NO ₂ concentration of the inlet (CNO _x) and outlet (CNO _x) gases was analyzed by means of chemilunescence analyzer (Rosemount Analytical Model 951A) , whereas the CO ₂ and N ₂ O concentration in the outlet gases was determined with a gas chromatographer (HP 6890 Series) and a TCD detector . Before entering the gas analysis system, the gases were bubbled trough an aqueous solution of phosphoric acid (3-20 wt%) in order to remove the NH ₃
NH ₃ -SCR of NO at low temperatures over sulphated vanadia on carbon-coated monoliths: Effect of H ₂ O and SO ₂ traces in	Garcia-Bordeje E.	2006	Quartz micro-reactor	Mass spectrometer (Blazers) was used

Appendices

the gas feed				
Alumina-and titania-based monolithic catalysts for low temperature SCR OF NO _x	Blanco J.	2000	Reactor working close to an isothermal axial profile	The inlet and outlet NO and NO ₂ concentrations were determined by chemiluminescence with a signal NO+NO ₂ analyzer Series 4000 . Analysis of N ₂ O and NH ₃ were carried out by IR spectroscopy with a signal 7000FT GFC analyzer and with an ADC Double Beam Luft type Infra-red gas analyzer, respectively
Low temperature SCR of NO with NH ₃ over carbon nanotubes supported vanadium oxides	Huang B.	2007	Quartz fixed-bed	NO concentrations in the inlet and outlet gases were measured by an on-line FSI Model flue gas analyzer. N ₂ O and NO ₂ concentrations in the outlet gases were measured continuously by a gas chromatograph with Porapak Q column.
Low-temperature selective catalytic reduction of NO _x by metal oxides supported on active carbon fibers	Yoshikama M.	1998	Fixed-bed flow reactor	NO and NO ₂ concentrations were analyzed continuously at the inlet and outlet of the reactor by chemical luminescence NO _x meter (ECL-88AO, YANACO). Other gaseous species at the outlet of the reactor such as NH ₃ , N ₂ O, CO and CO ₂ were analyzed by FT-IR spectrophotometer (FT-IR 8200pc, Shimadzu) using optical gas cell (Long Path Mini-Cell model 6, infrared analysis).
Low temperature SCR of NO with NH ₃ over AC/C supported manganese-based monolithic catalysts	Tang X.	2007	Quartz tube reactor	NO _x , O ₂ , and SO ₂ concentration in the inlet and outlet gases were simultaneously measured by Quintox flue Gas Analyzer (KM9106, Kane-May)
Low temperature SCR of NO over modified activated carbon fibres	Muniz J.	2000	Fixed bed reactor made of quartz	NO concentration in the inlet and outlet gases was analyzed by means of NO/NO ₂ chemiluminescence analyzer (Rasemount Analytical, Mod. 951A)

Appendices

Assessment of low-temperature Envinox variant for catalytic N ₂ O abatement over steam-activated FeZSM-5	Miguel A.G.	2008	Quartz micro-reactor	Reactant and product gases were analyzed by a gas chromatograph (Agilent 6890N) equipped with HP-PLOT and DB-FFAP columns ND TCD and FID detectors
Catalytic DeNO _x activity of cobalt and copper ions in microporous MeALPO-34 and MeAPSO-34	Frache A.	2002	Quartz fixed bed micro-reactor	The concentration of NO, NO ₂ , N ₂ O, and O ₂ were monitored by using Hartmann and Braunn continuous analyzers for NO and N ₂ O (URAS 10E), O ₂ (MAGNOS 6G) and a catalytic converter (CGO-K) for NO ₂
catalytic conversion of CO, NO and SO ₂ on the supported sulfide catalyst	Zhuang S. X.	2000	Fixed bed flow reactor	The feed gas was passed trough a catalyst bed and then entered into an on-line trap coiled in an ice bath to condense sulfur before entering a sampling valve of GC with a TCD detector using a Porapak Q column for separating CO, CO ₂ , COS and SO ₂ .
On the SCR of NO _x with methane over Ag-ZSM-5 catalysts	Shi C.	2002	Microcatalytic reactor	The effluent gases from the reactor were analyzed by gas chromatograph (GC 14B) with a TCD detector
	Rahkamaa-Tolonen K.		Tubular quartz reactor heated by IR	The outlet gas was analyzed by FT-IR analyzer (Gasmeter FT-IR gas analyzer)
Ultra-active Fe/ZSM-5 catalyst for SCR of nitric oxide with ammonia	Qi G.	2005	Fixed-bed quartz reactor	The NO and NO ₂ concentrations were continually monitored by chemiluminescent NO/Nox analyzer (Thermo Environmental Instruments Inc. Model 42C) The products were also analyzed by a gas chromatograph (Shimadzu, 8A) at 50°C with 5A molecular sieve column for N ₂ and Porapak Q column for N ₂ O
Low-temperature SCR of NO _x with NH ₃ over carbon ceramic supported catalysts	Valdes-Solis T.	2003	Vertical furnace, using Vycor reactors	NO and NO ₂ concentrations in the inlet and outlet gases were measured continuously by a chemiluminescence analyzer (ROSEMOUNT Analytical, 951A)

Appendices

A novel carbon-supported vanadium oxide catalyst for NO reduction with NH ₃ at low temperatures	Zhu Z.	1999	fixed-bed quartz reactor of 8mm of diameter	The concentrations of NO, NO ₂ , SO ₂ and O ₂ both at the inlet and the outlet of the reactor were simultaneously monitored by an On-line Flue Gas Analyzer (KM9006 Quintox, Kane International Limited) equipped with NO, NO ₂ , SO ₂ and O ₂ sensors.
Catalytic reduction of NO _x with H ₂ /CO/CH ₄ over PdMOR catalysts	Johannis A.Z.	2007	Quartz reactors with an internal diameter of 0.5 cm	The quantitative analysis of the gas phase components was performed using a Compact GC Inter-science, C2002000A equipped with TCD and FID and a NOx analyzer (M&C Indumation, Eco Physics CLD822) . Data were collected from 673 to 363 K using a ramp of 5 K/min with preconditioning at each temperature. NOx conversion versus time The quantitative analysis of the gas phase components was performed using either a FTIR spectrometer MIDAC (model I1803) equipped with a gas cell (path length 3 m)
Selective catalytic reduction of NO and NO ₂ at low temperatures	Koebel M.	2002	Tubular glass reactor of 30 mm i.d. and of about 500 mm length	Multi-component gas analysis was performed by means of an FT-IR spectrometer (Nicolet Magna IR 560, OMNIC QuandPad software) equipped with a multiple pass gas cell (Graseby Specac G-2-4-BA-AU, path length 2 m) and a liquid nitrogen cooled MCT detector. The method developed allowed the simultaneous determination of NO, NO ₂ , N ₂ O, HNO ₃ , NH ₃ , and H ₂ O

7.3 ANNEX II: Instrumentation list of the rig

Instrument	Supplier	Comment
Afrox scientific regulators	Afrox	<ol style="list-style-type: none"> 1. W019110 Air/Argon/Helium/Oxygen/NFT S 2. W020170 Mix flammable/Corrosive 1S 3. W020120 SC Ammonia 1S 4. W021060 SC Mix corrosive
Infra-red heaters	Elstein, 750W, 230W, 230V	Part N° UHI – LYHLS - 0750
Control unit box with controller and indicator	Unitemp	Part N°: UCH - Control box
Gas analyzer	Agilent Technologies	HP 7890 A GC system
Ammonia trap	Cole Palmer	I E Gas wash bottle
Moisture trap	Cole Palmer 55 ml volume 1/8" fitting	
Manometers	Swagelok Pressure Gauge	PGI – 63B – SG250 - CAOX
Rota meters	AALBORG	Single tube flow meters (Built in valves)
Mol Sieve 5A 1/8" SS 80/100 mesh column	Thermo Fischer	Max temp 273° C
Hayesep Q 1/8" SS 80/100 mesh column	Thermo Fischer	Max temp 273 ° C